Molecular Mechanisms that Regulate Neurotransmission and Establish Presynaptic Homeostasis at the *Drosophila melanogaster* Neuromuscular Junction

Inaugural Dissertation

to obtain the academic degree

Doctor rerum naturalium (Dr. rer. nat.)

submitted to the Department of Biology, Chemistry and Pharmacy

of Freie Universität Berlin

by

Anthony William McCarthy

from Dublin, Ireland

February 2020

The experimental part of this thesis was conducted from September 2015 to November 2019 under the supervision of Dr. Alexander Walter at the Leibniz-Forschungsinstitut für Molekulare Pharmakologie (FMP) and at the CharitéCrossOver, Charité Campus Berlin Mitte.

1st Reviewer: Dr. Alexander Walter

2nd Reviewer: Prof. Dr. Stephan Sigrist

Date of Defence: 15th June 2020

Statement of Authorship

I hereby declare that I am the sole author of this thesis and that I have not used any sources or tools other than those quoted. Use of work by any other author is identified as such and appropriately referenced.

Berlin, February 2020

Anthony William McCarthy

Acknowledgments

I would like to take the opportunity to thank all the people who have been important and made an impact on me during my time in Berlin. I would first like to thank my supervisor, Dr. Alexander Walter, for his guidance and supervision over the years. His passion for science and expert knowledge as well as approachable nature made for insightful conversation, projecting me forward with my projects.

I would also like to thank Prof. Dr. Stephan Sigrist for his valuable input during thesis committee meetings and for acting as a reviewer. I am grateful to Prof. Dr. Volker Haucke, the members of his lab and all those at the FMP in Buch for the plentiful feedback I received following thesis committee meetings and progress presentations.

Many thanks go to my colleagues in AG Walter for making the lab an enjoyable and productive place to work. I would specifically like to thank the following people: Dr. Mathias Böhme for his mentorship, particularly regarding fly genetics and microscopy, and for sharing his knowledge and experience with me during the long walks home; Meida Jusyte for sharing the struggles of electrophysiology and pharmacology but always pushing through with a smile on her face, ready to lend a hand; Andreas Grasskamp for his help with IT-related issues, expert MATLAB tips, proofreading and for the constant stream of ‘dad jokes’; Sabine Hahn for her upbeat attitude and keeping us all well stocked with recording solutions. Thanks go to all the members of the Sigrist lab in Mitte not only for the fun and pleasant atmosphere but for providing an environment full of lively discussion and interaction.

Outside of the lab, I am grateful to all my friends and family for their continued encouragement, not just during the last few years but throughout life. Finally, and most importantly, I would like to thank my mother. She has been the most supportive loving person a son could hope for, working hard to provide the best upbringing possible and always there for a chat, night or day.

Table of Contents

1 Summary

Accurate and efficient neurotransmission is achieved through a complex interplay of proteins and lipids at the presynaptic active zone (AZ). Action potentials (APs) trigger the fusion of synaptic vesicles (SVs) with the plasma membrane at AZs in a coordinated manner. The subsequent release of neurotransmitter (NT) into the synaptic cleft and activation of postsynaptic receptors elicits a response in the opposing cell. Synapses are plastic structures and this feature aids in modulating neurotransmission depending on the situational requirements. Plasticity is thought to form the basis of information processing including learning and memory and its dysregulation is linked to neurological disorder. This thesis presents work that explores the molecular contributions of AZ proteins and lipid signalling to neurotransmission and plasticity, using electrophysiology and microscopy at the *Drosophila melanogaster* larval neuromuscular junction (NMJ).

In the first part of the thesis, the role of lipid signalling is investigated. The ability to load and activate an initially chemically caged $PI(4,5)P_2$ is confirmed in mammalian cell culture, with observed changes in actin organisation. At the *Drosophila* NMJ, acutely uncaged $PI(4,5)P_2$ provides a possible protective effect against decreasing responses to stimulation. $PI(4,5)P_2$ is metabolised to diacylglycerol (DAG), and application of a functionally analogous phorbol ester (PMA) is also shown here to greatly enhance evoked but not spontaneous NT release.

Neurotransmission during presynaptic homeostatic plasticity provides a primary focus for this thesis. This form of plasticity maintains stable neurotransmission in response to a reduction in postsynaptic NT sensitivity, induced rapidly by pharmacological application of a postsynaptic NT receptor antagonist or chronically by genetic deletion of the receptors. Functionally, presynaptic homeostatic potentiation (PHP) occurs as NT release increases to compensate for postsynaptic challenge. This is accompanied by structural reorganisation of AZs proteins, involving an increase in presynaptic protein levels.

It is shown here that the SV priming factor and release site generating protein Unc13A is vital for rapid PHP, and the N-terminal portion of Unc13A is specifically identified as being essential for this process. Interestingly, the AZ cytomatrix scaffold protein Bruchpilot (BRP) is necessary for the structural aspect of homeostatic plasticity but is dispensable for functional PHP. However, following the long-term chronic induction of presynaptic homeostatic plasticity, BRP is found to be necessary for both functional PHP and structural AZ reorganisation. Additionally, axonal transport is required for both manifestations during long-term homeostatic plasticity.

The results outline the similarities and differences between acutely and chronically induced presynaptic homeostatic plasticity and they suggest how core AZ proteins differentially regulate this process depending on the timescale. The disparity between the functional and structural components of homeostatic plasticity is unveiled, indicating that PHP does not necessarily require AZ structural change on short timescales, instead being important for consolidation of potentiation.

2 Zusammenfassung

Präzise und effiziente Neurotransmission wird durch ein komplexes Zusammenspiel von Proteinen und Lipiden an der präsynaptischen aktiven Zone (AZ) erreicht. Aktionspotentiale (AP) lösen die koordinierte Fusion von synaptischen Vesikeln (SV) mit der Plasmamembran der AZ aus. Die anschließende Ausschüttung von Neurotransmittern (NT) in den synaptischen Spalt und die Aktivierung von postsynaptischen Rezeptoren löst eine Erregung der postsynaptischen Zelle aus. Die Eigenschaft von Synapsen, plastische Strukturen darzustellen, erlaubt die Modulation von Neurotransmission je nach bestehenden Anforderungen. Synaptische Plastizität wird als Grundlage für Informationsverarbeitung sowie für Lernen und Gedächtnisbildung angesehen. Ihre Dysregulierung wird mit neurologischen Erkrankungen in Verbindung gebracht. Diese Arbeit befasst sich mit der Beteiligung von AZ Proteinen und Lipid-Signalkaskaden an Neurotransmission sowie synaptischer Plastizität, die mithilfe von Elektrophysiologie und Mikroskopie an der larvalen neuromuskulären Synapse von *Drosophila melanogaster* untersucht wurde.

Im ersten Teil dieser Arbeit wird die Rolle, die Lipide bei der Signalübertragung spielen, untersucht. Zunächst wird gezeigt, wie kultivierte Zellen mit einer anfangs durch einen chemischen „Käfig“ inaktivierten Form von $PI(4,5)P_2$ geladen werden können. Es wird desweiteren verifiziert, dass diese Komponente aktiviert werden kann und dass dies zu Änderungen der Aktinorganisation führt. An der neuromuskulären Synapse von *Drosophila* wird zudem gezeigt, dass akut aktiviertes $PI(4,5)P_2$ als möglicher Mechanismus zum Schutz gegen abnehmende Übertragungsstärke dient. $PI(4,5)P_2$ wird zu Diacylglycerol (DAG) metabolisiert und es wird in dieser Arbeit demonstriert, dass sein Analogon Phorbolester (PMA) AP-induzierte postsynaptische Antwortstärke stark verändert, während es keinen Effekt auf spontane synaptische Aktivität hat.

Neurotransmission im Kontext von präsynaptischer homöostatischer Plastizität (PHP) stellt den Hauptfokus dieser Dissertation dar. Im Zuge einer verringerten NT-Sensitivität von postsynaptischen Rezeptoren , die entweder durch

pharmakologische Interferenz durch postsynaptische Rezeptorantagonisten oder den genetisch erzielten Verlust der Rezeptoren erzielt werden kann, stellt PHP eine beständige Neurotransmission sicher. Funktionell beinhaltet PHP eine Kompensation einer solchen postsynaptischen Herausforderung, die durch den Anstieg von freigesetztem NT durch die Präsynapse erzielt wird. Begleitet wird dies durch die strukturelle Umgestaltung von präsynaptischen Proteinen, was ihren Anstieg an der AZ beinhaltet.

Das AZ Protein Unc13A spielt eine essentielle Rolle für die Vorbereitung der SV für ihre Fusion und wurde zudem als das Molekül identifiziert, das ihre Freisetzungsstelle definiert. In dieser Arbeit wird gezeigt, dass Unc13A und im Spezifischen der N-terminale Teil des Proteins, unabdingbar für die funktionelle Komponente von PHP ist. Zwar ist das AZ Strukturprotein Bruchpilot (BRP) notwendig für den strukturellen Aspekt der PHP, interessanterweise ist es jedoch entbehrlich für funktionelle PHP. Im Zuge der chronischen Induktion von homeostatischer Plastizität hingegen, ist BRP sowohl für die funktionelle als auch für die strukturelle Komponente notwendig. Zudem wird axonaler Transport von synaptischem Material für beide Aspekte von PHP über längere Zeiträume gebraucht.

Die Ergebnisse dieser Arbeit stellen die Gemeinsamkeiten und Unterschiede der schnellen und chronisch induzierten PHP einander gegenüber und skizzieren, wie Kernproteine an der AZ diesen Prozess in Abhängigkeit von seiner Zeitskala regulieren. Die Unterschiede zwischen den molekularen Komponenten der funktionellen und strukturellen PHP werden aufgedeckt und es werden Hinweise dafür aufgezeigt, dass PHP nicht zwingend die strukturelle Ummodellierung der AZ benötigt.

3 Introduction

3.1 The Action Potential

Debate surrounds the emergence of nervous system in animals (Metazoa). Comb jelly fish (Ctenophora) possess a nervous system yet sponges (Porifera), which are apparently more recent in the phylogenetic tree, lack a nervous system (Liebeskind et al., 2017). Regardless of the specific timeline of their evolution, neurons exist in all complex bilaterally symmetrical animals and form the basis of the nervous system.

Neurons are a type of excitable cell specialised for conveying electrical signals that facilitated the development of rapid and diverse behaviour in animals (Liebeskind et al., 2017). As is the case in many other cells, a concentration gradient of charged ions exists across the neuronal plasma membrane. While the concentration of K^+ ions is higher intracellularly, the concentration of Na^+ ions is higher extracellularly (Kandel et al., 2000). At rest, the membrane is more conductive for K^+, which moves down its concentration gradient out of the cell. Compared to the positive exterior, the default state of neuronal membranes is therefore to be negatively charged inside, as cations (K^+) exit. The unequal charge distribution between the intracellular and extracellular space is a fundamental aspect of neuronal membranes. The electrical potential (voltage) difference across the membrane is referred to as the resting membrane potential. Na^+/K^+ pumps actively transport Na^+ and K^+ against their ion gradient in an ATP and hence energy dependent process, supporting the maintenance of neuronal membrane resting potential (Kandel et al., 2000). It is important to consider the equilibrium potential of specific ions, which describes the potential at which there is a net flow of zero across the membrane for that particular ion. This information aids in predicting membrane potential behaviour in certain situations. The membrane potential will tend to move towards the equilibrium potential of the ions it has the greatest conductance for at a point in time. Therefore, the opening and closing of ion channels is one of the greatest determinants of the membrane potential. As an example, the resting potential is

close to the equilibrium potential of K^+ due to a high proportion of K^+ leak channels constitutively open.

Neurons make use of alterations in the membrane potential to propagate signals known as action potentials (APs) along elongated protrusions, which extend toward other cells (Kandel et al., 2000). In most neurons, APs move away from the cell body (soma) via axons and towards it via similar structures referred to as dendrites. An AP is a wave of depolarisation and repolarisation of the membrane potential. AP initiation and propagation was described by Hodgkin and Huxley (1952) in the squid giant axon.

For an action potential to be initiated, the membrane must depolarise sufficiently in relation to the resting membrane potential, crossing a threshold potential in the process (Figure 1) (Zhang and Stewart, 2010b). This can happen at several sites of the neuronal membrane, but commonly occurs at the axon hillock, and is caused by the opening of ion channels embedded in the membrane. Current passing into the neuron overcomes the resting membrane potential, leading to positive feedback. At the threshold potential the probability for voltage gated Na^+ channels to open, and for Na^+ to enter the cell drastically increases. Na^+ conductance is increased, and the membrane potential rapidly moves towards the equilibrium potential of Na^+ (Figure 1). Towards the peak of membrane depolarisation, the opening probability of voltage gated K^+ channels increase. Na^+ channels enter an inactive state, which serves to limit further entrance of Na^+ ions while K^+ exits the cell. Further AP initiation is not possible until Na^+ channels have exited the inactive state, a period called the absolute refractory period.

The membrane potential starts to repolarise again, and K^+ conductance is at its peak (Zhang and Stewart, 2010b). The potential moves towards the equilibrium potential of K^+. While repolarising, the membrane passes the resting membrane potential and become hyperpolarised due to a combination of delay in closure of voltage gated K^+ channels and permanently open K^+ leak channels. A relative refractory period exists during this hyperpolarisation: The possibility to initiate another AP is reduced as the extremely polarised membrane is less likely to be sufficiently stimulated to reach the threshold potential than it would be at the

resting potential. Gradually, most of the remaining open voltage gated K^+ channels close and the membrane returns to the resting potential. APs propagate in an all-or-nothing fashion by influencing the potential of the membrane in close proximity to the initiation site, moving as a wave and opening voltage gated ion channels as they travel. Various properties of axons can increase or decrease the conduction velocity and kinetics of APs, including the axon diameter, ion channel density, and the presence/absence of insulating myelin (Freeman et al., 2016). Electrical resistance in the axon is inversely related to axon diameter. This means that larger axons will permit faster AP conduction (Kandel et al., 2000). In some axons, a myelinating sheath reduces the membrane capacitance and increases resistance between regions of the axon known as nodes of Ranvier (Castelfranco and Hartline, 2015). In a process known as salutatory conduction APs are forced to jump between these nodes, at which voltage gated Na^+ channels are concentrated, vastly increasing conduction velocity (Kandel et al., 2000).

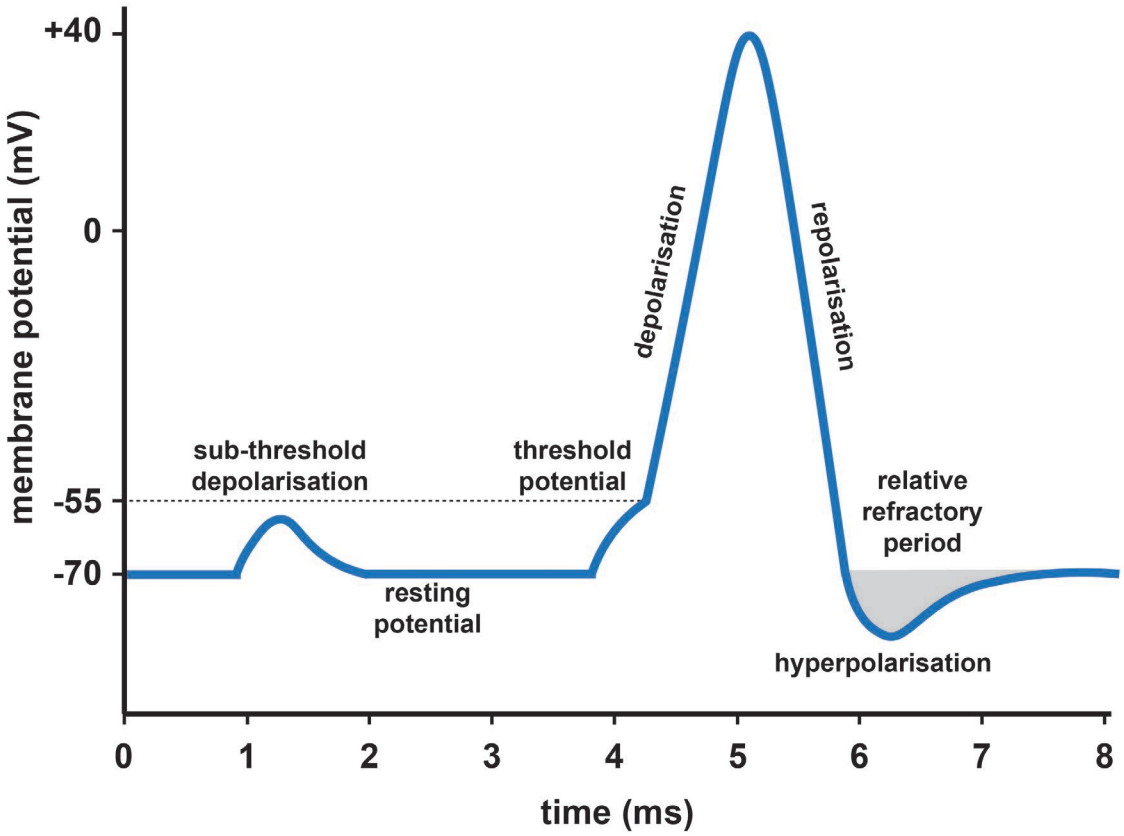

Figure 1: The Action Potential: Example time course and stages.

From rest, membrane depolarisations of the neuronal membrane must reach a threshold potential to initiate an AP. On doing so, voltage gated Na^+ channels open and the membrane rapidly depolarises further as Na^+ enter the cell. Towards the peak of an AP, Na^+ channels begin to close and voltage gated K^+ channels begin to open and K^+ exiting the cell increases. At the peak, Na^+ channels have entered a refractory inactive state. K^+ channels are open but begin to close as the membrane repolarises. Closure of K^+ channels is delayed and the membrane potential passes the resting membrane potential, becoming hyperpolarised. Remaining K^+ channels close soon after and the membrane returns to the resting potential.

3.2 Chemical synapses

Neurons communicate with each other at specialised sites called synapses. At chemical synapses, the presynaptic neuron releases chemical messengers called neurotransmitters (NTs) that bind to receptors on the membrane of the postsynaptic neuron or muscle. Active Zones (AZs) are presynaptic regions specifically configured to respond to the arrival of APs and release neurotransmitter accordingly (exocytosis) (Südhof, 2012). NTs are stored in

sac-like synaptic vesicles (SVs) and those localised at the plasma membrane are said to be docked. A small proportion is prepared for AP-induced exocytosis of their contents (primed). SVs that are docked and primed for plasma membrane fusion do so due to acute Ca^{2+} influx through a cluster of voltage gated Ca^{2+} channels following membrane depolarisation (Südhof, 2012). Fusion occurs when the two lipid bilayers (of the SV and the plasma membrane) merge (Han et al., 2017). NT is subsequently released into the synaptic cleft, the extracellular space between the presynapse and the postsynapse, prior to binding and activating postsynaptic NT receptors. Synapses do not only transmit information; they also modulate and transform it (Südhof, 2012). A feature of the presynaptic AZ is its ability to plastically react to changes in neuronal activity, achieved via the function of a host of regulatory proteins, lipids and signalling pathways (Zhai and Bellen, 2004).

SVs at the presynapse are proposed to exist in three separate pools: the readily releasable pool (RRP), the reserve pool and the recycling pool (Rizzoli and Betz, 2005). The RRP consists of SVs that are docked at the AZ and primed to fuse with the membrane in response to an AP, in other words, fully release competent. They are immediately releasable on stimulation and strong stimulation will successfully deplete the pool (Rizzoli and Betz, 2005). When an AP arrives at the presynapse, there is an associated probability due to Ca^{2+}-influx that individual SVs will be released, so called release probability (Böhme et al., 2018). The distinction between docking and priming is important as docked SVs are not necessarily immediately releasable (Verhage and Sørensen, 2008). Labelling of recycled SVs at the frog NMJ revealed docked SVs at AZ membranes that are not released following stimulation (Rizzoli and Betz, 2004). *Drosophila* priming mutants display a near complete loss of neurotransmission but maintain approximately half the number of docked SVs at AZs compared to wild-type (Böhme et al., 2016). However, debate surrounds the separation of docking and priming (Imig et al., 2014). At mouse hippocampal synapses in slice culture, the number of observed docked SVs seems to correlate with previous estimations of the RRP (Stevens and Tsujimoto, 1995) and it is argued that docked SVs are primed (Imig et al., 2014). SVs in the recycling pool may be recruited with appropriate stimulation

but many SVs in the reserve pool are unlikely to ever be released at physiological conditions (Denker and Rizzoli, 2010). While it was initially thought that the recycling and reserve pool were spatially distinct there is now evidence that they are mixed (Denker et al., 2009). Reserve pool SVs may be tethered to the scaffold, and mobile recycling SVs can mature to enter a similar state (Denker and Rizzoli, 2010).

3.3 The quantal nature of synaptic transmission

Bernard Katz and colleagues performed pioneering experiments at the frog NMJ, discovering “miniature end-plate potentials” in muscle membranes at rest. These spontaneous events could be unveiled to be the minimum unit of neurotransmission by reducing extracellular Ca^{2+} to the point where presynaptic stimulation produced muscle responses of equal amplitude and no lower (Fatt and Katz, 1952). It was established that synaptic transmission is underpinned by the release characteristics of defined all-or-none packets of neurotransmitter and summation of these formed the basis of larger responses (del Castillo and Katz, 1954). Shortly afterwards, the first electron micrographs of synaptic vesicles were published (Robertis and Bennett, 1955). From the work of Katz one can derive the following formula to explain the postsynaptic depolarisation of the muscle membrane in response to presynaptic nerve stimulation: $I = Npq$, where N is the number of independent SV release sites, p is the probability of SV release and q, the amplitude of the postsynaptic response to individual SVs (quantal size) (Figure 2a) (Takahashi, 2015). Put simply, an AP that stimulates NT release at the synapse will produce a postsynaptic response that is a function of the number of SVs positioned and ready for release, the probability of individual SVs to be released (independent of each other) and the size of the postsynaptic response to NT contained within each SV.

N is dependent on SVs docking and priming at appropriate sites on the plasma membrane called release sites. There is debate regarding the term “release site” and whether it should refer to the entirety of an AZ, as in many cases, SVs are released individually at AZs (Pulido and Marty, 2017). This is not always true however, because at certain AZs, multiple SVs can be released at once

(Rudolph et al., 2015). Thus, it is accurate to refer to release sites as the specific location within an AZ where SVs dock and fuse, as I do here. Unc13 is the likely candidate protein for localising SVs with a defined distribution at AZs and subsequent priming, and release is limited by it (Reddy-Alla et al., 2017; Sakamoto et al., 2018).

The probability that SVs will release (q) is influenced by their placement at the membrane in relation to Ca^{2+}-channels, as tighter coupling (nanometre range) in the case of Unc13A-localised SVs will have a higher probability of triggering fusion via the Ca^{2+}-sensor synaptotagmin (Böhme et al., 2016). Experiments at Calyx of Held synapses involving homogenous uncaging of presynaptic Ca^{2+}, visualisation with fluorescent dye and electrophysiology allowed the relationship between intracellular Ca^{2+} and NT release to be determined (Schneggenburger and Neher, 2000). The Ca^{2+}-sensor binds multiple Ca^{2+} ions and is not saturated under normal stimulation conditions, making it and hence p quite sensitive to changes in intracellular Ca^{2+} concentration (Schneggenburger and Neher, 2000). Ca^{2+} buffering at greater distances from the Ca^{2+} source and the action of Ca^{2+} pumps will reduce p (Walter et al., 2018).

q is determined as the amplitude of the response to spontaneous events and is influenced by not only NT filling and content of SVs but also characteristics of the postsynapse such as the function, availability and density of NT receptors (Karunanithi et al., 2002). Alterations in postsynaptic responses can complicate the accurate determination of presynaptic function, for example due to NT receptor desensitisation (Koike-Tani et al., 2008).

Spontaneous fusion of SVs represent individual quantal events (Takahashi, 2015). The postsynaptic response is a summation of many quanta. Dividing the evoked postsynaptic response amplitude by the average spontaneous SV fusion event amplitude allows the determination of the number of SVs released by stimulation (quantal content) (Figure 2b). A situation relevant to this thesis is depicted in Figure 2c, whereby postsynaptic sensitivity to NT is reduced (either by pharmacological receptor blockade or deletion of receptors) leading to smaller spontaneous responses (smaller q) (Böhme et al., 2019). Plastic adaptation of the synapse compensates, maintaining the evoked response (I).

Assuming q is not altered due to presynaptic changes (e.g. lower SV NT content), either the number of SV release sites (N), the probability of SV fusion (p) or both, are increased. The number of released SVs is thus drastically increased in response to stimulation.

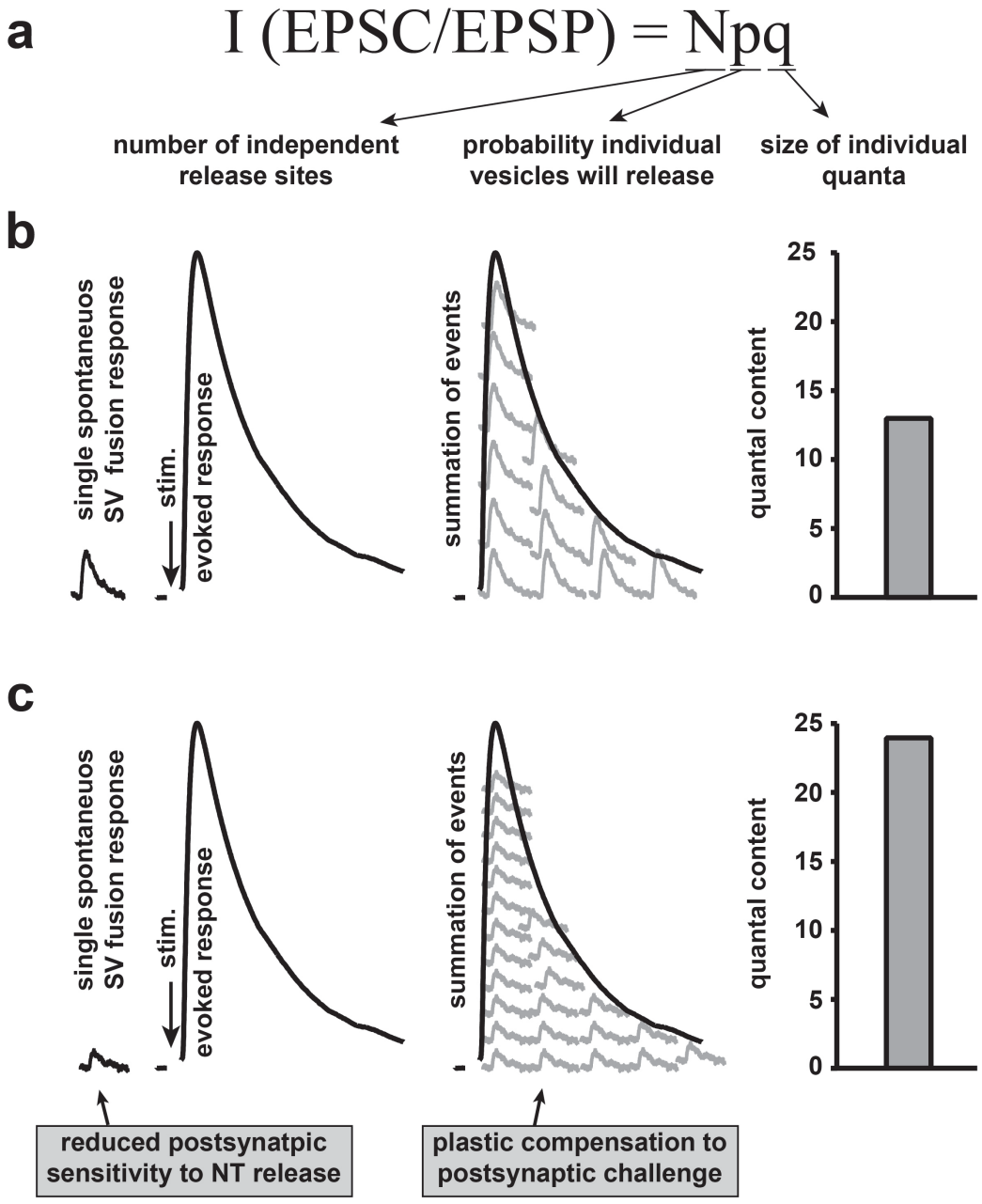

Figure 2: The postsynaptic response to presynaptic stimulation depends on several key variables.

(a) The evoked postsynaptic response (I: eEPSC or eEPSP) is determined by: 1) N: The number of independent SV release sites. 2) p: The probability that SVs will release in response to an AP. 3) q: The size of the response to a single vesicular NT release

event (quanta). **(b)** A single spontaneous event produces a postsynaptic response of particular amplitude and represents a fusion of a single SV (quanta). An evoked stimulation produces a much larger postsynaptic response. The evoked response is a summation of many SV fusion events. The evoked response can be divided by the mean spontaneous response to determine the total number of SVs released as a result of stimulation, also referred to as the quantal content. **(c)** Postsynaptic challenge reduces the sensitivity to NT of single SV events (q). This does not lead to a reduction in the evoked response, however. The evoked response is a summation of an increased number of individual quanta. The quantal content has increased in the depicted situation. Considering $I = Npq$, if q is lowered, N/p must increase to maintain I.

3.4 Components of the presynaptic active zone

A structured and conserved array of proteins at the presynapse, the AZ cytomatrix, is responsible for localising proteins, lipids and SVs in close proximity to the membrane to accurately promote fusion reactions (Südhof, 2012). Electron microscopy (EM) reveals the electron dense projections of the cytomatrix. These structures vary widely in appearance between different synapses and species, from the ribbon-like dense projections of skate electroreceptors to the pyramid-like dense projections in the mammalian hippocampus. The *Drosophila* NMJ exhibits a distinctive “T-bar”, consisting of a pedestal extending from the membrane capped by a platform (Zhai and Bellen, 2004). Much of these earlier EM studies were performed by chemical fixation and crosslinking of protein, which is quite disruptive to the AZ ultrastructure structure (Südhof, 2012). More recently, high-pressure freeze or freeze substitution EM and cryoelectron tomography has been employed to provide a complementary view of the AZ structure (Bruckner et al., 2015). This approach reveals the filamentous nature of the cytomatrix with filaments appearing to link SVs at the AZ. The diversity in AZ structure is likely forms the basis of the various functional demands at different synapses (Zhai and Bellen, 2004).

APs arriving at the presynapse activate voltage gated Ca^{2+} channels, permitting Ca^{2+} influx. Initial voltage gated Ca^{2+} channels experiments made use of various antagonists and toxin blockers to unveil different channel types, classifying them into L-,N-, P/Q-, R- and T-type channels accordingly (Catterall, 2011). These channels have varying characteristics such as being activated by high or low membrane voltage depolarisations and exhibit differential expression

depending on their subunit composition (Simms and Zamponi, 2014). Channels consist of an essential $Ca_V\alpha1$ subunit plus auxiliary subunits. $Ca_V\beta$ are involved in channel inactivation and transcriptional repression while $Ca_V\alpha2\delta$ subunits are involved in channel density modulation and channel targeting (Simms and Zamponi, 2014). Some channels may also possess a Cavγ subunit. The Cavα1 subunit determines the channel subfamily (Ca_V1, Ca_V2 or Ca_V3) Cavα1 are pore-forming proteins of four large repeated domains, each domain consisting of six transmembrane spanning α-helices (Catterall, 2010). The Ca_V2 subfamily are central for synaptic transmission and interact extensively with presynaptic proteins involved with NT release (Catterall, 2011). Ca^{2+} influx at the *Drosophila* NMJ presynapse occurs to a large extent through the Dmca1A subunit Ca^{2+} channel, homologous to the $Ca_V2.1$ Ca^{2+} channel. The α1 subunit is encoded by the gene cacophony (cac) (Smith et al., 1998).

Fusion of SVs is opposed by repulsive forces (electrostatic and hydration repulsion) acting against the two lipid bilayers coming together. An array of proteins at the presynapse assist in overcoming this energy barrier for SV fusion, culminating in the formation of the SNARE complex (Han et al., 2017). SNARE (Soluble N-ethylmaleimide sensitive factor Attachment protein REceptor) proteins are located at either the plasma membrane (t-SNAREs: syntaxin-1 and SNAP-25) or on the vesicular membrane (v-SNAREs: synaptobrevin/VAMP2) (Han et al., 2017; Sollner et al., 1993). These three proteins arrange themselves as four alpha helical bundles at the junction of the SV and plasma membrane (Sutton et al., 1998). The priming protein Munc18 is proposed to hold syntaxin-1 in a closed state, inhibiting SNARE complex formation (Genç et al., 2014). Priming involves the weakening of this interaction, and phosphorylated Munc18 has a reduced affinity for syntaxin-1. Despite this, Munc18 remains associated with the SNARE complex. Ca^{2+} influx into the presynapse stimulates SV fusion via binding to the Ca^{2+} sensor, synaptotagmin, embedded in the SV (Mackler et al., 2002). Synaptotagmin-1 (syt-1) triggers NT release through the function of two Ca^{2+} binding C2 domains. Additionally, binding of synaptotagmin to either the SNARE complex, lipids in the plasma membrane, or both, aids in exocytosis (Walter et al., 2011).

3.5 (M)unc13

SVs docked at the membrane require priming prior to fusion and Unc13 is vital for this process (Augustin et al., 1999; Böhme et al., 2019; Richmond et al., 1999; Varoqueaux et al., 2002). Sydney Brenner identified *unc-13* in the nematode worm *Caenorhabditis elegans* as a protein with a phorbol ester/diacylglycerol binding domain, which were known at the time to enhance neurotransmitter release (Maruyama and Brenner, 1991). Worms possess two isoforms of UNC-13, a short isoform (UNC-13S) and a long isoform (UNC-13L) (Hu et al., 2013). Mammals possess five Munc13 genes, Munc13-1, Munc13-2, Munc13-3, Munc13-4 and BAP3. Only Munc13-1, Munc13-2 and Munc13-3 are expressed in the brain (Südhof, 2012). Munc13-2 is further divided into two differentially expressed isoforms, one brain specific (bMunc13-2) and one ubiquitously (ubMunc13-2) expressed (Brose et al., 1995; Song et al., 1998; Südhof, 2012). Munc13-1 was identified as being vital for neurotransmission by priming SVs for release at murine excitatory glutamatergic synapses (Augustin et al., 1999). In cortical and hippocampal neurons, Munc13-1 is expressed at all presynapses (Kawabe et al., 2017). bMunc13-2 is expressed along with Munc13-1 at only 10% of synapses. Interestingly only bMunc13-2 localisation and stability are dependent on the scaffold ELKS (discussed below) and interference with this interaction reduces SV priming.

Munc13 is an essential priming and release site generating protein (Reddy-Alla et al., 2017). The priming activity of Munc13 is performed via a MUN domain (Basu et al., 2005; Stevens et al., 2005). It is likely that the MUN domain removes a lock on SNARE complex formation, consequently promoting exocytosis. Munc13 appears to assist in relieving the syntaxin-1/Munc18 closed conformation, allowing SNARE complex formation (Ma et al., 2011). Munc13-1 interacts directly with RIM1, an interaction that is important to maintain the number of releasable SVs (Betz et al., 2001). Worm UNC-13L contains a C_2A domain (Zhou et al., 2013), and this domain is known to activate the UNC-13 via RIM (Liu et al., 2019). The C_2A domain is conserved in mouse Munc13-1 and ubMunc13-2, interacting with RIM proteins (Andrews-Zwilling et al., 2006). The C_2A domain of Munc13 undergoes homodimerization, inhibiting the priming action of the MUN domain, and it is thought that RIM prevents this autoinhibition

(Camacho et al., 2017; Deng et al., 2011). Rescue with a Zn^{2+}-finger fragment from the N-terminus of RIM can rescue the SV priming defect observed on conditional double knockout of all RIM isoforms. Conversely, monomeric constitutively active ubMunc13-2 (point mutant in C_2A domain) was able to rescue the priming defect brought about by RIM loss (Deng et al., 2011). RIM-BP2 is required specifically for Munc13-1 clustering at mossy fibre synapses and in autaptic (self-synapsing) granule neurons, loss of RIM-BP2 leads to a reduction in docked SVs and the RRP (Brockmann et al., 2019). Monomeric constitutively active Munc13-1 (C_2A mutation mentioned above (Deng et al., 2011)) was able to bypass RIM-BP loss in these granule neurons and rescue impaired neurotransmission (Brockmann et al., 2019). The interaction of Munc13 and RIM-BP might be indirect, for example via RIM. These studies have illustrated that Munc13 relies on significant interaction with AZ scaffold proteins for reliable function.

The functional domains of Munc13 are varied (Figure 3). The C1 domain of Munc13 can bind diacylglycerol (DAG) and the functionally analogous phorbol esters (Basu et al., 2007). DAG, a derivative of the membrane lipid $PI(4,5)P_2$, can be substituted experimentally with the phorbol esters, phorbol 12-myristate 13-acetate (PMA) (Song et al., 2002) or 4β-phorbol-12, 13-dibutyrate (PdBu) (Basu et al., 2007). Translocation of Munc13-1 to plasma membranes is observed when the phorbol ester PMA is applied to cells (Blanco et al., 2019). Stimulated and spontaneous neurotransmission are greatly enhanced by C1 activation of Munc13 (Rhee et al., 2002). It has been proposed that C1 acts as a partial autoinhibitory domain that limits neurotransmitter release by interfering with MUN function unless activated (Basu et al., 2007). Phorbol esters increase C1 domain membrane binding which would compete with the intramolecular inhibition by the C1.

The C_2B domain facilitates Ca^{2+}-dependent phospholipid binding by Munc13 (Shin et al., 2010). Mutations that enhance or abolish the function of this domain positively or negatively affect neurotransmission during sustained stimulation (Shin et al., 2010). Deletion of the C_2B domain can enhance release, indicating that the C_2B may be autoinhibitory (functioning with the C1 domain) and that Ca^{2+} binding removes this inhibition (Michelassi et al., 2017). Munc13-1 and

ubMunc13-2 contain a Ca^{2+}/calmodulin-binding domain (CaM binding domain) that enhances priming, the RRP and the response to residual Ca^{2+} due to repetitive stimulation (short-term plasticity) (Junge et al., 2004; Lipstein et al., 2013; Zikich et al., 2008). Potential CaM binding sites have also been identified in bMunc13-2 and Munc13-3 (Lipstein et al., 2012).

In *Drosophila*, Unc13 exists as a single gene that is expressed as at least two different isoforms, Unc13A and Unc13B, differing at their N-terminal end (Xu et al., 1998). Like mammalian Munc13, *Drosophila* Unc13 is essential for neurotransmitter release (Aravamudan et al., 1999). Neither *Drosophila* Unc13 isoform contains a C_2A domain and only Unc13A possesses a CaM binding site (Figure 3) (Böhme et al., 2016; Reddy-Alla et al., 2017). Unc13A loss results in nearly complete loss of AP-induced exocytosis. Each isoform is responsible for localising SVs with a specific nanoscopic distribution at the AZ. Unc13A and consequently SVs localise close to Ca^{2+}-channels at the centre of the cytomatrix AZ (Böhme et al., 2016). These are SVs with a high probability of release. Unc13B on the other hand makes only a minor contribution to release and localises further from the centre of the AZ (Böhme et al., 2016). The N-terminal portion of Unc13A is vital for its appropriate localisation at the AZ while the C-terminal portion provides the priming function (Reddy-Alla et al., 2017). Deletion of the N-terminus results in loss of defined Unc13A localisation. Unc13A and SVs are found across the surface of the membrane, resulting in a decrease in release probability of SVs and an increase in asynchronous release. Confirming that Unc13 is the release site generating molecule, deletion of the priming C-terminus of Unc13A and expression of the localising N-terminus, block endogenous Unc13A from forming release sites at the AZ (Reddy-Alla et al., 2017).

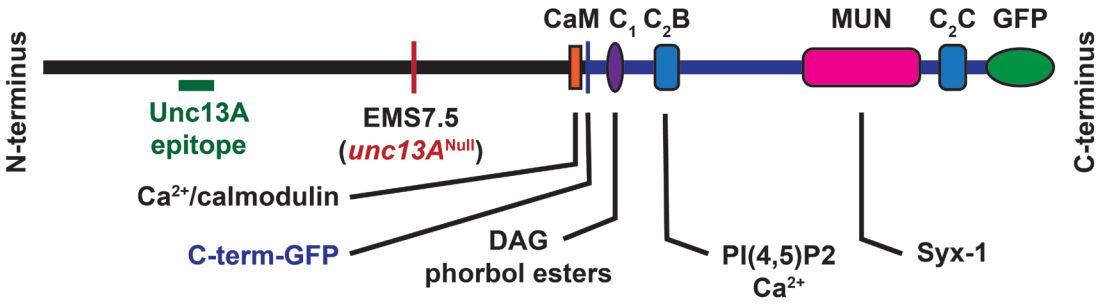

Figure 3: Structure of *Drosophila* Unc13A.

Unc13A includes several functional domains that bind other proteins or lipids, shown are the MUN, C1, C_2B, C_2C and CaM domains. Unc13A can be tagged with GFP at the C terminus without removing protein function. An identified Unc13A epitope permits isoform specific immunohistochemistry. Additionally, genetic manipulations such as expression of only the C-terminus (C-term-GFP) or complete deletion of the protein (EMS7.5) are possible.

3.6 The role of PI(4,5)P_2 during exocytosis at the AZ

The plasma membrane is not relevant purely as the site of SV fusion. It contains a variety of signalling lipids that regulate exocytosis (Khuong et al., 2013; Walter et al., 2017). Although a number of phospholipids are involved in synaptic transmission, a partial focus of this thesis is PI(4,5)P_2. Phospholipids such as PI(4,5)P_2 may influence exocytosis in several ways, which I will discuss in the following section (Martin, 2012). Firstly, PI(4,5)P_2 directly changes the physical properties of the membrane. Secondly, they recruit, localise and regulate proteins vital for SV exocytosis. Finally, their metabolism to secondary messengers and signalling lipids initiates signalling pathways that modulate exocytosis (Martin, 2012).

Membrane curvature changes induced by the physical properties of lipids such as PI(4,5)P_2 may aid or inhibit physical fusion of SVs. As an inverted cone-shaped lipid, PI(4,5)P_2 tends to bulge in the direction of the polar head groups when in a lipid monolayer. This acts to prevent the formation of a high negative curvature stalk, an important step in vesicular membranes fusing with the plasma membrane (Chernomordik and Kozlov, 2008). This characteristic of

$PI(4,5)P_2$, promoting positive curvature, inhibits SNARE-dependent fusion (James et al., 2008).

Interaction and binding of proteins at the AZ is one of the most well studied functions of $PI(4,5)P_2$ during exocytosis. SNARE proteins interact extensively with $PI(4,5)P_2$. $PI(4,5)P_2$ was implicated in altering the movement of syntaxin-1/SNAP-25 heterodimers in the plasma membrane (Wagner and Tamm, 2001). In PC12 cells, docked SVs also locate to areas of $PI(4,5)P_2$ and syntaxin-1 clustering (Aoyagi et al., 2005; Barg et al., 2010; Kabachinski et al., 2014; Lang et al., 2001). It seems syntaxin-1 may be clustered by $PI(4,5)P_2$, particularly as the $PI(4,5)P_2$ degrading phosphatase synaptojanin-1 inhibits syntaxin-1 clustering (van den Bogaart et al., 2011). It is suggested that syntaxin-1 acts to remove the fusion resistant characteristics of $PI(4,5)P_2$ by sequestering it away from the direct fusion site (James et al., 2008). Supporting these findings, syntaxin-1 lipid binding mutants exhibit exocytotic defects (James et al., 2008; Lam et al., 2008).

Beyond SNAREs, proteins involved in priming docked SVs interact with $PI(4,5)P_2$. Munc13 binds $PI(4,5)P_2$ via its Ca^{2+}-dependent C_2B domain. Disturbance of this domain severely affects exocytosis (Shin et al., 2010). Munc13 promotes SNARE function to facilitate release (Ma et al., 2013). In PC12 cells, Munc13-1 has been observed translocating to the membrane due to Ca^{2+} influx from stimulation. Further supporting the importance of the C_2B domain of Munc13, mutants of Ca^{2+} dependent $PI(4,5)P_2$ binding do not translocate to the membrane (Kabachinski et al., 2014).

The Ca^{2+} sensor syt-1 possesses a C_2B domain that interacts with $PI(4,5)P_2$ (Shin et al., 2009). By binding $PI(4,5)P_2$ via the C_2B domain, affinity of this sensor for Ca^{2+} is increased (Radhakrishnan et al., 2009). A specific polylysine motif in the C_2B domain is vital for function and interfering with this motif affects exocytosis (Loewen et al., 2006). Membrane bridging is an essential process as SVs dock at the plasma membrane and prepare to fuse. This process involves syt-1, likely due to $PI(4,5)P_2$ interactions (Kuo et al., 2011; Seven et al., 2013). It has also been proposed however that a single syt-1 could bridge two SNARE complexes via its C_2B domain (Zhou et al., 2017). $PI(4,5)P_2$ potentiation of

exocytosis via Munc13-2 and syt-1 has been confirmed by acutely uncaging $PI(4,5)P_2$ in chromaffin cells (Walter et al., 2017).

3.7 RIM and RBP

Various scaffold proteins comprise the presynaptic AZ. The scaffold protein RIMs (Rab3 interacting molecules) are essential for neurotransmission in several species (Han et al., 2011; Müller et al., 2012; Schoch et al., 2002). In mice and worms, RIM has been shown to be vital for SV localisation at the AZ membrane. Mutants lacking RIM show disturbed distribution in relation to dense projections in EM (Han et al., 2011; Weimer et al., 2006). Additionally, RIMs have been found to confine Ca^{2+}-channels at the AZ (Han et al., 2011; Kaeser et al., 2011). In *Drosophila*, loss of RIM reduces Ca^{2+}-influx and the RRP (Müller and Davis, 2012). As I will mentioned previously, mammalian RIM interacts with Munc13 to regulate the docking and priming of SVs (Camacho et al., 2017; Deng et al., 2011).

RIM-Binding Protein (RIM-BP) is likewise vital for NT release. In *Drosophila*, RIM-BP was found to regulate the AZ ultrastructure, Ca^{2+}-channel clustering, Ca^{2+} influx and the RRP (Liu et al., 2011; Müller et al., 2015). In mammals it is also heavily involved in Ca^{2+}-channel localisation (Grauel et al., 2016). Following knockout of RIM-BP2, $Ca_V2.1$ channels were mislocalised. Ca^{2+} influx was unaffected but the probability of vesicular release was reduced (Grauel et al., 2016). The relationship of RIM-BP to RIM is well established, particularly in regard to Ca^{2+} regulation (Hibino et al., 2002). At Calyx of Held synapses, singular deletion of RIM and RIM-BP does not block NT release. Double deletion of both however nearly completely abolishes evoked neurotransmission, unveiling that there is redundancy between RIM/RIM-BP (Acuna et al., 2016).

3.8 ELKS / CAST / BRP

ELKS/CAST family proteins are large presynaptic AZ scaffold proteins that are known to interact extensively with many other AZ proteins. During the

identification of members of this family, two individual vertebrate ELKS/CAST proteins were named several times leading to a degree of confusion in the nomenclature. CAST is also known as Erc2 or ELKS2. ELKS is also known as Rab6IP2a, Erc1 or CAST2. CAST and ELKS differ in their expression; CAST is primarily expressed in the mammalian brain and ELKS expression is ubiquitous with the ELKS2α isoform being brain specific (Hida and Ohtsuka, 2010). A high degree of homology exists between CAST and ELKS, and a member of this family is present in *C. elegans*, indicating that it is evolutionarily conserved (Deguchi-Tawarada et al., 2004).

At hippocampal synapses ELKS regulates SVs in seemingly disparate ways. Hippocampal cultures neurons conditionally lacking both CAST and ELKS displayed disrupted neurotransmission at inhibitory synapses with a reduction in the probability of release (Liu et al., 2014). Ca^{2+} influx is also reduced without a change in the Ca^{2+}-channels themselves, perhaps due to an alteration of channel opening. At small excitatory synapses on the other hand, loss of both CAST and ELKS reduces the readily releasable pool without affecting the probability of vesicular release (Held et al., 2016). Based on these double knockout experiments, CAST and ELKS maintain the frequency of spontaneous vesicular release at both inhibitory and excitatory synapses (Held et al., 2016; Liu et al., 2014). Single knockout experiments in mice produced different findings than double knockout of ELKS/CAST in culture. CAST was found to generally increase vesicular release only at inhibitory synapses in mice (Kaeser et al., 2009). Conflicting with this however, a recent single CAST knockout experiment in mice found increased spontaneous vesicular quantal size and decreased probability of vesicular release but only at excitatory synapses, (Kobayashi et al., 2016). It is difficult to make strict comparisons between these experiments due to the large differences in experimental design (in-vivo vs. in-vitro) and use of single or conditional double knockouts. Regardless, ELKS/CAST family proteins play diverse and important roles at mammalian AZs.

The CAST/ELKS homolog Bruchpilot (BRP) is a major component of the presynaptic *Drosophila* AZ. The N-terminus of BRP is highly homologous to CAST/ELKS while the coiled coil domain rich C-terminus is similar to

cytoskeletal proteins such as plectin and myosin heavy chain (Wagh et al., 2006). Loss of BRP results in the disappearance of the T-bar at AZs. Similarly, truncation of BRP results in shortened T-bars (Fouquet et al., 2009). BRP is essential for Ca^{2+} channel clustering and the release probability is reduced in the absence of BRP (Kittel et al., 2006).

Two isoforms of the protein exist in *Drosophila*, Brp-190 and Brp-170, which differ in their N-terminus (Matkovic et al., 2013). They localise distinctly and do not overlap at the AZ when viewed by high resolution STED microscopy. Removal of either of these isoforms individually interferes with the number of SVs readily available to exocytose, as uncovered by sustained stimulation. Vesicular release probability is similar however, indicating that localisation of SVs is possible with one isoform (Matkovic et al., 2013). Supporting the hypothesis that BRP is involved in tethering SVs to the AZ, loss of the extreme C-terminus of BRP, leads to a reduction in the number of SVs observed at the AZ, reduced probability of vesicular release and reduced SV recovery (Hallermann et al., 2010). This reinforces the importance of the C-terminus of BRP for proper neurotransmission.

3.9 Presynaptic plasticity

Synapses dynamically adapt to neuronal firing or changes in their environment to upregulate, downregulate or maintain neurotransmission, according to the situational requirements. Together, these varied processes are referred to as synaptic plasticity and can take several different forms at the chemical presynapse. Synaptic plasticity underlies memory, learning, filtering and sensory adaptation as well as supporting consistent neurotransmission (Delvendahl and Müller, 2019).

Use-dependent short-term plasticity (STP) operates on timescales of milliseconds to minutes. It is divided into three categories: facilitation, depression and augmentation/posttetanic potentiation (Regehr, 2012). Closely successive APs arriving at synapses most often do not elicit the same degree of postsynaptic activation. Facilitation occurs when a stimulus produces a larger release of NT than preceding stimuli. Similarly, depression occurs when

subsequent stimuli produce reduced NT release. Posttetanic potentiation can be observed following sustained high frequency stimulation as a general enhanced responsiveness to stimuli and increase in the number of spontaneous SV fusion events (Regehr, 2012). STP is heavily influenced by release probability (p) and SV pool characteristics such as the size of the RRP or pool repopulation (Böhme et al., 2018; Regehr, 2012). Receptor desensitisation at the postsynapse can compound STP estimation (Koike-Tani et al., 2008).

On extended timescales, long term plasticity takes the form of depression (LTD) or potentiation (LTP). LTP or LTD at the presynapse is extremely diverse and can be initiated by signalling pathways with their origin in the postsynapse (retrograde signalling), presynapse or even nearby synapses (Yang and Calakos, 2013). Signalling can occur in a wide number of different ways, from endocannabinoid activation of presynaptic CB_1 receptors, to metabotropic glutamate receptors, and even nitric oxide (Atwood et al., 2014; Stanton et al., 2003). Downstream, LTP can be positively or negatively regulated by cyclic adenosine monophosphate (cAMP) via cAMP-dependent protein kinase A (PKA) or Ca^{2+}-signalling involving calmodulin and CaMKII. (Atwood et al., 2014; Yang and Calakos, 2013).

Presynaptic homeostatic plasticity is a form of plasticity that maintains neurotransmission, for example in response to external or environmental challenge to the synapse (Böhme et al., 2019). Postsynaptic NT receptor blockade or loss is compensated by an increase in presynaptic release. At the rat NMJ, a nicotinic acetylcholine receptor blocker α-bungarotoxin (αBTX) was found to decrease the size of detected spontaneous vesicular release. However, over the course of a several weeks, up to a month, presynaptic NT release gradually increased (Plomp et al., 1992). At the mouse NMJ, αBTX was again used to determine that postsynaptic receptor blockade results in compensatory presynaptic release (Wang et al., 2010). This phenomenon is best described at the *Drosophila* NMJ (Frank et al., 2006), and the increase in NT release is generally referred to as presynaptic homeostatic potentiation (PHP). Additionally, homeostatic vesicular NT loading and homeostatic depression have been reported (Gaviño et al., 2015; Gois et al., 2005). For plasticity to occur, following postsynaptic receptor challenge, the postsynapse

must effectively signal retrogradely across the synapse to the site of presynaptic release at the AZ (Delvendahl and Müller, 2019). A structural rearrangement of AZ proteins including Ca^{2+} channels coincides with increased SV exocytosis (Böhme et al., 2019). Much of this thesis will explore fundamental aspects of this form of plasticity at the *Drosophila* NMJ.

3.10 Aims and goals

I aimed to investigate the contribution of presynaptic AZ proteins to the initiation and maintenance of homeostatic plasticity, with a particular interest in the priming protein Unc13A and scaffold protein BRP. I sought to answer the question if either or both of these proteins is required for presynaptic homeostatic plasticity, and what aspects of this process they regulate (functional PHP or structural reorganisation). Making use of electrophysiology and microscopy, I applied a combination of pharmacological, genetic and immunohistochemical techniques at the fruit fly (*Drosophila melanogaster*) NMJ to answer this question.

Additionally, I aimed to investigate the acute uncaging of the phospholipid $PI(4,5)P_2$ and assess its contribution to exocytosis at the NMJ, as well as application of PMA to assess DAG-mediated modulation of neurotransmission.

4 Methods

4.1 The fruit fly as a model organism

The fruit fly *Drosophila melanogaster* has been utilised for over a century to pursue the study of a wide range of biological processes such as genetic heredity, embryonic/larval development and as an animal model of human disease (Markow, 2015). First produced in large numbers by Charles W. Woodworth, he recommended it to William E. Castle who introduced it to his laboratory. Thomas Hunt Morgan and his graduate student Herman J. Muller went on to win individual Nobel Prizes, using *Drosophila* to explore chromosomal heredity and X-ray mutagenesis respectively (Markow, 2015). *Drosophila* was and continues to be an attractive choice as a model organism for a number of reasons which I will briefly detail here.

Drosophila has a short lifespan allowing study of multiple generations and production of genetic crosses in a brief space of time; roughly 10 days from egg to adult at 25˚C (Figure 4) (Allocca et al., 2018). Life stages are distinct; starting with the embryo, progressing through three larval moulting stages (instar), a pupal stage and finally the emergence of the adult fly. Large numbers of offspring can be produced by a single female, laying over a hundred eggs a day during peak oviposition and many hundreds more during a lifetime (Shapiro, 1932). Flies are relatively cheap and easy to maintain. Adults and larvae can be immobilised using carbon dioxide or volatile anaesthetics for the purposes of crossing or dissection (Campbell and Nash, 1994).

Flies only have four pairs of chromosomes, three pairs of autosomes and one pair of sex chromosomes (Allocca et al., 2018). Balancers are homozygous lethal and possess multiple inversions to prevent undesirable recombination; both of these characteristics protect against loss of the allele/genotype of interest (Ashburner et al., 2005). Balancers also express dominant identifiable phenotypic markers. Balancer chromosomes are used extensively to maintain stocks of particular genes or mutations of interest as well as aiding in sorting during fly crossing or selection of larvae for experiments.

Analysis of fly gene function has been greatly supported by the fact that the *Drosophila* genome has been sequenced and available for nearly two decades (Adams et al., 2000). Genetic manipulation is possible using a number of methods that has expanded over the years. Transposon mediated integration, gene targeting by homologous recombination, site specific integrase insertion, bacterial artificial chromosomes and more recently the CRISPR/*Cas9* system are examples of genetic manipulation tools in *Drosophila* (Allocca et al., 2018). Traditionally mutagenesis using transposable P-elements, potent chemical agents such as Ethyl Methanesulfonate (EMS) or X-rays combined with genetic screening had been used to generate fly lines for study (Allocca et al., 2018). With the advent of the CRISPR/Cas9 system, the specificity and accuracy of genetic modification has increased vastly.

Use of the *Drosophila* model system benefits from the commercial availability of many fly lines for targeted gene expression. The UAS-Gal4 system involves genes placed under the control of Upstream Activation Sequence (UAS) sites (Brand and Perrimon, 1993). These gene specific lines are crossed with lines possessing tissue specific expression of the transcription factor GAL4. GAL4 binding of the UAS site in the progeny of these crosses achieves controlled expression of genes in desired cells and tissue. For even greater control of expression and temporal specificity, lines exist for pharmacological or temperature-sensitive activation of the UAS/GAL4 system (Osterwalder et al., 2001; Zeidler et al., 2004). Finally, there is a huge degree of homology between flies and humans. Approximately 65% of human genes implicated in disease have *Drosophila* homologs (Ugur et al., 2016).

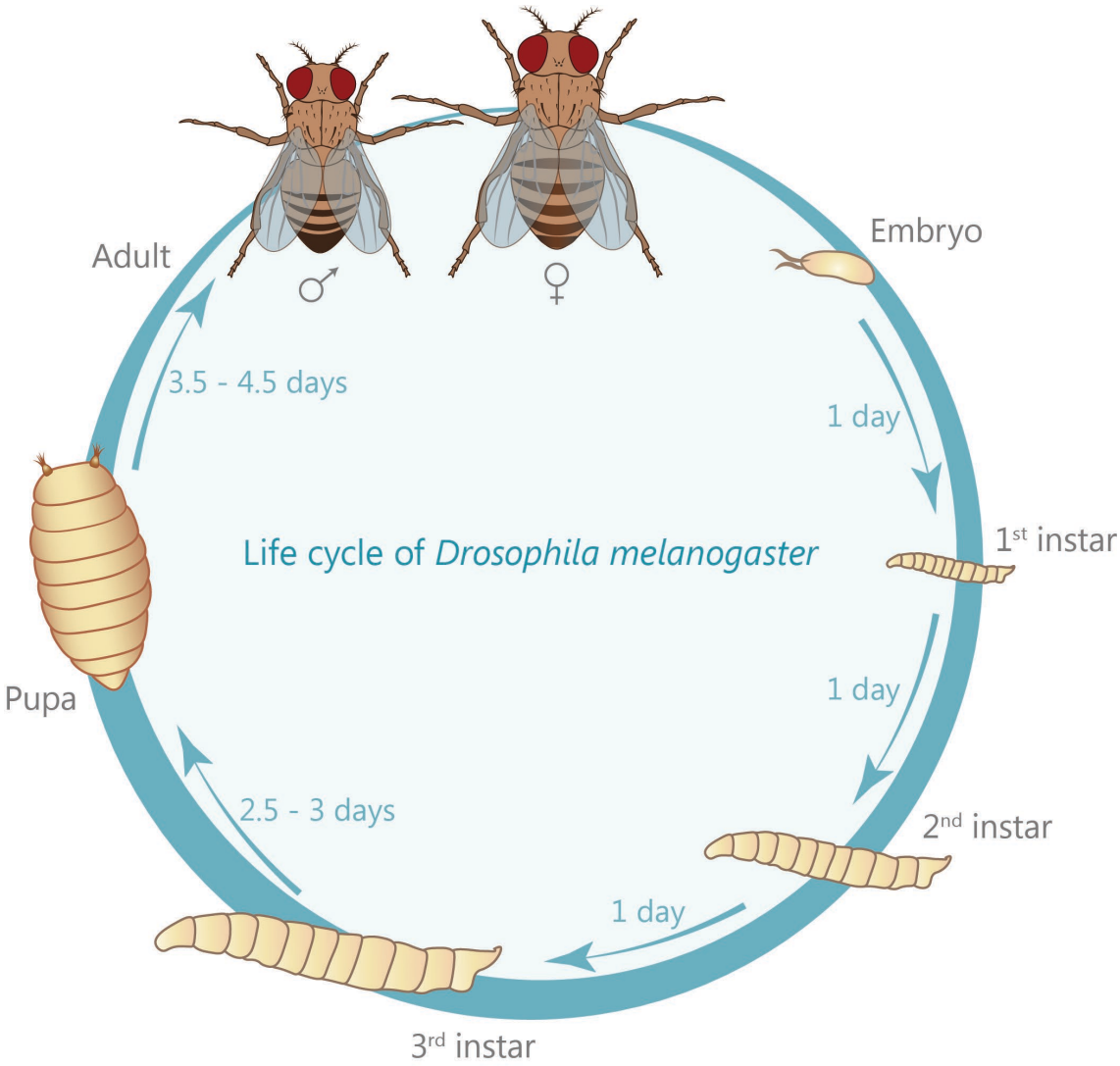

Figure 4: The *Drosophila* melanogaster life cycle.

The timing and developmental stages of *Drosophila* at 25°C is depicted. Provided by Meida Jusyte.

4.2 The *Drosophila* neuromuscular junction

Much of the work in this thesis was performed at the *Drosophila* larval neuromuscular junction (NMJ). Electrophysiology at the larval NMJ was first described by Jan and Jan (1976). Motoneuronal bundles propagating from the ventral ganglion approach each hemisegment anteriorly from the ventral midline on the left and the right. Branching out into the hemisegment, each nerve bundle innervates the various muscles of that segment terminating at clusters of boutons. Motoneurons can be subdivided into classes based on their differing morphology, neurotransmitter type, firing characteristics and muscle innervation

(Pérez-Moreno and O'Kane, 2019). Type I are glutamatergic and can be subdivided further into Type Ib and Type Is. Type 1b, so called for their 'big boutons', display less branching and tonic firing (Menon et al., 2013; Pérez-Moreno and O'Kane, 2019). Type 1s on the other hand have smaller boutons, tend to innervate many more muscles than 1b, fire in phasic fashion, have a larger proportion of SVs in the RRP and have greater release efficacy. Type II (octopaminergic) and Type III (peptidergic) nerves have neuromodulatory functions (Pérez-Moreno and O'Kane, 2019; Stocker et al., 2018).

A major benefit of the *Drosophila* NMJ is the regular and easily identifiable muscle pattern (Keshishian et al., 1993). There are 400 striated muscle cells in third instar larvae, each possessing 10-20 nuclei (Jan and Jan, 1976). Intracellular recordings are usually performed at muscle 6,7,12 and 13 due to their large size, easy access and ventral positioning (Zhang and Stewart, 2010a). *Drosophila* NMJs are not cholinergic like those of mammals., ionotropic excitatory glutamate receptors are permeable to Na^+, K^+, Mg^{2+} (Jan and Jan, 1976) but also highly permeable to Ca^{2+} and share some sequence and structural similarities with vertebrate AMPA and kainate receptors. Importantly however they are neither AMPA or kainite receptors and do not pharmacologically respond in the same way (Han et al., 2015). They are composed of five subunits. All possess subunits GluRIIC, GluRIID, GluRIIE, an accessory subunit Neto, but differ in their fifth subunit. This subunit can be either GluRIIA or GluRIIB, influencing receptor properties such as desensitisation kinetics and gating properties (DiAntonio et al., 1999; Petzoldt et al., 2014).

In the following sections I will describe in detail the pharmacology, electrophysiology, immunohistochemistry and microscopy techniques I employed to investigate neurotransmission at the *Drosophila* NMJ. However, I will first describe the techniques used to confirm the loading and acute activation of a caged $PI(4,5)P_2$ compound, followed by application to the *Drosophila* NMJ. For more information on all experiments, particularly the reasoning and outcomes; please refer to the Results section.

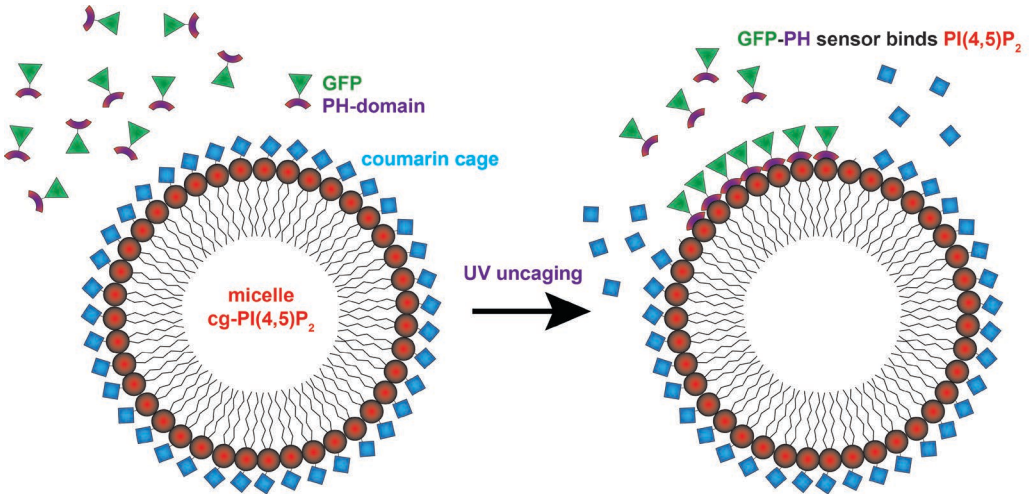

Figure 5: UV light uncages cg-PI(4,5)P_2.

cg-PI(4,5)$_2$ in solution forms micelles. A high affinity PI(4,5)P_2 sensor consisting of a lipid binding PH domain and a fluorescent GFP will not bind PI(4,5)P_2 when the coumarin cage is present on the lipid. The lipid sensor binds PI(4,5)P_2 following photocleavage of the coumarin group with intense UV light.

4.3 Uncaging PI(4,5)P_2

The following PI(4,5)P_2 uncaging experiments were performed as described in Walter et al. (2017) and so the procedural details are also largely as published there (Section 4.3).

4.3.1 PI(4,5)P_2 uncaging in vitro

A loading solution was made by adding 20 µM cg-PI(4,5)P_2 (stored in a 20 mM DMSO-stock) to imaging buffer (HBSS with 5% FCS), making sure that cg-PI(4,5)P_2 was only exposed to red light to avoid premature uncaging. The high-affinity PI(4,5)P_2-sensor PLCδ1-PH-GFP (stored as a 1.8 mg/ml PBS/20% Glycerol stock) was also added in a 1:20 ratio to the cg-PI(4,5)P_2 imaging buffer solution (e.g. 5 ml in 100 ml). The solution was pipetted onto a glass coverslip in an incubation chamber (37°C), and imaged on a TIRF microscope (Nikon Ti Eclipse), featuring a 60X TIRF objective (Apo TIRF 1.49NA, Nikon), a sCMOS camera (Neo, Andor), four excitation laser lines: (405,488 nm, 568 nm, 647 nm)

an appropriate dichroic mirror (Di01-R405/488/561/635), filter (FF01-446/523/600/677) and operated with ImageJ micromanager software. At 50% (30MW) 488 nm laser power, images were taken of the glass coverslip with 200 ms exposure every second. Following the 488 nm frame an uncaging frame with the 100% (60 MW) 405 nm laser (200 ms exposure) was used to uncage $PI(4,5)P_2$ before returning to a 488 nm frame. Using Fiji (ImageJ) software, cg-$PI(4,5)P_2$ on the glass was identified in the 405 nm channel. ROIs were placed on this cg-$PI(4,5)P_2$ and transferred to the corresponding 488 nm channel images. The fluorescence intensity of PLCδ1-PH-EGFP before and after the uncaging frame was compared.

4.3.2 Culture and transfection of cell lines

HEK 293T (Figure 7b) and COS-7 (Figure 8a) cells were purchased from ATCC, who confirmed the identity of the cells by performing short tandem repeat profiling. Cell lines were also tested for mycoplasma contaminations monthly. Cells were cultured in DMEM (Lonza) supplied with 10% fetal bovine serum (FBS, Gibco 10270–106) and 1% penicillin/streptomycin. Cells were not used beyond passage 30 from original (splitting of cells). COS-7 cells were transfected using Lipofectamine 2000 (Life Technologies) according to manufactures instructions with the following DNA concentrations: 1 µg of mCherry-INPP5E-CAAX plasmid (Posor et al., 2013) and 2 µg DNA of EGFP-PH-PH (PLCδ1) plasmid from Michael Krauss (Leibniz-Forschungsinstitut für Molekulare Pharmakologie, Berlin, Germany).

The LifeAct-RFP experiments depicted in Figure 8b were performed in HEK 293T cells provided by Dr. Therese Schaub and Prof. Dr. Victor Tarabykin (Institute of Cell Biology and Neurobiology, Charité Berlin). These were cultured in DMEM GlutaMAX (Thermo Fisher/Gibco) supplied with 10% fetal bovine serum (FBS, Gibco 16140063) and 1% penicillin/streptomycin at 37°C in a humidified atmosphere (5% CO2). Cells were not used beyond passage 40 from original. This cell line was not tested for mycoplasma contaminations. Cells were transfected using Lipofectamine LTX (Thermo Fisher Scientific) according to manufactures instructions with 1.8 µg DNA of LifeAct-RFP (pmRFPruby-

N1*LifeAct (GB lab plasmid nr 28) in pmRFPruby-N1) provided by Geert van den Bogaart (Radboud University Medical Center, Nijmegen, the Netherlands). Cells were used 18–24 hours following transfection with LifeAct-RFP.

4.3.3 Cellular loading of cg-PI(4,5)P_2

Loading solution was made for HEK 293T (Figure 7b) and COS-7 (Figure 8a) cells by adding 20 µM cg-PI(4,5)P_2 (stored in a 20 mM DMSO-stock) and 0.02% Pluronic F-127 (Sigma-Aldrich, MO, USA, stock (20% solution in DMSO)) to imaging buffer (HBSS with 5% FCS). Preparation of loading solution was performed under red light to prevent premature uncaging. The control solution contained an equal volume of DMSO in the place of cg-PI(4,5)P_2. The resulting solutions were vortexed for 3 minutes to prevent formation of lipid micelles. A cell plate was taken from a CO_2-incubator (5%) and cell medium removed with a pipette from the wells to be loaded, making sure to avoid drying out of the cells. cg-PI(4,5)P_2/control loading solution was gently pipetted into the wells, avoiding disruption of the cells by pipetting onto the wall of each well. The cell plate was returned to the incubator for 30 minutes (37˚C). The plate was again taken from the incubator and the loading solution removed from each well. Wells were washed twice with cg-PI(4,5)P_2/Pluronic-free imaging buffer.

Loading of cg-PI(4,5)P_2 was performed for HEK 293T (Figure 8b) cells as described above, substituting cell culture medium for imaging buffer as the loading solvent (20 µM cg-PI(4,5)P_2, 0.02% Pluronic F-127 in cell culture medium). Following 30 minutes incubation (37˚C) in a CO_2-incubator (5%), cells were washed twice with a solution containing: (in mM) NaCl 145, KCl 3, HEPES 10, $CaCl_2$ 1, $MgCl_2$ 1 and Glucose 6, pH adjusted to 7.4 and with an osmolarity of 290 mOsm/l.

4.3.4 Visualisation of cellular PI(4,5)P_2 localisation and uncaging

CellMask Deep Red plasma membrane stain (Thermo Fisher Scientific, stored at room temperature in the dark as a 5 mg/ml stock in DMSO) was added as a 1:1000 dilution to imaging buffer (Figure 7b). HEK 293T cells were incubated for

5 minutes in the CellMask imaging buffer solution before washing twice with fresh imaging buffer. The cells were then subsequently loaded with cg-PI(4,5)P_2 or control DMSO as described above. Cells were then placed in an incubation chamber (37°C) and imaged on a Spinning Disk Confocal Microscope (Nikon TI-Eclipse) featuring a 60X objective (P-Apo NA 1.40, Nikon), Yokogawa spinning disk (CSU-X1), an EMCCD camera (AU-888 Andor), four excitation laser lines: (405, 488 nm, 561 nm, 638 nm), a Borealis unit (Andor), an appropriate dichroic mirror (Di01R405/488/561/635), specific filters (BP450/50 and BP700/75 for coumarin and CellMask, respectively) and operated with NIS Elements (Nikon) software. Images were captured at 0.5 s intervals (200 ms exposure) for 30 seconds using a 638 nm laser at 20% power (100 mW) to visualise the CellMask. Each 638 nm frame was followed by a frame captured with a 405 nm laser at 30% power (100 mW) to visualise the coumarin-caging group of cg-PI(4,5)P_2 and uncage it. Using Fiji (ImageJ) software, line profile ROIs were placed in the CellMask imaging channel (excitation 638 nm) across the plasma membrane (90˚ angle in relation to the membrane) of individual cells, crossing from the extracellular space into nucleus-free cytosol. Only one membrane ROI was selected per cell. The site of maximum CellMask fluorescence intensity along each line was deemed to be the midpoint of the plasma membrane (calculated using the second output parameter of the built-in MATLAB function 'max' ((MATLAB vers. 7.12.0 R2011a)). For each line profile ROI, a 3 µm long section was aligned at each frame (using a custom MATLAB script) such that the calculated plasma membrane midpoint was 1.5 µm along the section (i.e. each frame of each line profile ROI was centred at the plasma membrane). The Cell Mask fluorescence intensity values along the line profile were noted at 15 positions preceding (-1.5 µm) and 15 positions succeeding (+1.5 µm) the mid-point. Each line profile ROI, following alignment to plasma membrane as explained above, was transferred as is to the corresponding coumarin channel (405 nm excitation) frame. The coumarin fluorescence intensity values were noted at the exact same line positions as the CellMask channel values. In both channels, the pixel intensity value of the 1st position on each line (i.e. 1.5 µm extracellular to the plasma membrane) was subtracted from values at all other positions to obtain background subtracted line profiles. The analysed aligned line profile sections were then averaged across all cells.

COS-7 cells were transfected with EGFP-PH (PLCδ1), mChINPP5E-CAAX and loaded with cg-PI(4,5)P_2 or DMSO control as described above (Figure 8a). Cells were imaged on the TIRF microscope setup describe previously for PI(4,5)P2 uncaging in vitro (Figure 7a). Images were captured at 1 s intervals (200 ms exposure) using a 488 nm laser at 50% power (30 MW) to visualise EGFP, immediately followed by a 561 nm laser at 100% power (50 MW) to visualise mCherry. This sequence cycled until the interval between the 10th and 11th cycle (10–11 s), where a single frame was introduced (400 ms exposure) using a 405 nm laser at 100% power (60 MW) to UV uncage PI(4,5)P_2. COS-7 cells expressing both the constitutive phosphatase and lipid sensor were analysed using Fiji (ImageJ) software. ROIs of plasma membrane were selected in the EGFP (488 nm excitation) channel only (3 per cell) and the mean fluorescence intensity noted over time. A ratio of EGFP fluorescence intensity change (before/after UV uncaging) in these ROIs was calculated by dividing intensities after the UV uncaging frame by the corresponding intensities prior to the UV uncaging frame. Values were then averaged across ROIs.

4.3.5 LifeAct-RFP imaging

HEK 293T cells were transfected with LifeAct-RFP and loaded with cg-PI(4,5)P_2 or DMSO control as previously described. Cells were placed in an incubation chamber (37°C) and imaged on a TIRF microscope (Nikon Ti eclipse) featuring a x100 objective (Apo TIRF 1.49NA, Nikon), an EMCCD camera (iXon 888 Andor, EM gain set to 300), four excitation laser lines: (405,488 nm, 561 nm, 647 nm), suitable filter sets and controlled by the Nikon NIS-Elements AR Software (vers. 4.51.01). Images were acquired at 0.5 second intervals (100-200 ms exposure) with a 561 nm laser (2% intensity) to visualise LifeAct-RFP. After 5 frames, three consecutive UV frames (100 ms exposure) were introduced with the same interval to uncage PI(4,5)P_2, produced using the 405 nm laser (25% intensity). Imaging was then resumed at the same 0.5 second intervals (100-200 ms exposure) with a 561 nm laser (2% intensity) to visualise LifeAct-RFP. Using Fiji (ImageJ), circular ROIs of equal size were

selected on cellular footprints resembling filamentous structures in the LifeAct-RFP channel (561 nm excitation), presumed to be LifeAct-RFP bound actin (white circles, Figure 8b). The mean fluorescence intensity of a single ROI, placed outside the cell, was subtracted from those of all cellular ROIs at each frame to account for background fluorescence (yellow circle). The mean fluorescence intensities of all cellular ROIs were averaged for each frame per cell and then normalised to the very first frame. Cells were then divided based on treatment group and averaged at each frame.

4.4 Fly handling and stocks

All *Drosophila* larvae were raised at 25˚C under standard laboratory conditions (Sigrist et al., 2003) on semi defined medium (Bloomington recipe). Fly crosses and stocks were kept at room temperature. Experiments were performed using male and female third instar larvae.

Table 1: List of fly lines used.

Fly line	Figure	Source
Wild-type: +/+ (*w*^{1118})	11-12, 15, 17-19	Bloomington Drosophila Stock Center
brp^{mCherry}*/III*	9, 16	(Matkovic et al., 2013)
Mhc-myr-GCaMP5G/III	10	(Reddy-Alla et al., 2017)
unc13A^{Null}: *EMS7.5/P84200*	12	(Böhme et al., 2016) P84220 from DGRC
Unc13A-GFP*: elav-GAL4/+;;UAS-Unc13A-GFP/+;P84200/P84200*	13-14	(Böhme et al., 2016) P84220 from DGRC
C-term-GFP*: elav-GAL4/+;;UAS-C-term-GFP/+; P84200/P84200*	13-14	(Reddy-Alla et al., 2017) P84220 from DGRC
gluRIIA^{Null}*:AD9/df(2 L)cl*^{h4} or *gluRIIA*^{SP16}*/gluRIIA*^{SP16}	17-19	(Petersen et al., 1997)
brp^{Null}*: brp*$^{\Delta 6.1}$*/brp*^{69}	15, 18	(Kittel et al., 2006) (Fouquet et al., 2009)
gluRIIA^{Null},*brp*^{Null}: *gluRIIA*^{SP16},*brp*$^{\Delta 6.1}$/*gluRIIA*^{SP16}, *brp*^{69}	18	(Petersen et al., 1997) (Kittel et al., 2006) (Fouquet et al., 2009)
aplip-1^{ek4}*:aplip-1*^{ek4}/Df(3L)BSC799	19	Bloomington Drosophila Stock Center
gluRIIA^{Null}*;aplip-1*^{ek4}*: AD9/df(2L)cl*^{h4}*; aplip-1*^{ek4}*/Df(3L)BSC799*	19	(Petersen et al., 1997) Bloomington Drosophila Stock Center

DGRC = Drosophila Genome Research Center

The following procedures for dissection, incubation, electrophysiology and immunohistochemistry (in relation to Homeostatic Plasticity) were performed as described in Böhme et al. (2019) and so the details are also as published there.

4.5 Electrophysiology

4.5.1 Dissection and incubation of larvae for electrophysiology

Third instar larvae were individually placed on Sylgard (184, Dow Corning, Midland, MI, USA) and pinned at the head and the tail. The pins were placed close enough together so as to not stretch the larvae. A small incision was made with a sharp scissors in the dorsal cuticle near the tail pin. Starting from this posterior incision, a cut was made along the length of the larva extending beyond the head pin, being sure not to stretch the larva when cutting.

The following solutions were used to incubate larvae prior to recording;

- *PMA incubation (Figure 10):* HL3 for TEVC recording (values in mM: NaCl 70, KCl 5, $MgCl_2 \cdot 6H_2O$ 20, $NaHCO_3$ 10, trehalose 5, sucrose 115, HEPES 5, $CaCl_2$ 0, pH adjusted to 7.2) (Stewart et al., 1994) containing 2 µM Phorbol 12-myristate 13-acetate (PMA) (Sigma-Aldrich, MO, USA (stored at -20˚C as 10 mM stock in DMSO)). Control incubations contained an equal volume of DMSO instead of PMA.
- *Phtx incubation (Figures 12-13, 15, 17a):* Modified HL3 for current clamp recording (values in mM: NaCl 70, KCl 5, $MgCl_2 \cdot 6H_2O$ 10, $NaHCO_3$ 10, trehalose 5, sucrose 115, HEPES 5, $CaCl_2$ 0, pH adjusted to 7.2) containing 20 µM PhTx-433 (Sigma-Aldrich, MO, USA (stored at -20˚C as 4 mM stock in dH_2O)). Control incubations contained an equal volume of dH_2O instead of PhTx.

40 µl of the incubation solution was gently pipetted into the larval abdominal cavity using minimal force. Larvae were incubated for 10 minutes at room temperature (~22˚C). Dissection was completed in the incubation solution as below.

Larvae in Figures 11, 14, 17e, 18-19 were not pre-incubated; 40 µl of modified HL3 for current clamp only (values in mM: NaCl 70, KCl 5, $MgCl_2 \cdot 6H_2O$ 10, $NaHCO_3$ 10, trehalose 5, sucrose 115, HEPES 5, $CaCl_2$ 0, pH adjusted to 7.2) was gently pipetted onto the larva before dissection.

The cuticle was pinned down twice on either side. The intestines and trachea were cut at the posterior and held firmly with forceps as the remaining connections to the body were cut before being fully removed, taking care not to pull on the preparation. The brain was held slightly raised above the preparation and the segmental nerves cut without touching the underlying muscle. Finally the brain was removed.

Larvae in Figures 12-13, 15. 17a were minimally washed of incubation solution with HL3 three times. Larvae in Figures 10-11, 14, 17e, 18-19 were not washed.

Dissection and incubation with cg-PI(4,5)P_2

Larvae in Figure 9 were dissected on ice under red light in HL3 for TEVC recording (values in mM: NaCl 70, KCl 5, $MgCl_2 \cdot 6H_2O$ 20, $NaHCO_3$ 10, trehalose 5, sucrose 115, HEPES 5, $CaCl_2$ 0, pH adjusted to 7.2) (Stewart et al., 1994). Following dissection they were incubated on ice for 30 minutes in 100 µl HL3 containing 40 µM cg-PI(4,5)P_2 (stored at -80 ˚C, 20 mM stock in DMSO) and 0.04% Pluronic F-127 (Sigma-Aldrich, MO, USA, stock (20% solution in DMSO) stored at room temperature and preheated to 40˚C prior to use). After incubation, larvae were washed once with HL3.

4.5.2 Current clamp recording

The Sylgard block and completed larval preparation was placed in the electrophysiological recording chamber. Prior to recording, $CaCl_2$ (1M stock stored at 4˚C) was added to modified HL3 for current clamp recording (values in mM: $CaCl_2$ 0.4, NaCl 70, KCl 5, $MgCl_2 \cdot 6H_2O$ 10, $NaHCO_3$ 10, trehalose 5, sucrose 115, HEPES 5, pH adjusted to 7.2). The recording chamber was filled with 2 ml HL3.

Recordings were performed at room temperature in current clamp mode at muscle 6 (Figures 11-15, 17-19) in abdominal segments A2/A3 as previously described (Zhang and Stewart, 2010a) using an Axon Digidata 1550A digitizer, Axoclamp 900A amplifier with HS-9A x0.1 headstage (Molecular Devices, CA, USA) and on a BX51WI Olympus microscope with a 40X LUMPlanFL/IR water immersion objective. Sharp intracellular recording electrodes were made using a Flaming Brown Model P-97 micropipette puller (Sutter Instrument, CA, USA) with a resistance of 20-35 MΩ and back-filled with 3 M KCl. Cells were only considered with a membrane potential less than -60 mV and membrane resistances greater than 4 MΩ. All recordings were acquired using Clampex software (v10.5) and sampled at 10-50 kHz, filtering with a 5 kHz low-pass filter. eEPSPs were recorded by stimulating the appropriate nerve at 0.1 Hz, 5 times (8 V, 300 μs pulse) using an ISO-STIM 01D stimulator (NPI Electronic, Germany). Stimulating suction electrodes were pulled on a DMZ-Universal Puller (Zeitz-Instruments GmbH, Germany) and fire polished (width of axon bundle, differs depending on genotype) using a CPM-2 microforge (ALA Scientific, NY, USA).

Spontaneous mEPSPs in Figure 11 were recorded for 30 seconds. 1 ml of solution was then removed without disturbing the preparation or electrodes and exchanged for 1 ml of HL3 added containing PhTx-433 (Sigma-Aldrich, MO, USA), mixing gently with the pipette to a final concentration of 4 μM PhTx. Spontaneous mEPSPs were recorded immediately, again for 30 seconds. Stimulation was performed at 10 Hz for 10 seconds to measure eEPSPs or in the case of control recordings, 10 seconds without stimulation. Finally, mEPSPs were recorded for 30 seconds.

For current clamp recordings in Figures 14 and 17, cells with an initial membrane potential greater than −55 mV, resistances less than 5MΩ were rejected. eEPSPs were recorded by stimulating the appropriate nerve at 0.2 Hz, 10 times (6 V, 300 μs pulse) (Figure 17) or 0.2 Hz continuously (8 V, 300 μs pulse) (Figure 14).

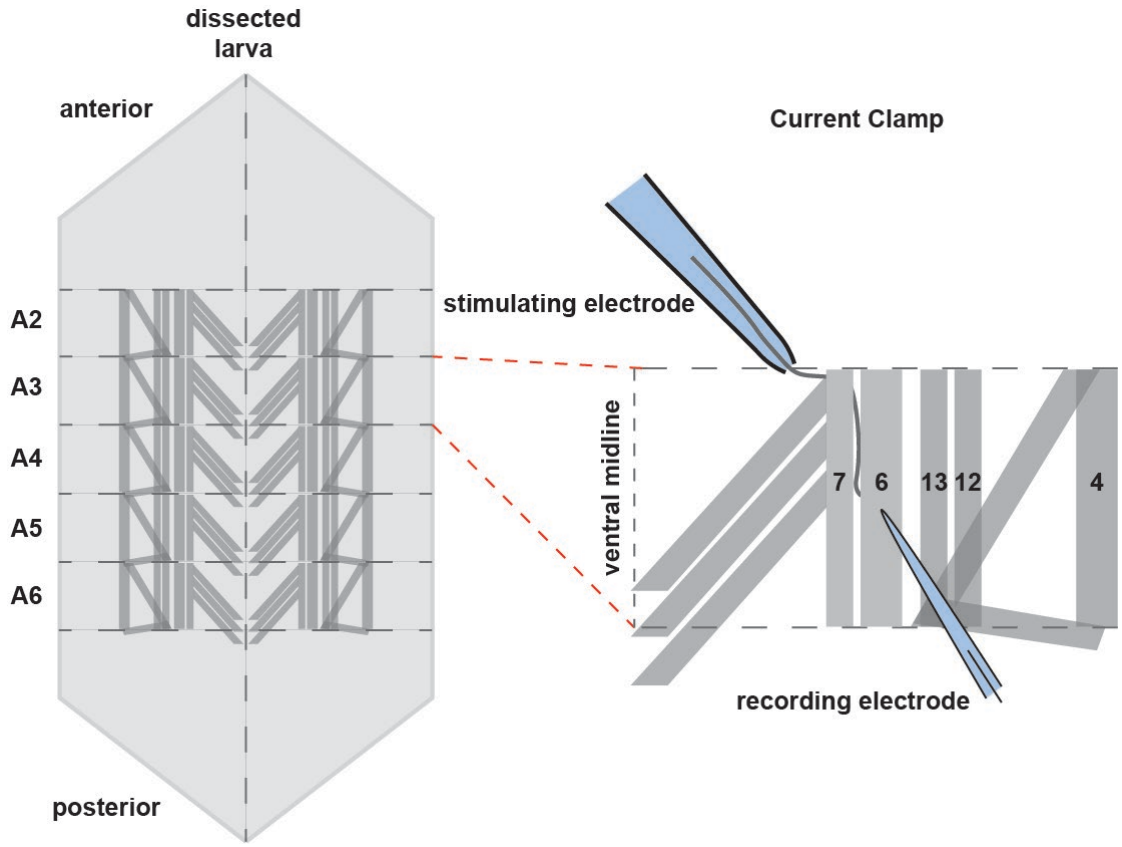

Figure 6: Dissected larva and current clamp recording configuration.

Left: Dissected larval preparation showing muscle pattern in abdominal segments A2-A6. Right: Example placement of electrodes for Current Clamp recording in right A3 hemisegment. The cut end of the segmental motoneuron bundle is sucked into the stimulating electrode and the sharp recording electrode is inserted into muscle 6.

4.5.3 Two electrode voltage clamp (TEVC) recording

The Sylgard block and completed larval preparation was placed in the electrophysiological recording chamber. $CaCl_2$ (1M stock stored at 4˚C) was added to HL3 for TEVC recording (NaCl 70, KCl 5, $MgCl_2 \cdot 6H_2O$ 10, $NaHCO_3$ 10, trehalose 5, sucrose 115, HEPES 5, $CaCl_2$ 0, pH adjusted to 7.2) to a final concentration of 2 mM (Figure 9) or 1.5 mM (Figure 10). The recording chamber was filled with 2 ml HL3. TEVC recordings were performed as previously described (Zhang and Stewart, 2010c) in muscle 6 (Figure 9) or muscle 4 (Figure 10) of abdominal segments A2/A3. Cells were only considered with a membrane potential less than -50 mV and membrane resistances greater than 4 MΩ. UV uncaging in combination with paired-pulse TEVC recording (Figure 8) was performed using a JML-C2 UV flash lamp (Rapp OptoElectronic GmbH,

Germany) with ET 405/40 bandpass filter. A UV flash (C2) was given 2 seconds after the first paired-pulse.

4.5.4 Electrophysiological analysis

Analysis of eEPSPs/eEPSCs and mEPSPs/mEPSPCs was performed with Clampfit 10.5. Average eEPSP/eEPSC amplitudes were measured. High frequency trains in Figure 9 were analysed using a custom MATLAB script (MATLAB vers. 7.12.0 R2011a). mEPSPs/mEPSCs traces were filtered with a 500 Hz Gaussian low-pass filter. An mEPSP/mEPSC template was generated for each cell in Figures 10-11, 15, 18-19. A single mEPSP template was used to identify individual mEPSPs in Figures 12-13. mEPSPs were analysed with a genotype specific template in Figures 14,17. The mean mEPSP amplitude per cell and mEPSP frequency was calculated in all experiments. Quantal contents were calculated by dividing the mean eEPSP by mean mEPSP for each cell/stimulation cycle.

4.6 *Drosophila* Imaging

4.6.1 Live imaging of axonal transport

Third instar larvae were dissected and transferred to a recording chamber as described above for current clamp electrophysiology, filling the recording chamber with 2 ml modified HL3. Imaging was performed on a BX51WI Olympus microscope equipped with a 60X water immersion objective (LUMFL NA 1.10, Olympus, Tokyo, Japan), Lumencor SPECTRA X light engine (Lumencor, OR, USA), EGFP/mCherry filter (59022x, Chroma Technology Corporation, VT, USA) and operated with ImageJ micromanager software. Prior to recording 1 ml of modified HL3 was removed from the recording chamber and exchanged for 1 ml of modified HL3 (values in mM: $CaCl_2$ 0.4, NaCl 70, KCl 5, $MgCl_2 \cdot 6H_2O$ 10, $NaHCO_3$ 10, trehalose 5, sucrose 115, HEPES 5, pH adjusted to 7.2) containing PhTx-433 (Sigma-Aldrich, MO, USA (stored at -20˚C as 4 mM stock in dH_2O)) or control dH_2O, gently mixing with the pipette to obtain a final concentration of 20 µM PhTx. Imaging was commenced

immediately at nerve bundles above muscle 4, abdominal segments A2-A4. Image stacks were acquired at 15 second intervals with a z-step of 1 µm, 800 ms exposure and 550/15 nm light at maximum power (260 mW). Image stacks were analysed using Fiji (ImageJ) software. A max projection of each stack was generated, and fluorescent particles manually tracked with the ImageJ Manual Tracking plugin. Fluorescent particles were placed into two categories based on their individual movement over 10 minutes; anterograde-/retrogradely or stable/slowly oscillating particles. The proportion of particles in each category out of the total observed particles in a nerve bundle was calculated.

4.6.2 Dissection and Immunohistochemistry

Individual third instar larvae were selected and placed on a rubber dissection puck and pinned at the head and the tail. A 40 µl drop of HL3 (values in mM: NaCl 70, KCl 5, $MgCl_2 \cdot 6H_2O$ 20, $NaHCO_3$ 10, trehalose 5, sucrose 115, HEPES 5, $CaCl_2$ 0, pH adjusted to 7.2) (Stewart et al., 1994) was pipetted onto the larva. A small incision was made with a pair of sharp scissors in the dorsal cuticle near the tail pin. Starting from this posterior incision, a cut was made along the length of the larva extending beyond the head pin. The cuticle was stretched and pinned down twice on either side. The intestines and trachea were cut at the posterior and held firmly with forceps as the remaining connections to the body were cut before being fully removed. The HL3 was removed and the larva fixed with ice-cold methanol for 5 minutes. The methanol was then removed before washing 5 times with PBS containing 0.05% Triton X-100 (0.05% PBT). Fixed larvae were transferred and stored in a 1.5 ml Eppendorf tube containing ice-cold 0.05% PBT until blocking. Larvae were blocked for an hour in 0.05% PBT containing 5% normal goat serum (NGS), rotating on a wheel at room temperature. The blocking solution was then removed and larvae were incubated overnight on a wheel at 4°C in the primary antibody solution (BRP and Unc13A) consisting of 0.05% PBT containing mouse NC 82 (1:200 dilution, Developmental Studies Hybridoma Bank, University of Iowa, Iowa City, USA) and guinea pig Unc13A (1:500, (Böhme et al., 2016)). Larvae were washed 5 times over 2 hours on a wheel by

exchanging the solution in the tube every 30 minutes for 1.5 ml of fresh 0.05% PBT. Larvae were incubated for 4 hours on a rotating wheel at room temperature in the secondary antibody solution consisting of PBT (0.05%) containing goat anti-mouse Cy3 (1:500, Jackson ImmunoResearch, PA, USA, 115–165–146), goat anti-guinea pig Alexa-Flour-488 (1:500, Life Technologies, CA,USA, A11037) and goat anti-HRP Alexa-Flour-647 (1:250, Jackson ImmunoResearch, PA, USA, 123–605–021). Larvae were again washed 5 times over 2 hours (every 30 mins) on a rotating wheel, each time exchanging the solution in the Eppendorf tube with 1 ml of fresh 0.05% PBT. After the last wash, the larvae were washed overnight on a rotating wheel at 4°C. All solution was then removed from the larvae and they were mounted on a glass slide in Vectashield (Vector Laboratories), and sealed under a coverslip with nail varnish. Microscope slides were stored in the dark at -20°C.

4.6.3 Confocal Imaging and synaptic intensity analysis

Confocal imaging was performed on a Leica SP8 microscope (Leica Microsystems, Germany) equipped with a 63X 1.4 NA oil immersion lens, four excitation laser lines (405 nm (not used), 488 nm, 552 nm, and 638 nm), suitable filter sets and controlled with LCS AF software. Fixed larval preparations were viewed at room temperature and NMJ images acquired at type 1b boutons, muscle 4 in abdominal segments A2-A5. Image stacks were acquired with a z-step size of 0.25 µm, a pixel size of 100 nm, zoom factor 1.8, 1024x256 pixel resolution, line averaging of 3, and scanned at 400 Hz. Fiji (ImageJ) software was used to process image stacks, including enhancement of brightness/contrast. A custom script was used, selecting 3 points on the image stack 40 pixels from the NJ/signal, to subtract background fluorescence. The image stack was separated into its 3 individual channels and a max projection generated for each channel. The HRP-647 channel (stained neuronal membrane) was used to create a mask, drawing an outline around the NMJ of interest. A Gaussian blur filter (1.00 Sigma radius) was applied and the threshold adjusted to remove signal outside the NMJ, making sure the HRP signal remained continuous. Additional areas of signal outside the NMJ were removed with the freehand tool. The final binary HRP mask was saved, and

then applied to each of the other two channels (Subtract) to restrict analysis to the NMJ. For image analysis in Figures 17 and 19, a custom script was used to further restrict analysis to AZs (BRP staining was used as an AZ marker). The script identified and measured points of high intensities in the BRP channel, the mean intensity was calculated. The intensities at these exact same points was measured in the Unc13A channel and the mean intensity calculated. In Figure 18, no script was used and instead the mean intensity across the entire NMJ (as defined by the HRP mask) was measured and calculated for both channels (BRP and Unc13A).

4.7 Statistics

Statistical analysis for all experiments was performed in GraphPad Prism 6 software. Data sets were tested for normality (D'Agostino & Pearson omnibus normality test) and compared for equal variances (F test). Student's t-test was used to compare the mean of two unpaired groups and for those that were not normally distributed or were of unequal variance; a Mann-Whitney U test was used. For paired recordings, paired t-test was used. For comparing multiple groups, nonparametric one-way analysis of variance (ANOVA) with Tukey's multiple comparison test was used. For specific statistical information on individual datasets, including n values, p values and statistical tests used, please see Table 2 (Appendix 8.4).

5 Results

5.1 Loading and uncaging $PI(4,5)P_2$

In addition to the formation of membranes, lipids play a central role in several important cellular processes. They act as targets for protein localisation, substrates for the generation of secondary messengers and as modulators of various cellular signalling pathways. In order to study the biological activity of signalling lipids, a chemically caged, membrane permeant phosphatidylinositol 4,5-bisphosphate ($PI(4,5)P_2$) was used that could be loaded into cells and optically uncaged, hence becoming biologically available. Prior to this however, it was necessary to test the ability to uncage the lipid and test its binding to a lipid sensor. Advantage was taken of the tendency of lipids to form micelles when suspended in an aqueous solution. An imaging buffer was made up containing cg-$PI(4,5)P_2$ (to a final concentration of 20 µM) and a high affinity lipid sensor specific for $PI(4,5)P_2$. This sensor was a fusion protein of the pleckstrin homology (PH) domain of phospholipase C-delta 1 ($PLC\delta_1$) tagged with EGFP (5% final concentration). $PLC\delta_1$ is an enzyme that endogenously binds $PI(4,5)P_2$ with high affinity during its metabolism. The solution was only briefly vortexed so as not to break up the aggregated $PI(4,5)P_2$ and pipetted into a chamber containing a glass coverslip. On a TIRF microscope, which allows restricted illumination within nanometres of the coverslip (restricted background), these micelles of $PI(4,5)P_2$ could be observed on the surface of the glass in the GFP channel (488 nm) (Figure 7a). The $PI(4,5)P_2$ was visualised prior to uncaging due to some degree of binding to $PLC\delta_1$-PH-EGFP. The lipid sensor in solution was also observed in the background. The coverslip was illuminated with 405 nm light to uncage $PI(4,5)P_2$, and with excitation of the coumarin its fluorescence could be observed in the UV channel. Following uncaging, the relative fluorescence intensity of micelles in the GFP channel increased drastically indicating that these were indeed micelles of $PI(4,5)P_2$ and that the phospholipid was uncaged, hence facilitating additional $PLC\delta_1$-PH-EGFP binding which establishes that the coumarin cage indeed impedes binding.

As uncaging of $PI(4,5)P_2$ had been established to be effective in a simplified assay, it was now important to confirm loading of the lipid into cells. Human Embryonic Kidney (HEK) cells were stained with far-red dye (CellMask, Invitrogen) to visualise the plasma membrane of cells, which could be observed with a 638 nm laser without uncaging the UV-sensitive coumarin cage of $PI(4,5)P_2$ (405 nm). Following this, cells were loaded by incubating in imaging buffer containing cg-$PI(4,5)P_2$ (20 μM final concentration) and an equal volume of Pluronic F-127 (0.02% final concentration) for 30 minutes. Control cells were loaded with a solution containing only DMSO and Pluronic. Following loading the cells were observed on a spinning disk confocal microscope. Both the CellMask and coumarin cage of $PI(4,5)P_2$ could be clearly seen at the plasma membrane. Internal cellular fluorescence indicated that the $PI(4,5)P_2$ was not restricted to the plasma membrane and likely also localising to intracellular structures, e.g. endosomes. I was interested in the sub cellular distribution of $PI(4,5)P_2$ so examined line profiles of sections of the plasma membranes. Using a custom MATLAB script, these profiles were aligned in the $PI(4,5)P_2$ channel using the maximum fluorescence of the CellMask channel to determine the centre of the plasma membrane. The average of many of these line profiles illustrates the obvious presence of $PI(4,5)P_2$ at the plasma membrane and within the cell, which was absent extracellularly and in control cells. After 60 frames of UV imaging this had significantly decreased as the coumarin cage was cleaved by continuous UV light (Figure 7b). This confirmed that caged $PI(4,5)P_2$ could be loaded into cells, that it was visible at the plasma membrane/intracellularly and that it could be uncaged.

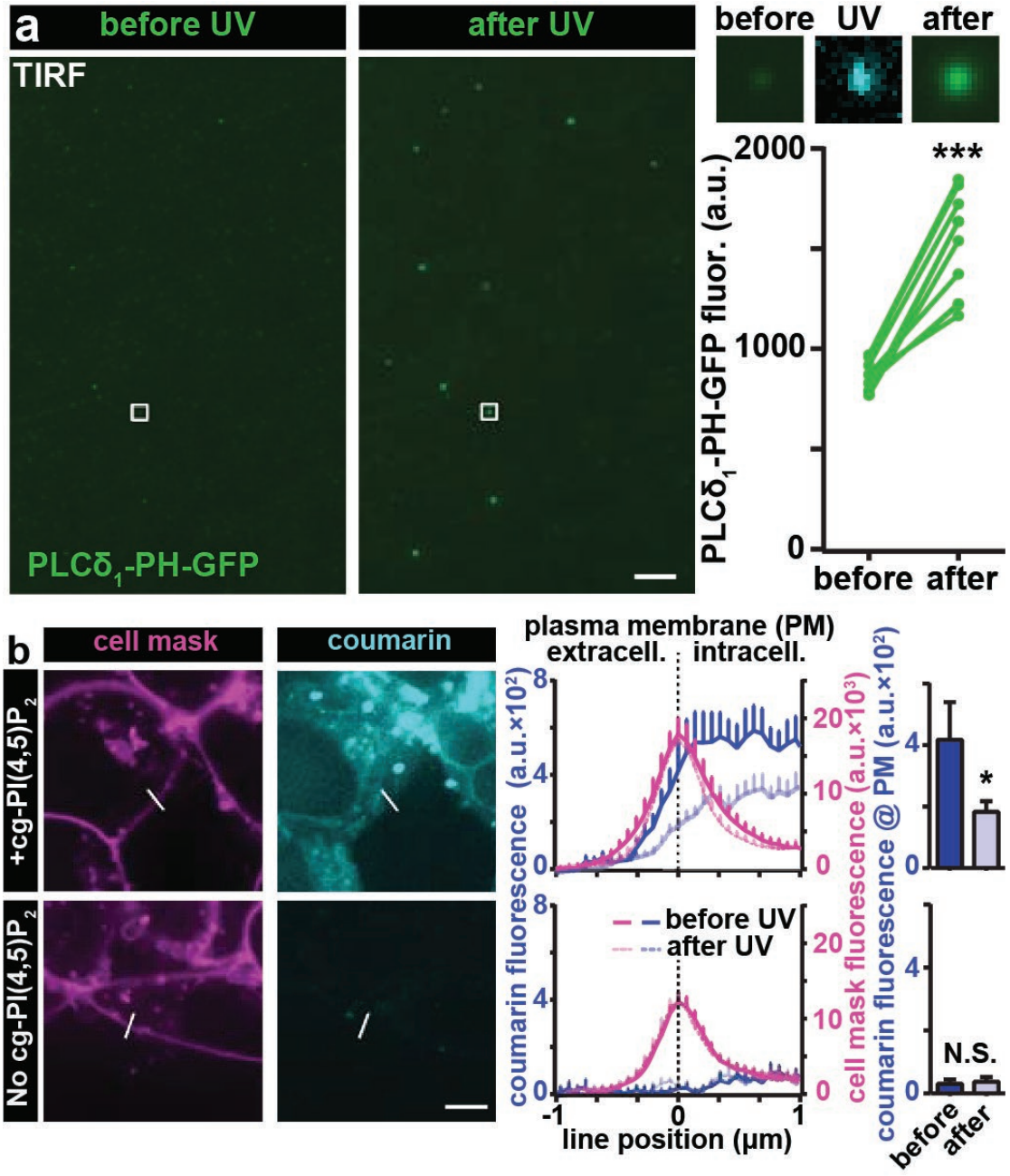

Figure 7: Confirmation of PI(4,5)P_2 UV uncaging and loading into HEK cells.

(a) Left panel: A solution containing cg-PI(4,5)P_2 and soluble PI(4,5)P_2 sensor, PLCδ$_1$-PH-EGFP, applied to a glass coverslip reveals lipid micelles accumulated on the surface using TIRF microscopy. PLCδ$_1$-PH-EGFP is also visible in the background. On the left a comparison of EGFP fluorescence (488 nm) before and after UV uncaging can be seen. The white box indicates and encompasses an example micelle on the glass coverslip. Right panel: The example micelle is shown before uncaging (EGFP fluorescence (488 nm)), during uncaging (UV fluorescence (405 nm)), and again after uncaging (EGFP fluorescence (488 nm)). Below this, quantification is shown of EGFP fluorescence at 10 such micelles before and after UV uncaging. **(b)** Left panel: HEK cells were incubated for 30 minutes at 37°C with cg-PI(4,5)P_2 (top) or without cg-PI(4,5)P_2 (bottom) in vehicle DMSO (0.02%) and Pluronic (0.02%). Cells were also

incubated with CellMask Deep Red plasma membrane stain. Line profiles are shown in white crossing the plasma membrane, with the plasma membrane identified by CellMask Deep Red fluorescence (638 nm). The line profiles are then transferred to the corresponding Coumarin fluorescence (405 nm) UV images. Line profiles in both channels are aligned based on the CellMask fluorescence maximum. Right panel: Mean fluorescence line profiles of Cell Mask (pink), Coumarin before UV uncaging (dark blue) and Coumarin after 30 s UV uncaging (light blue). The Coumarin is localised within the cg-PI(4,5)P_2 loaded cells (top) and at the position of the membrane is significantly lower after UV uncaging. It is absent from vehicle-only loaded cells (bottom). Statistics: Paired T-test, *$p \leq 0.05$, ***$p \leq 0.001$, not significant (n.s.) $p > 0.05$, mean ± SEM. For details see Table 2. Scale bars: 5 µm. Modified from Walter et al. (2017).

The question remained whether PI(4,5)P_2 loaded into cells was biologically active after uncaging. To investigate this, COS-7 cells were transfected with PLCδ_1-PH-EGFP to visualise uncaged PI(4,5)P_2 available for binding. In an attempt to degrade endogenous PI(4,5)P_2 that might bind the EGFP sensor prior to uncaging and would obscure observation of fresh lipid-sensor binding, the cells were also transfected with a mCherry tagged inositol polyphosphate 5-phosphatase targeted to the plasma membrane via a CAAX motif (mCh-INPP5E). I had previously observed sensor localising to the membrane, even in the absence of uncaging. Cells were loaded with cg-PI(4,5)P_2 or DMSO (control) as before and the large footprints of the COS-7 cells imaged on a TIRF microscope. The lipid sensor was to some extent already present at the plasma membrane and after imaging for 10 seconds a moderate degree of bleaching occurred (Fig 8a). Following the 10th frame a single UV uncaging frame was introduced to the sequence prior to the 11th frame. Small circular ROIs (of equal size) of the footprints of cells were analysed. The change of GFP fluorescence between subsequent frames was significantly different when comparing cg-PI(4,5)P_2 loaded cells and control cells. In PI(4,5)P_2 loaded cells, uncaging appeared to briefly counteract the bleaching, while no such effect was seen in control cells. This confirmed that upon uncaging, PLCδ_1-PH-EGFP was localised to the membrane and that PI(4,5)P_2 was available for binding.

PI(4,5)P_2 is well known to regulate actin organisation and bind actin regulator proteins, contributing to processes such as cellular migration and endocytosis (Senju and Lappalainen, 2019). To establish that loaded and uncaged

$PI(4,5)P_2$ would have identifiable effects on cellular processes, HEK cells were transfected with an RFP tagged LifeAct construct. This fluorescent peptide binds filamentous actin, allowing any cytoskeletal rearrangements due to increases in $PI(4,5)P_2$ to be examined. Cells were loaded with $PI(4,5)P_2$ or DMSO control as before and imaged on a TIRF microscope. After 5 frames in the RFP channel at 2 Hz, a UV frame to uncage $PI(4,5)P_2$ was introduced before resumption of imaging in the RFP channel. 10 ROIs of equal size were taken from the footprint of each cell, averaged and background subtracted. It was clear that uncaging $PI(4,5)P_2$ increased LifeAct fluorescence in these regions (Figure 8b), and presumably actin near the plasma membrane almost immediately. This is consistent with other studies that show that actin polymerisation is enhanced with increased $PI(4,5)P_2$ (Scholze et al., 2018) and provides evidence that uncaging $PI(4,5)P_2$ alters cellular processes.

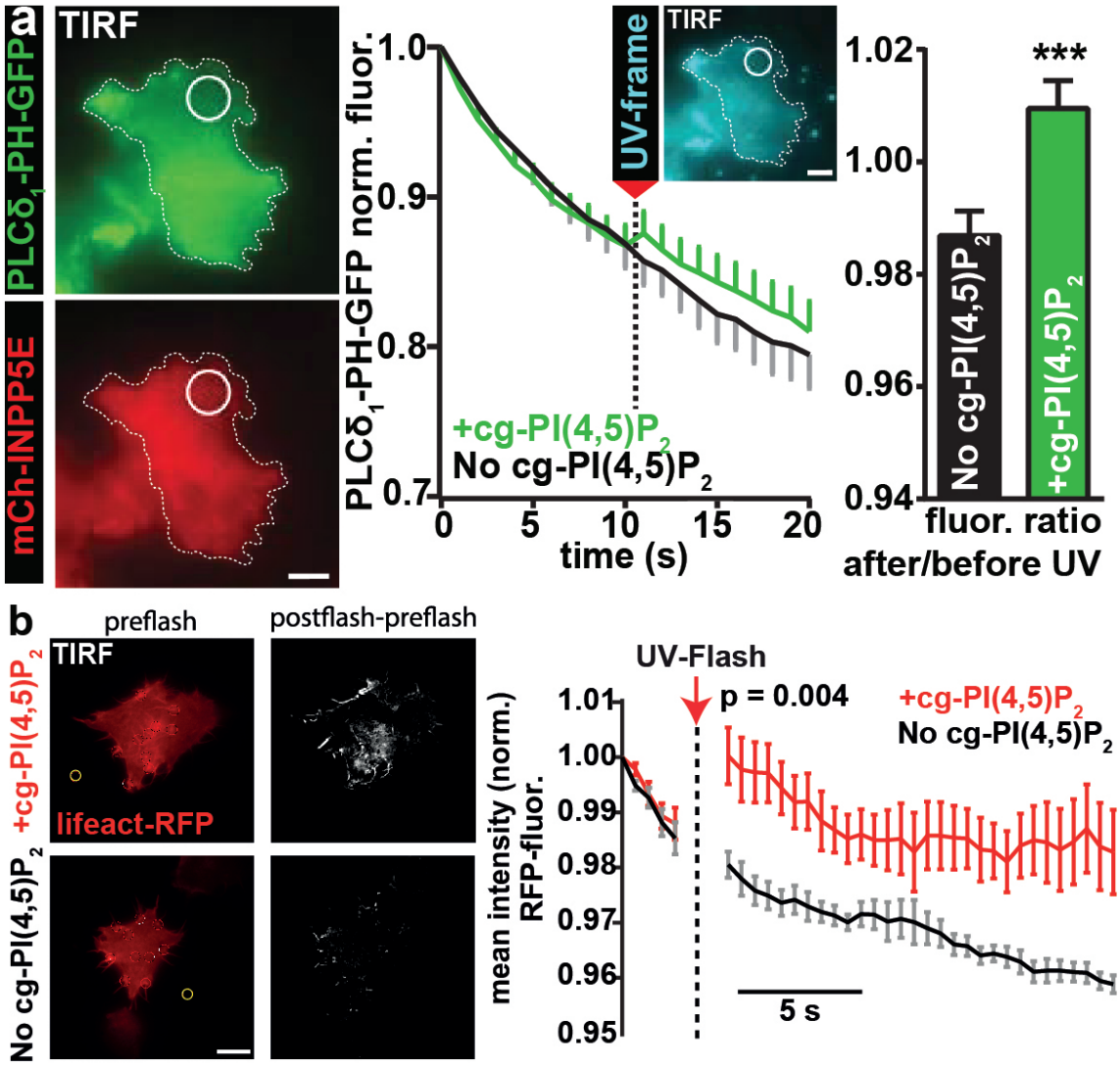

Figure 8: Uncaging PI(4,5)P_2 recruits a high affinity lipid sensor to the plasma membrane of COS-7 cells and triggers actin changes at the plasma membrane of HEK cells.

(a) Left panel: COS-7 cells transfected and expressing PLCδ$_1$-PH-EGFP (top) and mCh-INPP5E-CAAX (bottom) were incubated for 30 minutes at 37°C with cg-PI(4,5)P_2 or without cg-PI(4,5)P_2 in vehicle DMSO (0.02%) and Pluronic (0.02%). An example ROI is shown in white. Middle panel: Using TIRF microscopy, PLCδ$_1$-PH-EGFP fluorescence (488 nm) and mCh-INPP5E-CAAX fluorescence (561 nm) was imaged with a single UV uncaging frame (405 nm) between the 10th and 11th frames. Right panel: The ratio of PLCδ$_1$-PH-EGFP fluorescence change with UV uncaging is significantly higher in ROIs from cg-PI(4,5)P_2 loaded cells. **(b)** Left panel: HEK cells transfected with LifeAct-RFP were incubated for 30 minutes at 37°C with cg-PI(4,5)P_2 (top) or without cg-PI(4,5)P_2 (bottom) in vehicle DMSO (0.02%) and Pluronic (0.02%). ROIs of high LifeAct-RFP fluorescence were selected from areas of TIRF images and averaged per cell. A ROI of background fluorescence (outside each cell) was subtracted from each cell average. Right panel: After 5 frames at 2 Hz in the RFP channel (561 nm), 3 UV frames (405 nm) uncaged cg-PI(4,5)P_2 before resumption of

imaging at 2 Hz in the RFP channel (561 nm). LifeAct-RFP fluorescence increased at the membrane before (left) to after uncaging (right) in cg-PI(4,5)P_2 loaded cells. In control cells, there was no such increase in LifeAct-RFP fluorescence. Statistics: Students unpaired T-test or Mann-Whitney U test, ***$p \leq 0.001$, mean ± SEM. For details see Table 2. Scale bars: 5 µm. Modified from Walter et al. (2017).

5.2 Uncaging PI(4,5)P_2 at the *Drosophila* NMJ

To investigate the effect of uncaging PI(4,5)P_2 in vivo, I turned to the *Drosophila melanogaster* larval NMJ. C2 domains of several synaptic proteins can bind PI(4,5)P_2, such as unc13A and syt-1. Therefore I focused on possible modulation of neurotransmission with PI(4,5)P_2 uncaging. *Drosophila* larvae were incubated with PI(4,5)P_2 (40 µM) and an equal volume of Pluronic for 30 minutes before being washed and transferred to a recording chamber containing artificial haemolymph (HL3 (2 mM Ca^{2+})).

To measure neurotransmitter release, two electrode voltage clamp (TEVC) recordings were performed using intracellular sharp electrodes inserted into muscle cells (M6) of abdominal segments A2/A3, clamping the membrane potential at -70 mV. The measured readout of the experiment is the current required to keep the membrane potential at this holding potential (-70 mV). A suction electrode was used to stimulate an AP in the relevant nerve for the correct hemi segment. TEVC provides a measure of the postsynaptic receptor activation due to NT release following the generation of an AP and subsequent opening of presynaptic voltage gated Ca^{2+} channels. Paired stimulations allow an assessment of the probability of neurotransmitter release at synapses, determined as the ratio of the second amplitude divided by the first amplitude. A low probability of release will result in facilitation from the first to the second amplitude. A high probability of release will have the opposite effect, resulting in depression from the first to the second amplitude. Following a paired-pulse stimulation (25 ms ISI), a UV uncaging flash was delivered to the relevant NMJ 2 seconds later. Larvae expressing mCherry tagged BRP were used so that the appropriate NMJ could be identified for maximum effect. Control larvae were also loaded with PI(4,5)P_2 but received no flash. After another 2 seconds, an identical paired stimulation was delivered (Figure 9a). There was no change in the paired-pulse ratio before the UV flash to after the UV flash, indicating

negligible change in the release probability (Figure 9b). It is possible that loading Drosophila larvae with $PI(4,5)P_2$ is problematic as the NMJ is not as accessible as in the previous cell culture experiments. There was however a slight decrease in the amplitudes of the first responses in control larvae, which was reduced in uncaged larvae (Figure 9c). This indicates a protective effect of $PI(4,5)P_2$ on the slight depletion of release observed with repeated stimulations in a short space of time.

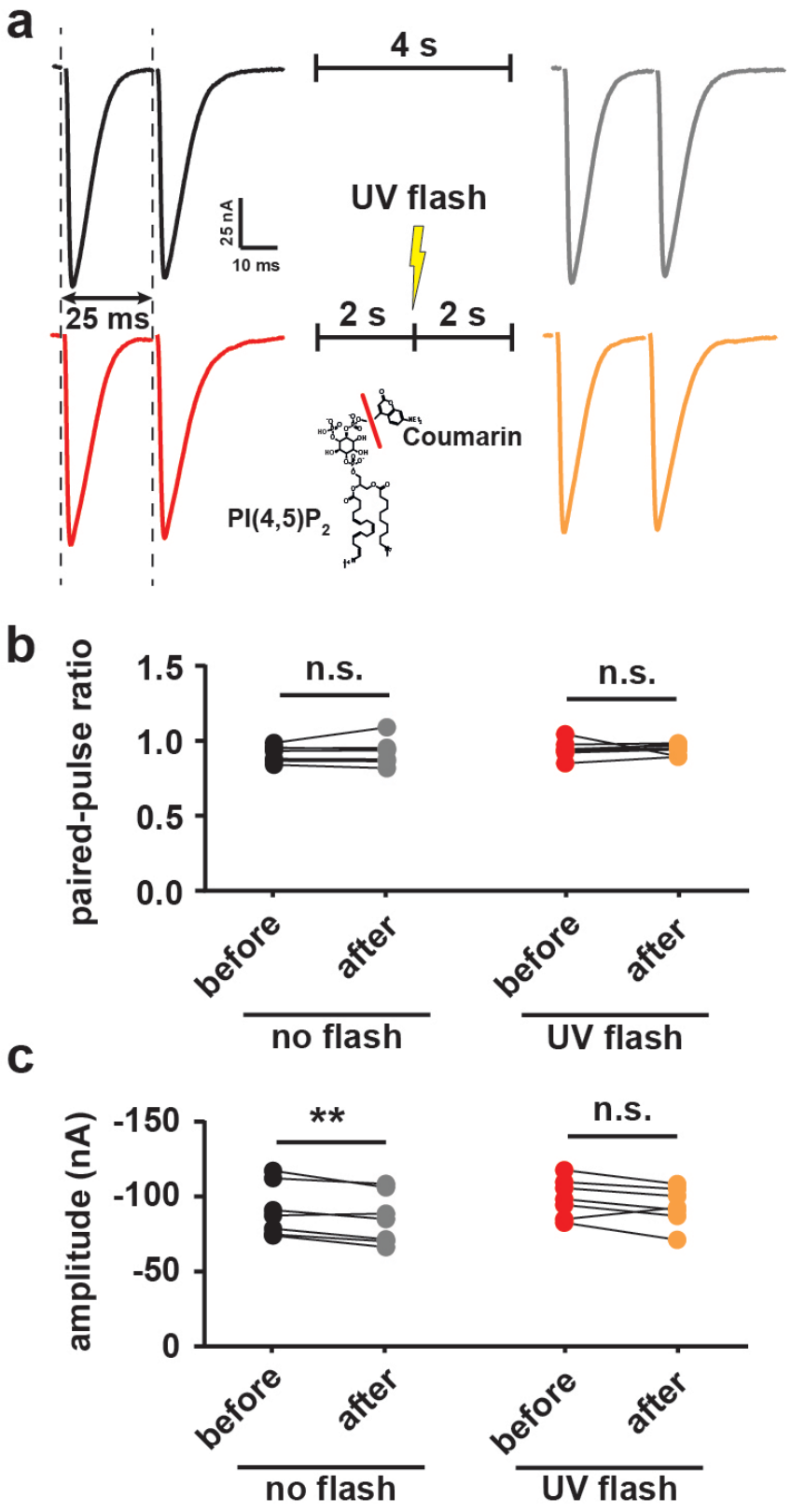

Figure 9: Uncaging PI(4,5)P_2 at the *Drosophila* NMJ.

(a) All BRP-mCherry larvae were loaded with cg-PI(4,5)P_2 for 30 minutes before TEVC recordings at muscle 6, abdominal segments A2/A3 (2mM Ca^{2+}). Top: Representative traces of evoked (eEPSC) paired-pulse stimulations (25 ms interstimulus interval)

performed 4 seconds apart without a UV uncaging flash (black-grey (control)) or with a UV uncaging flash (red-orange) midway between the paired stimuli (2 s). **(b)** The paired-pulse ratio (2nd EPSC amp./1st EPSC amp.), a measure of the release probability at synapses, did not differ between the first and second paired-pulse in control larvae or following a UV uncaging flash. **(c)** The 1st eEPSC amplitude of a paired-pulse stimulation is larger than the 1st eEPSC amplitude of another paired-pulse stimulation 4 seconds later (control larvae). In larvae that were exposed to a UV uncaging flash, the decrease in the 1st eEPSC amplitude from paired-pulse to paired-pulse was reduced. Cg-PI(4,5)P_2 from Walter et al. (2017). Statistics: Paired T-test, **$p \leq 0.01$, not significant (n.s.) $p > 0.05$, mean ± SEM. For details see Table 2.

5.3 PMA potentiation at the *Drosophila* NMJ

In addition to PI(4,5)P_2, exocytosis is influenced by a variety of signalling lipids, including its derivative DAG (Rhee et al., 2002). The phorbol ester PMA acts in much the same way as DAG by binding to C1 domains. PMA has been shown to increase exocytosis, both due to evoked stimulation and in the spontaneous release of single SVs (Song et al., 2002; Virmani et al., 2005). Unc13A is a likely target for the increased release due to phorbol ester application (Basu et al., 2007). To investigate the role of PMA and hence DAG in exocytosis at the *Drosophila* NMJ, larvae were incubated for 10 minutes in PMA (2 µM) or DMSO. Following incubation, they were fully dissected, transferred to a recording chamber containing artificial haemolymph (HL3 (1.5 mM Ca^{2+})) and TEVC recordings performed in muscle 4 of segments A2/A3. Miniature excitatory postsynaptic currents (mEPSCs), which occur spontaneously, are observed when single SVs fuse and release neurotransmitter resulting in a postsynaptic response. By recording these events I could determine the contents of single SVs and the frequency of their spontaneous fusion. Interestingly there was no increase in either the amplitude or frequency of these events (Figure 10c,d), as had been observed in other systems. This could suggest a different mechanism is present elsewhere and absent in *Drosophila* regarding activation of spontaneous events by PMA. High frequency train stimulations were also performed. As expected, the amplitude of the first peak was significantly increased, and this persisted for several further responses (Figure 10e, g). The emergence of depression and a lower paired-pulse ratio confirms a higher probability of release (Figure 10h). By dividing the first amplitude (eEPSC) by the average mEPSC amplitude, the total number of SVs

released in response to a single stimulation could be determined (quantal content). This was significantly increased with PMA treatment (Figure 10f). The number of released SVs had increased, while the content of these SVs had remained constant (mEPSC amplitude). To gain insight into the origin of this increase of release, I first calculated the cumulative release for every cell. This was done by adding the amplitude of each eEPSC (baseline to peak) to the amplitude of the previous eEPSC in the train (Figure 10i). Later in the train, steady state is reached, which is the point at which equilibrium exists between the release of SVs and recruitment of fresh SVs. By fitting a line (linear fit) to the cumulative release at this late portion of the train (stimuli 30 to 60) for each treatment, one can determine the number of SVs that were initially available for release (readily releasable pool (RRP)). This is calculated by back extrapolating to the y-intercept of each fitted line. The value of the y-intercept was significantly larger with PMA treatment, indicating an increased RRP (Figure 10j). This is in line with the effects of PMA potentiation on RRP size reported in experiments in other systems (Gillis et al., 1996; Stevens and Sullivan, 1998). The slope of each fitted line provides an insight into the priming rate of new SVs. There was no significant difference between treatments (Figure 10k). This experiment confirms that PMA, and presumably DAG, increases the RRP and hence the probability for neurotransmitter release at the *Drosophila* NMJ.

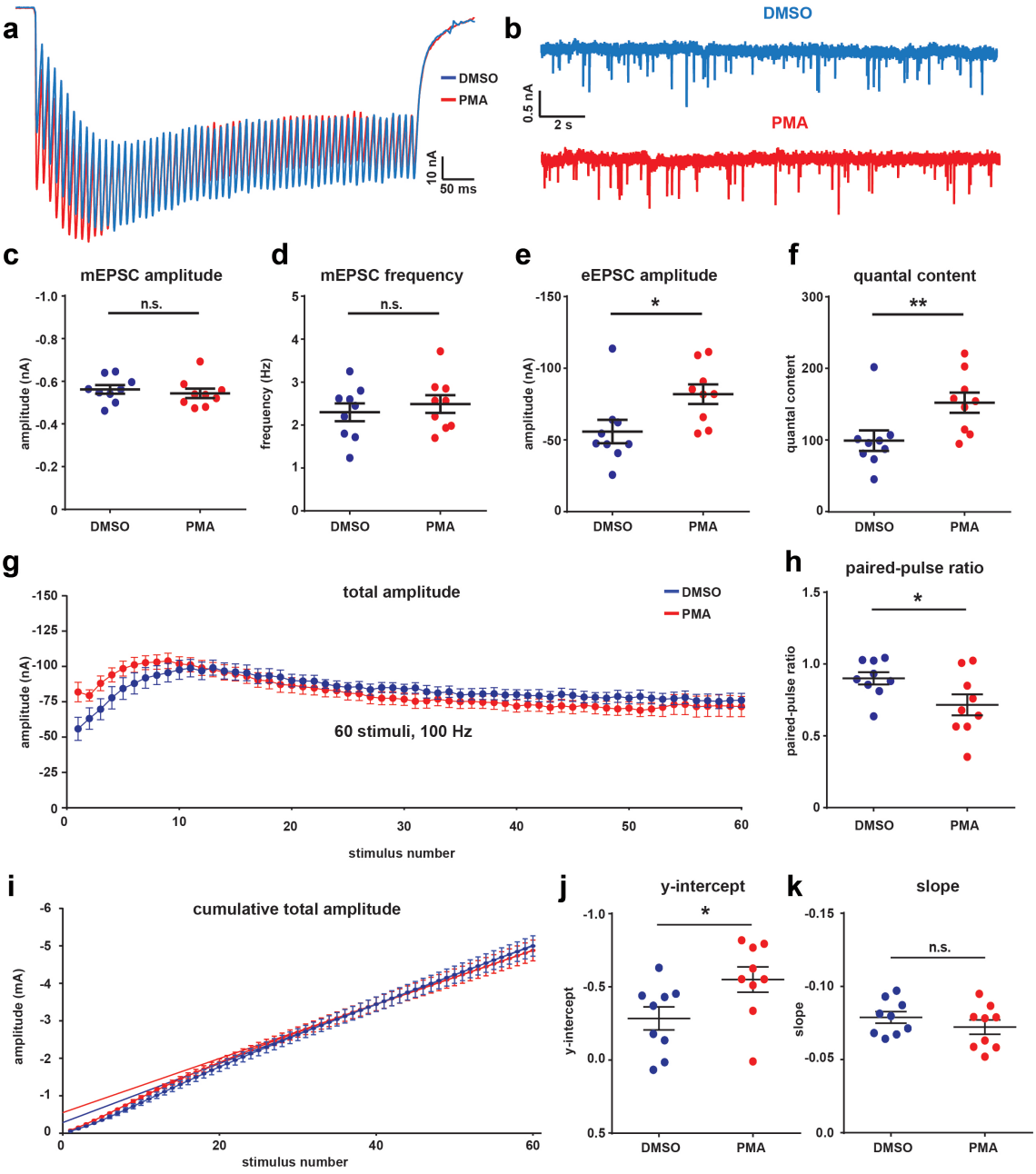

Figure 10: The phorbol ester PMA increases release probability and the readily releasable pool at the *Drosophila* NMJ.

(a) Average eEPSC (evoked) traces of 100 Hz trains (60 APs) in PMA (2 µM) treated (red) or DMSO treated (blue) third instar *Mhc-myr-GCaMP5G* larvae, recording from muscle 4 abdominal segments A2/A3 (1.5 mM Ca^{2+}) **(b)** Example mEPSC (spontaneous) traces in 2 µM PMA treated (red) or DMSO treated (blue) animals. **(c)** mEPSC amplitudes are unaffected by PMA treatment. **(d)** mEPSC frequencies are unchanged with PMA treatment **(e)** eEPSC amplitudes are increased with PMA treatment **(f)** Quantal content is increased with PMA treatment **(g)** Mean total amplitude for each train stimulus for 2 µM PMA (red) or DMSO. Initial amplitudes are increased with PMA treatment **(h)** Paired-pulse ratio decreases with PMA treatment, indicating a higher release probability **(i)** Mean cumulative total amplitude with back-extrapolation curve fitted after 30 stimuli for 2 µM PMA (red line) or DMSO (blue line). **(j)** Individual y-

intercepts from back-extrapolation are larger with PMA treatment, a measure of the readily releasable pool **(k)** There is no change in individual slopes from back-extrapolation, a measure of the forward vesicle priming rate. Statistics: Students unpaired T-test or Mann-Whitney U test, *$p \leq 0.05$, **$p \leq 0.01$, ***$p \leq 0.001$, not significant (n.s.) $p > 0.05$, mean ± SEM. For details see Table 2.

5.4 Investigating Synaptic Plasticity - Philanthotoxin

I concluded direct research of signalling lipids and pivoted towards investigating other mechanisms regulating synaptic transmission. I became interested in the homeostatic modulation of neurotransmission in response to postsynaptic receptor disruption. To investigate this, I would make use of the polyamine toxin, Philanthotoxin (PhTx), secreted in the venom of the European beewolf (*Philanthus triangulum*). PhTx is a potent and irreversible antagonist of invertebrate ionotropic glutamate receptors, which blocks receptors in a use-dependent manner while they are in the open conformation (i.e. in the presence of glutamate). To investigate induction of plasticity that occurs in response to the pharmacological block of glutamate receptors, it was first important to understand the characteristics of PhTx itself. Although similar experiments had been previously published (Peled et al., 2014), they lacked accurate quantification of spontaneous transmission, comparing responses before/after PhTx application and with/without presynaptic stimulation.

I performed current clamp recordings at the *Drosophila* NMJ. Unlike the previous TEVC recordings, where the potential of the membrane is fixed (measuring current injection into the muscle necessary to maintain this potential), current clamp recording measures the membrane potential of the muscle. Larvae were dissected and transferred to a recording chamber containing artificial haemolymph (HL3 (1.5 mM Ca^{2+})). A single intracellular recording electrode was inserted into muscle 6 of segments A2/A3 to measure the muscle membrane potential and a stimulation electrode positioned at the relevant nerve. Spontaneous miniature excitatory postsynaptic potentials (mEPSPs) were first recorded for 1 minute in the absence of toxin (Figure 11a). PhTx (4 μM) was then applied and recording immediately resumed for another minute. A significant decrease in mEPSP amplitude was observed. Thus, application of PhTx leads to an immediate reduction in the sensitivity of the

postsynapse to released glutamate. There was only a slight decrease in the frequency of these events. Strong AP stimulation was then performed. Initially, large postsynaptic eEPSP responses were observed. With repeated activation in the presence of PhTx, postsynaptic eEPSP responses declined, as expected by the use-dependence of the toxin (Figure 11b). This strong reduction of the postsynaptic response was not observed in the absence of PhTx (data not shown).

I next sought to understand the effect that stimulation in the presence of PhTx would have on spontaneous mEPSPs. Following stimulation, the frequency of mEPSPs was greatly reduced while mEPSP amplitude did not reduce further, compared to recordings from non-stimulated cells (Figure 11c, d). Stimulation increased the number of activated receptors, which were subsequently blocked upon opening. The fact that mEPSP frequency was also affected indicated that a portion of spontaneous events were becoming undetectable, due to the increased block of receptors at a number of AZs. Evoked and spontaneous release must activate the same postsynaptic glutamate receptors, and so I could conclude that it is acceptable to compare the postsynaptic response of both release modes.

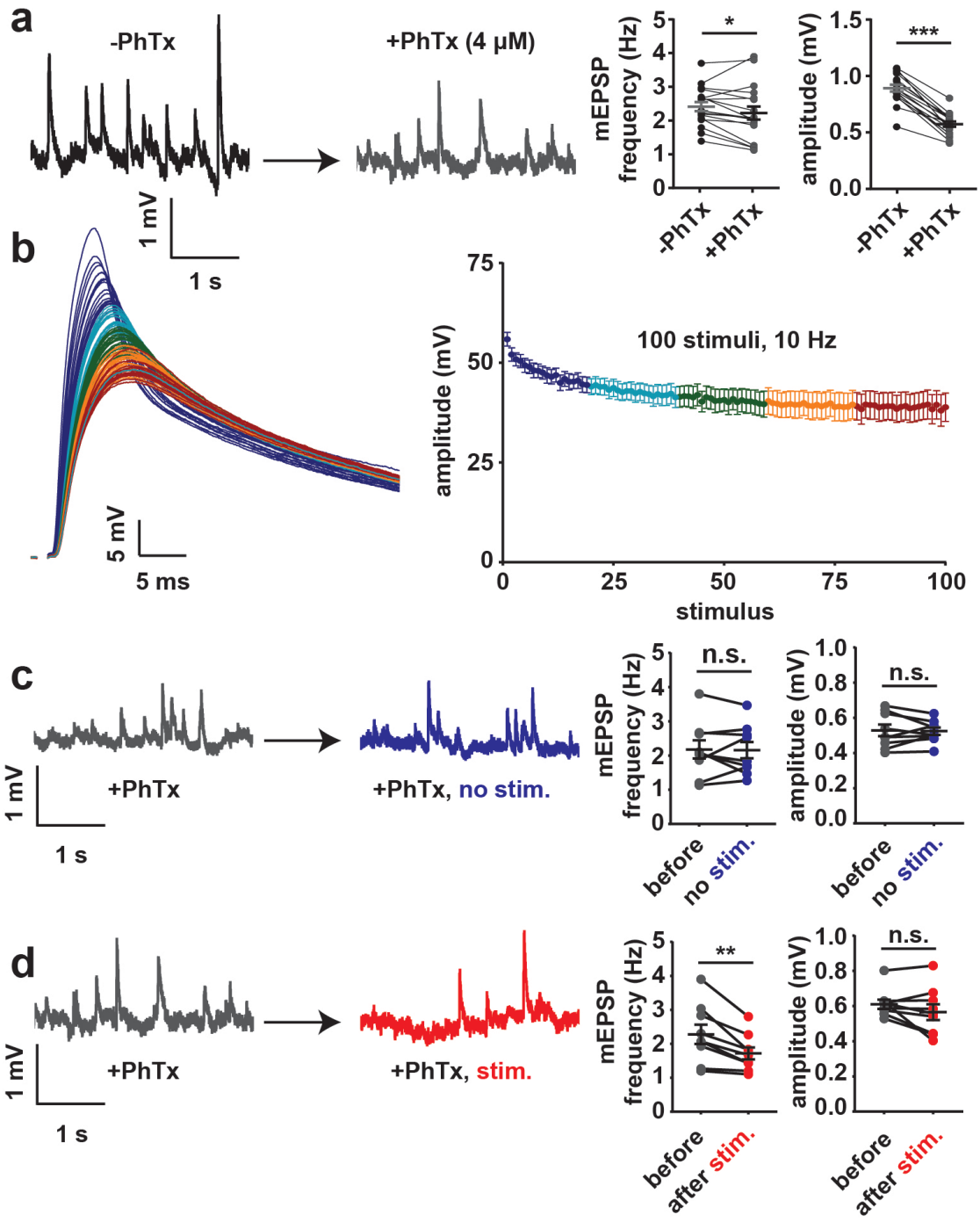

Figure 11: Characterisation of PhTx application and consequences of stimulation.

(a) Representative mEPSP (spontaneous) traces and quantification of mEPSP frequency and amplitude before and after PhTx (4 µM) (1.5 mM Ca^{2+}). mEPSP frequency is only slightly reduced immediately after PhTx application while mEPSP amplitude is strongly reduced. **(b)** Representative trace of eEPSP (evoked) response and quantification of 10 Hz 100 AP stimulation showing a strong PhTx use dependent decrease in eEPSP amplitude. **(c,d)** Representative mEPSP traces and quantification

of mEPSP frequency and amplitude comparing the effect of stimulation on spontaneous activity. (c) Both mEPSP amplitude and frequency are unaffected by a control 10 second rest period. (d) mEPSP frequency is strongly reduced by 10 Hz 100 AP stimulation while mEPSP amplitude is largely unaffected. Statistics: Paired T-test, *$p \leq 0.05$, **$p \leq 0.01$, ***$p \leq 0.001$, not significant (n.s.) $p > 0.05$, mean ± SEM. For details see Table 2.

5.5 Rapid Homeostatic Plasticity

PhTx allows the investigation of the consequences of postsynaptic sensitivity loss at the synapse. Homeostatic plasticity can be observed in two distinct ways: Firstly, as a structural re-arrangement and increase of proteins such as Ca^{2+} channels at AZs, and secondly as a functional increase in presynaptic neurotransmitter release (presynaptic homeostatic potentiation (PHP)). To illustrate PHP in action, I incubated wildtype larvae with PhTx (20 µM) for 10 minutes, washed them and performed current clamp recordings (M6, A2/A3) in toxin-free artificial haemolymph (HL3). This differs from the previous experiment where recordings were performed in the presence of PhTx. These animals exhibited reduced mEPSP amplitudes, as the postsynapse became less sensitive to glutamate detection. Despite this, evoked amplitudes (eEPSPs) remained largely unperturbed (Figure 12a,b). On calculation of the quantal content (average eEPSP/average mEPSP), one could clearly determine that there was a dramatic increase in neurotransmitter release to overcome the pharmacological challenge presented by PhTx. This illustrates that the presynapse had compensated by increasing the release that resulted from a single stimulus.

Evoked release is dependent on the release site protein Unc13A. I wanted to investigate its role in PHP as I suspected it to be of central importance in the upregulation of release. We had previously noted an increase in AZ proteins BRP, RBP and the Ca^{2+} channel subunit Cacophony (Cac) at *unc13A*^{Null} NMJs, although this increase was less than that observed in wildtype. In larvae expressing Unc13B but not Unc13A (*unc13A*^{Null}), evoked responses were greatly reduced to a mere fraction of the wildtype response (Fig 12c,d) as Unc13A is a vital release factor. mEPSP amplitudes were comparable between genotypes. Following incubation of wildtype and *unc13A*^{Null} larvae with PhTx,

larvae were washed and transferred to a recording chamber containing toxin-free artificial haemolymph. mEPSP amplitudes were reduced in both genotypes. As the control *unc13A*^{Null} eEPSP response was already significantly reduced, the PhTx treated larvae often exhibited complete failure to respond. For this reason, 5 stimulations were delivered and the resulting average amplitude was considered. PhTx treated *unc13A*^{Null} animals exhibited overall reduced evoked amplitudes compared to control treatment. In wildtype animals, evoked amplitudes were maintained despite treatment with PhTx. Due to the inability of *unc13A*^{Null} to maintain evoked amplitudes with PhTx treatment; one could calculate that the quantal content had indeed failed to increase, which is necessary to overcome PhTx challenge. Therefore, I could confirm that Unc13A is a vital component, not only for normal evoked release but also for the induction of homeostatic plasticity. The absence of PHP in the *unc13A*^{Null}, despite the presence of the Unc13B isoform, allows us to also conclude that Unc13B is not sufficient for this plasticity.

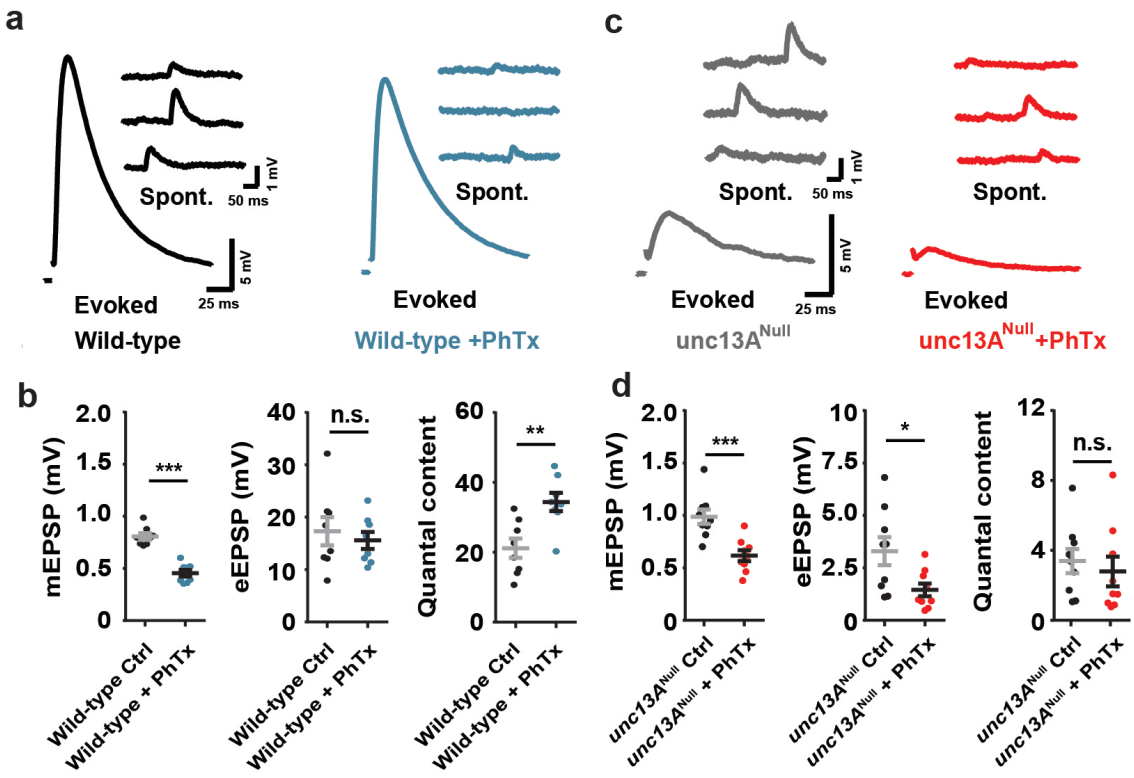

Figure 12: Unc13A is essential for rapid PHP.

(a) Representative eEPSP (evoked) and mEPSP (spontaneous) traces of wild-type control (black) and PhTx (20 µM) (blue) treated third instar larvae, recording from muscle 6 abdominal segments A2/A3 (0.4 mM Ca^{2+}). **(b)** Quantification of mEPSP

amplitude, eEPSP amplitude and Quantal content of wild-type control (black) and PhTx (blue) treated larvae. Quantal Content is increased in wild-type PhTx treated larvae as mEPSP amplitude is reduced with no change in eEPSP amplitude compared to controls. **(c)** Representative eEPSP (evoked) and mEPSP (spontaneous) traces of *unc13A*^{Null} control (grey) and PhTx (20 µM) (red) treated larvae. **(d)** Quantification of mEPSP amplitude, eEPSP amplitude and Quantal content of *unc13A*^{Null} control (grey) and PhTx (red) treated larvae. There is a decrease in both mEPSP amplitude and eEPSP amplitude and no change in Quantal content between *unc13A*^{Null} treatment groups. Statistics: Students unpaired T-test or Mann-Whitney U test, *$p \leq 0.05$, **$p \leq 0.01$, ***$p \leq 0.001$, not significant (n.s.) $p > 0.05$, mean ± SEM. For details see Table 2. Modified from Böhme et al. (2019).

It has been previously shown that the N-terminal region of unc13A was responsible for localising the protein to ensure proper Ca^{2+}-channel SV coupling distances at AZs (Reddy-Alla et al., 2017). I wanted to explore whether homeostatic plasticity could be induced in animals that were lacking both endogenous unc13A and unc13B but where a GFP tagged unc13A, lacking the N-terminal region, was re-expressed (C-term-GFP). This would leave the catalytic and interaction domains (e.g. MUN, C1 and C_2B domains) intact, with the exception of the Calmodulin binding site. In control larvae, a full length GFP tagged unc13A was expressed in the same null background (Unc13A-GFP). Both genotypes displayed comparable evoked eEPSP responses (Fig 13) confirming that animals expressing C-term-GFP retained the ability to generate a large response to single stimuli. While this genotype had been previously shown to have reduced amplitudes compared to Unc13-GFP, those experiments were performed at higher Ca^{2+} (1.5 mM) and Mg^{2+} (20 mM) concentrations and in a TEVC configuration (Reddy-Alla et al., 2017). The amplitudes of mEPSPs in both genotypes control treatments were also similar. NMJs of animals expressing C-term-GFP displayed a higher mEPSP frequency (data not shown), as had been previously reported. Larvae of both genotypes were incubated using the PhTx method described previously (Figure 12), before washing and transfer to a toxin-free recording chamber. Current clamp recordings revealed mEPSP amplitudes that were reduced following PhTx treatment in both genotypes. Evoked eEPSP responses were maintained in Unc13A-GFP but clearly reduced in C-term-GFP animals after PhTx treatment, compared to non-PhTx treated controls. On calculation of the quantal content,

PhTx treated Unc13-GFP animals possessed increased quantal release. Quantal content was lower for PhTx treated C-term-GFP compared to control treatment. Thus, the N-terminal region of Unc13A is required for PHP.

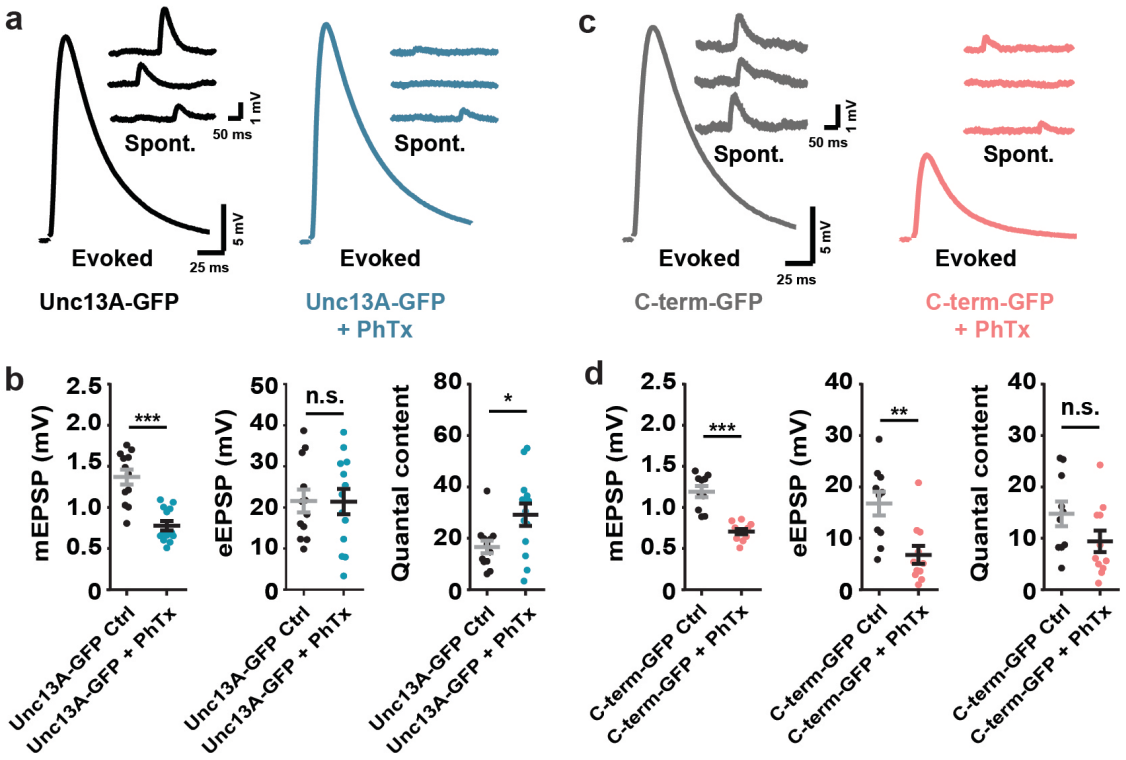

Figure 13: The N-terminal portion of Unc13A is essential for rapid PHP.

(a) Representative eEPSP (evoked) and mEPSP (spontaneous) traces of Unc13A-GFP control (black) and PhTx (20 µM) (blue) treated third instar larvae, recording from muscle 6 abdominal segments A2/A3 (0.4 mM Ca^{2+}). **(b)** Quantification of mEPSP amplitude, eEPSP amplitude and Quantal content of Unc13A-GFP control (black) and PhTx (blue) treated larvae. Quantal Content is increased in wild-type PhTx treated larvae as mEPSP amplitude is reduced with no change in eEPSP amplitude compared to controls. **(c)** Representative eEPSP (evoked) and mEPSP (spontaneous) traces of C-term-GFP control (grey) and PhTx (20 µM) (red) treated larvae. **(d)** Quantification of mEPSP amplitude, eEPSP amplitude and Quantal content of C-term-GFP control (grey) and PhTx (red) treated larvae. There is a decrease in both mEPSP amplitude and eEPSP amplitude and a slight non-significant decrease in Quantal content between C-term-GFP treatment groups. Statistics: Students unpaired T-test or Mann-Whitney U test, *p ≤ 0.05, **p ≤ 0.01, ***p ≤ 0.001, not significant (n.s.) p > 0.05, mean ± SEM. For details see Table 2. Modified from Böhme et al. (2019).

While the above experiments are well suited for examining the induction of PHP, they do not report on the time course of this plasticity. I wanted to

examine the induction of PHP in these genotypes and so recorded the response before, during and after PHP induction. Initial mEPSP and eEPSP (0.2 Hz) current clamp recordings were performed in the absence of PhTx. This allowed a cell-specific baseline for each parameter to be established. PhTx was then added to the recording chamber and remained continuously present from this point forward. Animals were allowed to incubate for 200 seconds without recording. Stimulation was then resumed at 0.2 Hz continuously for 500 seconds. Over 50 second intervals, spontaneous responses were identified to determine mEPSP frequency and the mean mEPSP amplitude. The average eEPSP amplitude was also determined over the same 50 second interval. A lower concentration of 4 μM PhTx was used (compared to 20 μM), as also used in Figure 11. PhTx was continuously present during long-term recording with stimulation.

In both Unc13A-GFP and C-term-GFP expressing animals, mEPSP amplitude was strongly decreased with PhTx addition and there was no divergence between genotypes over time (Figure 14b). mEPSP frequency following PhTx application was not initially reduced but did decrease noticeably in both genotypes over time (Figure 14c). The drop in frequency is likely caused by the continuous intermittent AP stimulation, as previously observed and described in Figure 11. Both of the mEPSP amplitude and mEPSP frequency observations were in line with that initial PhTx characterisation experiment. Despite eEPSP amplitudes in both genotypes initially being the same and both dropping after PhTx application, at later time points there is a stronger reduction in C-term-GFP animals compared to the Unc13A-GFP control (Figure 14d). It had previously been reported in an experiment with intermittent stimulation in the presence of PhTx that eEPSP amplitude and hence quantal content rises over time in controls (Frank et al., 2006). These animals did recover to pre-PhTx eEPSP amplitudes however. This is likely due to the continuous intermittent stimulation. As with mEPSP frequency (Figure 14c) and as shown in Figure 11, the toxin is use-dependent. An increase of quantal content was observed after PhTx application in Unc13A-GFP animals, which was on average maintained over the course of the experiment. While C-term-GFP animals also exhibited an initial slight increase in quantal content, it was lower and by 400 seconds

following PhTx application was significantly lower than the levels in Unc13-GFP animals (Figure 14e).

The reason behind the decrease of quantal content in the C-term-GFP genotype is perhaps again due to the loss of events with increased receptor blockade over time. This experiment confirmed the homeostatic plasticity defect previously seen in C-term-GFP. It also provided an overview of the time course of plasticity induction. C-term-GFP animals fail to deal with the pharmacological insult to glutamate receptors, diverging over time from Unc13A-GFP expressing animals, which maintain an increased quantal content.

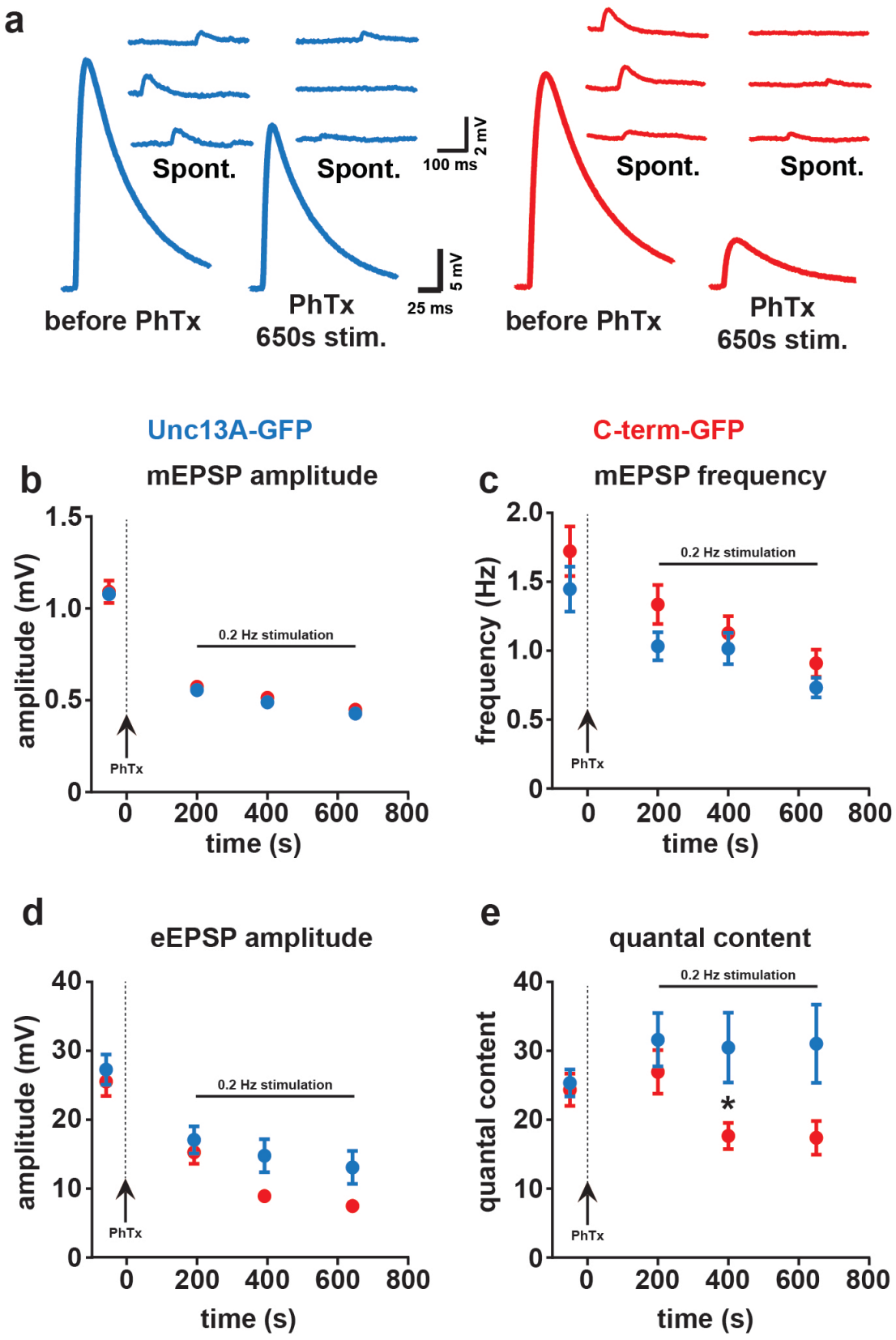

Figure 14: Time course of PHP induction following PhTx application in larvae expressing full length Unc13A or lacking the N-terminus of Unc13A (C-term-GFP).

(a) Representative eEPSP (evoked) and mEPSP (spontaneous) traces of Unc13A-GFP (blue) and C-term-GFP (red) before PhTx application and after 650 s PhTx (4 µM) treatment with 0.2 Hz stimulation in third instar larvae, recording from muscle 6 abdominal segments A2/A3 (0.4 mM Ca^{2+}). **(b)** Quantification of mEPSP amplitude; mEPSP amplitude is greatly reduced following PhTx application in both genotypes but further reduction with stimulation is minimal **(c)** Quantification of mEPSP frequency; mEPSP frequency only slightly decreases in both genotypes following PhTx application but continued stimulation reduces it further over time **(d)** Quantification of eEPSP amplitude; PhTx application reduces eEPSP amplitude in both genotypes, but with continued stimulation time, Unc13A-GFP amplitudes are maintained while C-term-GFP amplitudes continue to decrease **(e)** Quantification of Quantal Content: Quantal Content is slightly increased in both genotypes following PhTx application but diverges thereafter with time and continued stimulation, QC is maintained in Unc13A-GFP larvae but decreases in C-term-GFP larvae and the difference is significant 400 s after PhTx application. Statistics: Students unpaired T-test or Mann-Whitney U test, *$p \leq 0.05$, not significant (n.s.) $p > 0.05$, mean ± SEM. For details see Table 2.

We had seen that Phtx induced protein increases of Unc13A and Syx-1A at the AZ were dependent on BRP, as *brp*^{null} animals lacked such remodelling (Böhme et al., 2019). In order to explore the relevance of BRP for PHP, I made use of the same *brp*^{null} animals. Evoked responses and hence quantal release were lower in *brp*^{null} mutants compared to wildtype. Despite this, *brp*^{null} larvae displayed a relative increase in quantal content following PhTx treatment, as in wildtype (Figure 15b,d). This surprising result implied that even in a situation where the AZ structure is severely disrupted, PHP is possible on these rapid timescales. It also suggests that the structural reorganisation of the AZ and the compensatory increase in neurotransmitter release are independent of each other, at least at this short timescale (see Discussion).

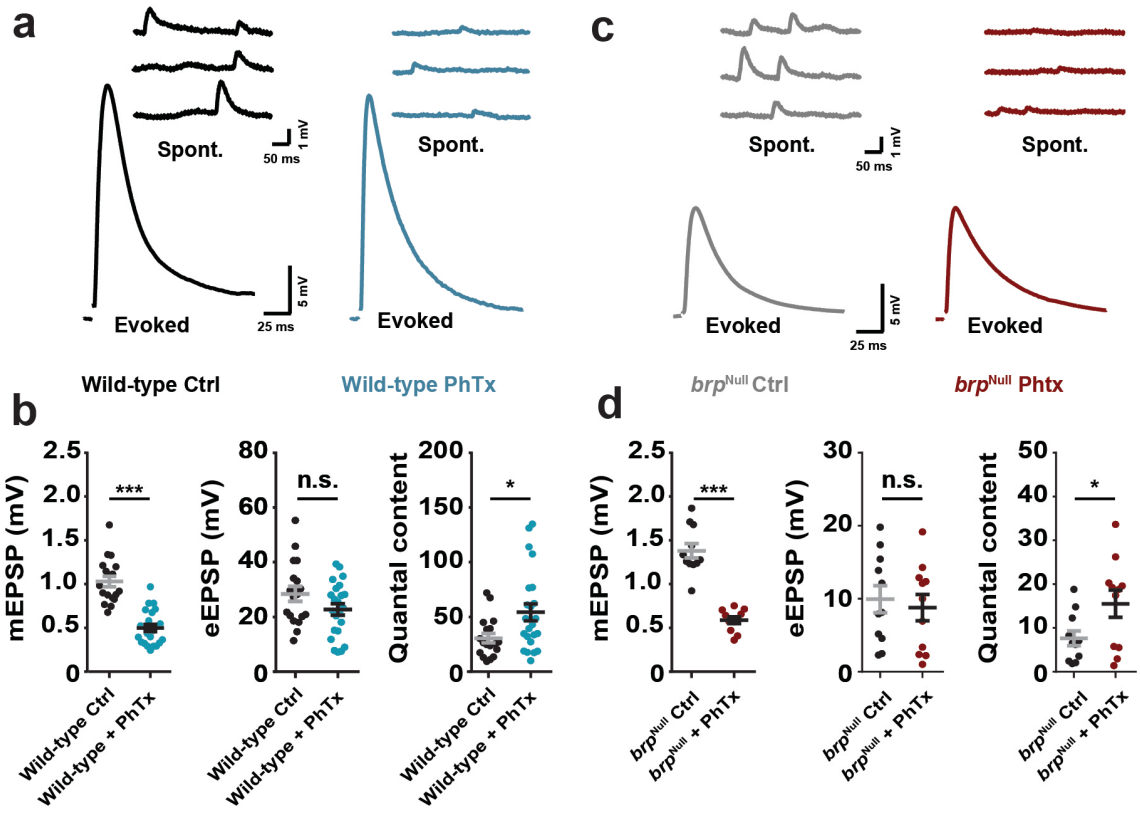

Figure 15: BRP is dispensable for rapid PHP.

(a) Representative eEPSP (evoked) and mEPSP (spontaneous) traces of wild-type control (black) and PhTx (20 µM) (blue) treated third instar larvae, recording from muscle 6 abdominal segments A2/A3 (0.4 mM Ca^{2+}). **(b)** Quantification of mEPSP amplitude, eEPSP amplitude and quantal content of wild-type control (black) and PhTx (blue) treated larvae. Quantal content is increased in wild-type PhTx treated larvae as mEPSP amplitude is reduced with no change in eEPSP amplitude compared to controls. **(c)** Representative eEPSP (evoked) and mEPSP (spontaneous) traces of *brp*^{Null} control (grey) and PhTx (20 µM) (red) treated larvae. **(d)** Quantification of mEPSP amplitude, eEPSP amplitude and Quantal content of *brp*^{Null} control (grey) and PhTx (red) treated larvae. Quantal Content is increased in *brp*^{Null} PhTx treated larvae as mEPSP amplitude is reduced with no change in eEPSP amplitude compared to controls. Statistics: Students unpaired T-test or Mann-Whitney U test, *$p \leq 0.05$, ***$p \leq 0.001$, not significant (n.s.) $p > 0.05$, mean ± SEM. For details see Table 2. Modified from Böhme et al. (2019).

5.6 Transport of BRP in the axon

PHP and the structural rearrangement of protein at AZs occur rapidly. Both are observed in larvae within 10 minutes of incubation with PhTx. I wondered what the source of additional protein being added to AZs might be. One possibility is that AZ proteins are freshly transported to synapses and so I decided to

investigate this using animals expressing mCherry tagged BRP. It was noted in this genotype that fluorescent particles of BRP-mCherry could be clearly seen in the motoneuronal axons of these animals. While some particles did not move, others moved in an anterograde or retrograde fashion (Figure 16a). This movement was not consistent and often involved brief pauses before a particle was seen to continue. PhTx was acutely applied to the extracellular solution and imaging initiated immediately. It was noted that the proportion of particles that were motile increased in both directions within 10 minutes (Figure 16b). In some cases, only motile particles were observed following PhTx application. If the motility of BRP in the axon increases with PhTx incubation but BRP is not required for functional PHP on short timescales (Figure 15), I wondered if this effect indicated a requirement for BRP on longer timescales.

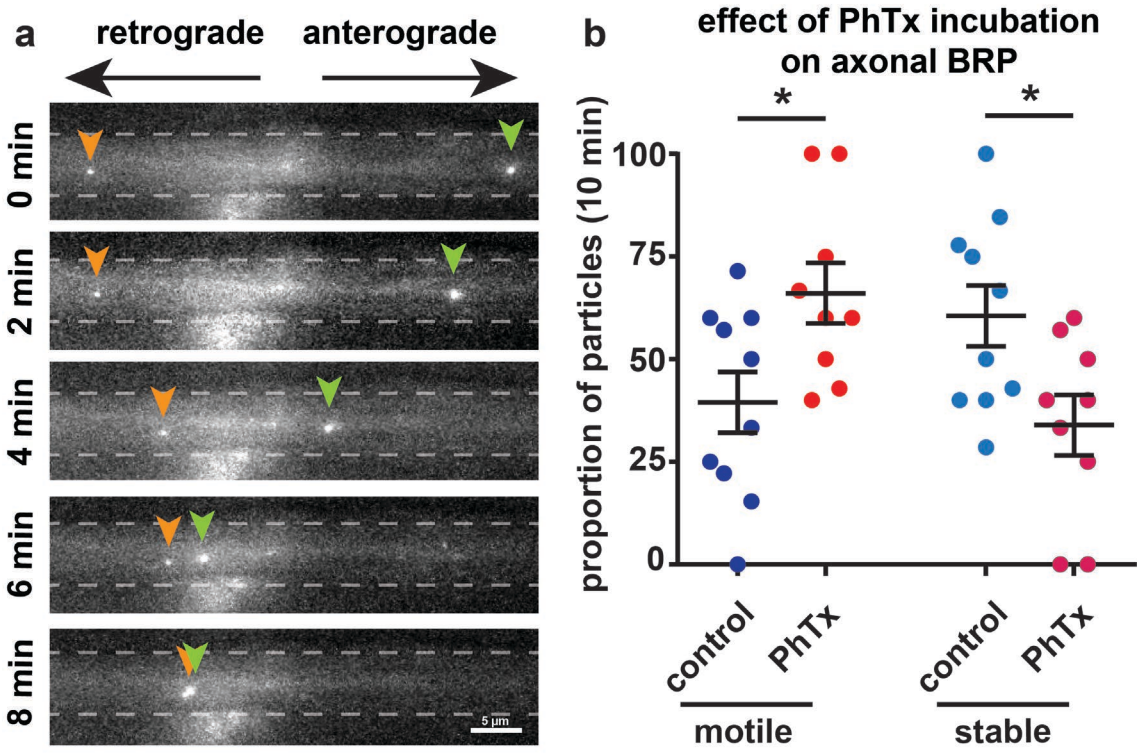

Figure 16: Axonal BRP motility increases following PhTx application.

(a) Fluorescent particles are observed moving in the axons near muscle 4, abdominal segments A2-A4 of third instar larvae expressing mCherry tagged BRP. Over time (0-8 min) particles move anterogradely towards the NMJ and retrogradely away from it (scale bar: 5 µm) **(b)** With PhTx application, there is a significant increase in the proportion of particles observed to be motile rather than stationary. Statistics: Students unpaired T-test, *p ≤ 0.05, mean ± SEM. For details see Table 2.

5.7 Chronic Homeostatic Plasticity

PHP can also occur in response to a more significant and long-term disruption of glutamate receptors at the postsynapse. Glutamate receptors at the *Drosophila* postsynapse can possess either GluRIIA or GluRIIB as their fifth subunit (DiAntonio et al., 1999). Loss of receptors containing GluRIIA results in expression of only receptors containing GluRIIB and reduces the general NT sensitivity of the postsynapse. Genetic removal of GluRIIA however does not lead to an obvious defect following evoked stimulation (Figure 17a,c). *gluRIIA*^{Null} animals have reduced mEPSPs, as with PhTx treatment, due to decreased sensitivity to released glutamate. Presynaptic release is subsequently increased to compensate, reaching eEPSP amplitudes comparable to wildtype. Levels of AZ proteins Unc13A and BRP also increase drastically at the NMJ upon GluRIIA loss (Figure 17b,d). This manipulation of GluRIIA is more severe than PhTx as it occurs over the lifetime of the animal and so this form of homeostatic plasticity differs in several key ways. It is for example dependent on translation, while PhTx-induced PHP is translation independent. The increase in quantal content is also more pronounced than with PhTx treatment.

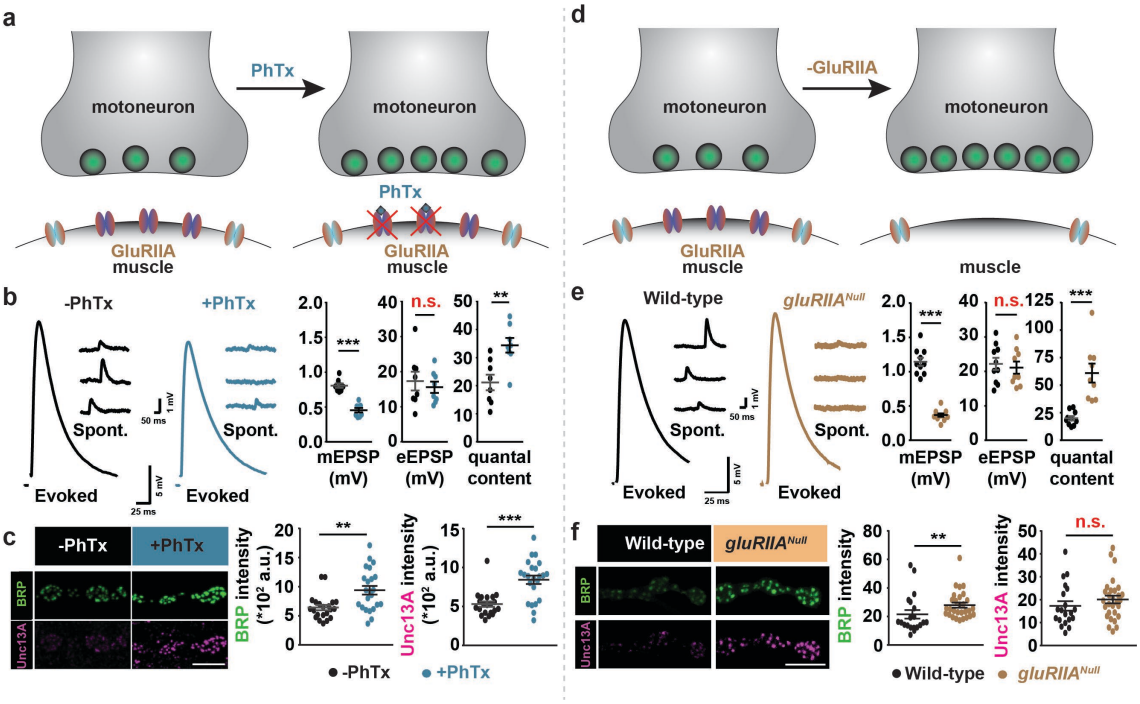

Figure 17: Chronic induction of PHP results in more robust functional and structural synaptic homeostatic plasticity.

(a,b,c) In wildtype animals, application of PhTx leads to an increase in quantal content within 10 minutes to compensate for glutamate receptor block. This is accompanied by a structural reorganisation (increase) of AZ proteins. b replotted from Figure 12 a, b **(d,e,f)** Genetic deletion of GluRIIA receptors over the life of the animal leads to a much more robust increase in quantal content and a greater increase in AZ proteins compared to the pharmacological experiment. Statistics: Students unpaired T-test or Mann-Whitney U test, **p ≤ 0.01, ***p ≤ 0.001, not significant (n.s.) p > 0.05, mean ± SEM. For details see Table 2. Scale bars: 5 µm. Data in c, f provided by Mathias Böhme. Modified from Böhme et al. (2019).

I wanted to identify if proteins that were non-essential for short-term functional PHP, instead played a role with long-term chronic induction of PHP. I made use of null mutants for both BRP and GluRIIA (*brp*^{Null};*glurIIA*^{Null}), to determine whether BRP played a more important role in chronically induced PHP, which is implied by the increase in BRP motility in the trafficking experiment (Figure 16). The primary point of interest was the loss of functional plasticity. Comparing *brp*^{Null} to *brp*^{Null};*glurIIA*^{Null}, evoked amplitudes were significantly reduced with GluRIIA loss and quantal content did not increase to compensate (Figure 18a,b).

Synaptic BRP levels increased comparing wildtype to *gluRIIA*^{Null}, as structural plasticity was induced. Synaptic BRP was absent in both *brp*^{Null} genotypes (Figure 18c,d).

I wanted to investigate the reorganisation of Unc13A. When considering changes in synaptic Unc13A levels, BRP is often used as a marker to identify AZs. As BRP was absent from the BRP null genotypes, Unc13A levels were instead analysed over the entire NMJ for all genotypes. There was a slight increase in average Unc13A levels comparing wildtype to *gluRIIA*^{Null} NMJs. This was not statistically significant however, likely due to the fact that in this case, analysis of Unc13A intensity was not restricted to AZs. As a result, regions with unspecific binding by the primary antibody were also considered (which is prone to background staining). Comparing *brp*^{Null} to *brp*^{Null}*;glurIIA*^{Null}, there was no increase in synaptic Unc13A levels (Figure 18c,d).

These data confirmed that on longer timescales BRP is vital for both structural and functional plasticity, uncovering a difference to short-term homeostatic plasticity, which only required BRP for structural rearrangement.

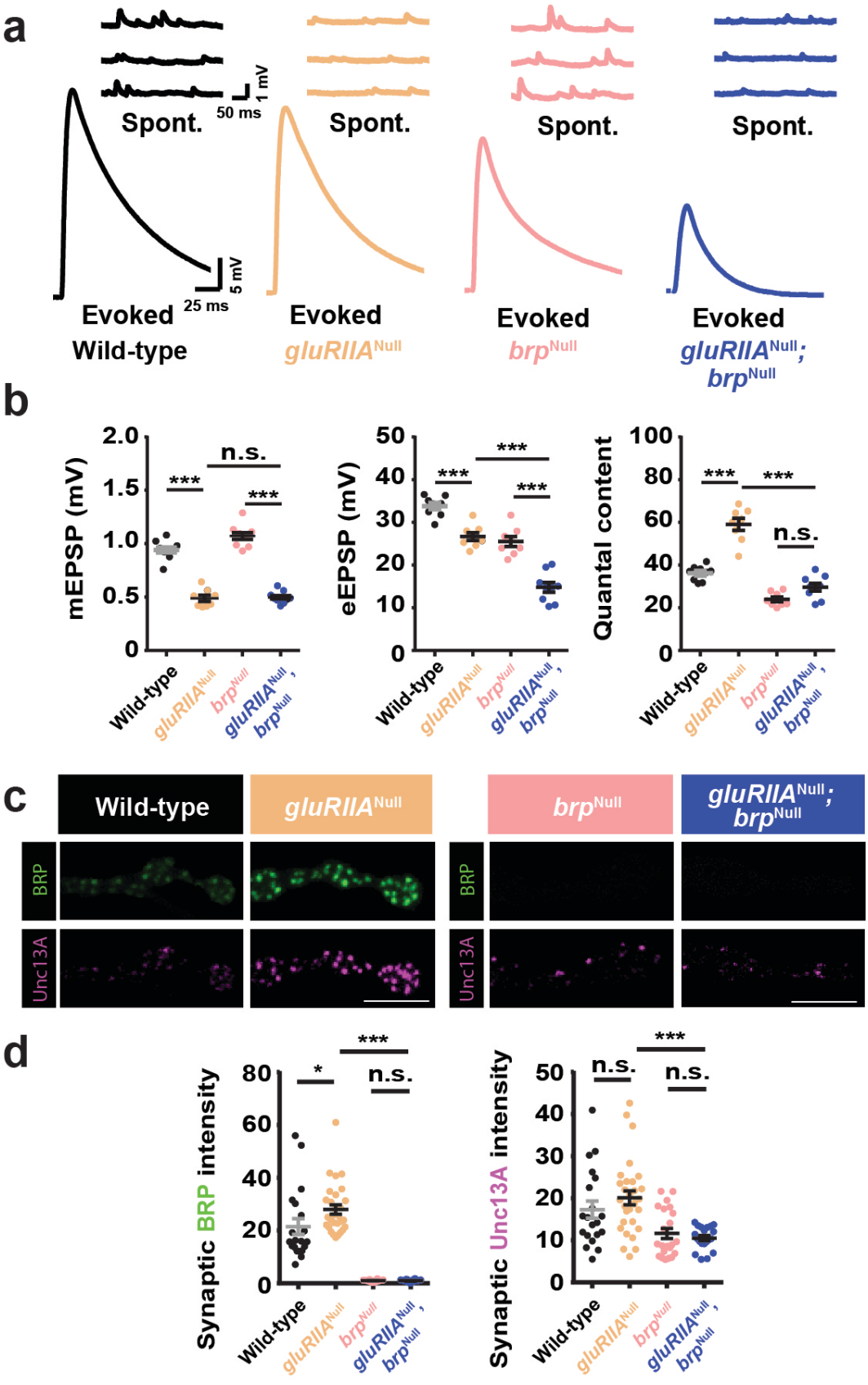

Figure 18: BRP is essential for both functional PHP and structural rearrangement with chronic loss of GluRIIA.

Figure 18 continued (a) Representative eEPSP (evoked) and mEPSP (spontaneous) traces of wild-type control (black), *gluRIIA*^{Null} (gold), *brp*^{Null} (pink) and *gluRIIA*^{Null};*brp*^{Null} (dark blue) larvae. **(b)** Quantification of mEPSP amplitude, eEPSP amplitude and Quantal Content. mEPSP amplitudes are decreased in both *gluRIIA*^{Null} genotypes. eEPSP amplitudes are reduced in *gluRIIA*^{Null} and *brp*^{Null} compared to wild-type but reduced to a much greater extent in *gluRIIA*^{Null};*brp*^{Null} double mutants. Quantal content is increased comparing *gluRIIA*^{Null} to wild-type animals but there is no change in Quantal Content in *brp*^{Null} animals, regardless of GluRIIA loss. **(c)** Representative confocal images of third instar NMJs at muscle 4 abdominal segments A2-A4 immunolabelled for BRP and Unc13A (scale bars: 5 µm) **(d)** Quantification of synaptic BRP and Unc13A. Left: BRP increased in *gluRIIA*^{Null} animals compared to wild-type. BRP was absent in both *brp*^{Null} genotypes. Right: Unc13A intensity was slightly increased in *gluRIIA*^{Null} animals compared to wild-type (non-significant: see text). Unc13A intensity was unchanged in both *brp*^{Null} genotypes. Statistics: One-way ANOVA with Tukey's multiple comparison test, *$p \leq 0.05$, ***$p \leq 0.001$, not significant (n.s.) $p > 0.05$, mean ± SEM. For details see Table 2. Data in a, b provided by Pragya Goel. Modified from Böhme et al. (2019).

Finally, I wondered if disrupting transport of AZ proteins to the NMJ could affect PHP in the chronic situation. I had already seen that BRP-mCherry movement in the axon is increased following PhTx application (Figure 16). App-like interacting protein (aplip-1) acts as an adapter protein for kinesin and cargo vesicles, facilitating transport along the axon towards the NMJ. It had been seen that aplip-1 knockdown lead to accumulations of BRP and Unc13A in the axon. I made use of larvae lacking GluRIIA and possessing a loss of function point mutation in aplip-1 (*gluRIIA*^{Null}*;aplip-1*^{ek4}), that prevents binding of aplip-1 to Kinesin Light Chain (KLC) (Horiuchi et al., 2005; Siebert et al., 2015).

Comparing wildtype to *gluRIIA*^{Null} and *aplip-1*^{ek4} to *aplip-1*^{ek4}*;glurIIA*^{Null}, mEPSP amplitudes decreased for both comparisons. There was also a trend for decreased evoked amplitudes upon GluRIIA loss. Quantal content however was significantly increased between wildtype and *gluRIIA*^{Null}. There was a comparatively smaller increase in quantal content for *aplip-1*^{ek4} vs. *aplip-1*^{ek4}*;glurIIA*^{Null}, indicating a partial defect in functional PHP (Figure 19a,b).

Average BRP intensity levels increased from wildtype to *gluRIIA*^{Null} animals but this was not the case when comparing *aplip-1*^{ek4} to *aplip-1*^{ek4}*;glurIIA*^{Null} (Figure 19c,d). While Unc13A levels increased for both comparisons, this was only statistically significant for w1118 vs. *gluRIIA*^{Null}, supporting the previous

observation of a partial defect in plasticity. From this I could conclude that aplip-1 plays a role in establishing PHP in the chronic situation. Aplip-1 is at least partially responsible for transportation of AZ proteins and the upregulation of release in PHP. This loss of plasticity was less pronounced than seen previously upon BRP deletion, likely due to the fact aplip-1 is only one of many such adapters and that extensive redundancy exists to overcome such perturbations.

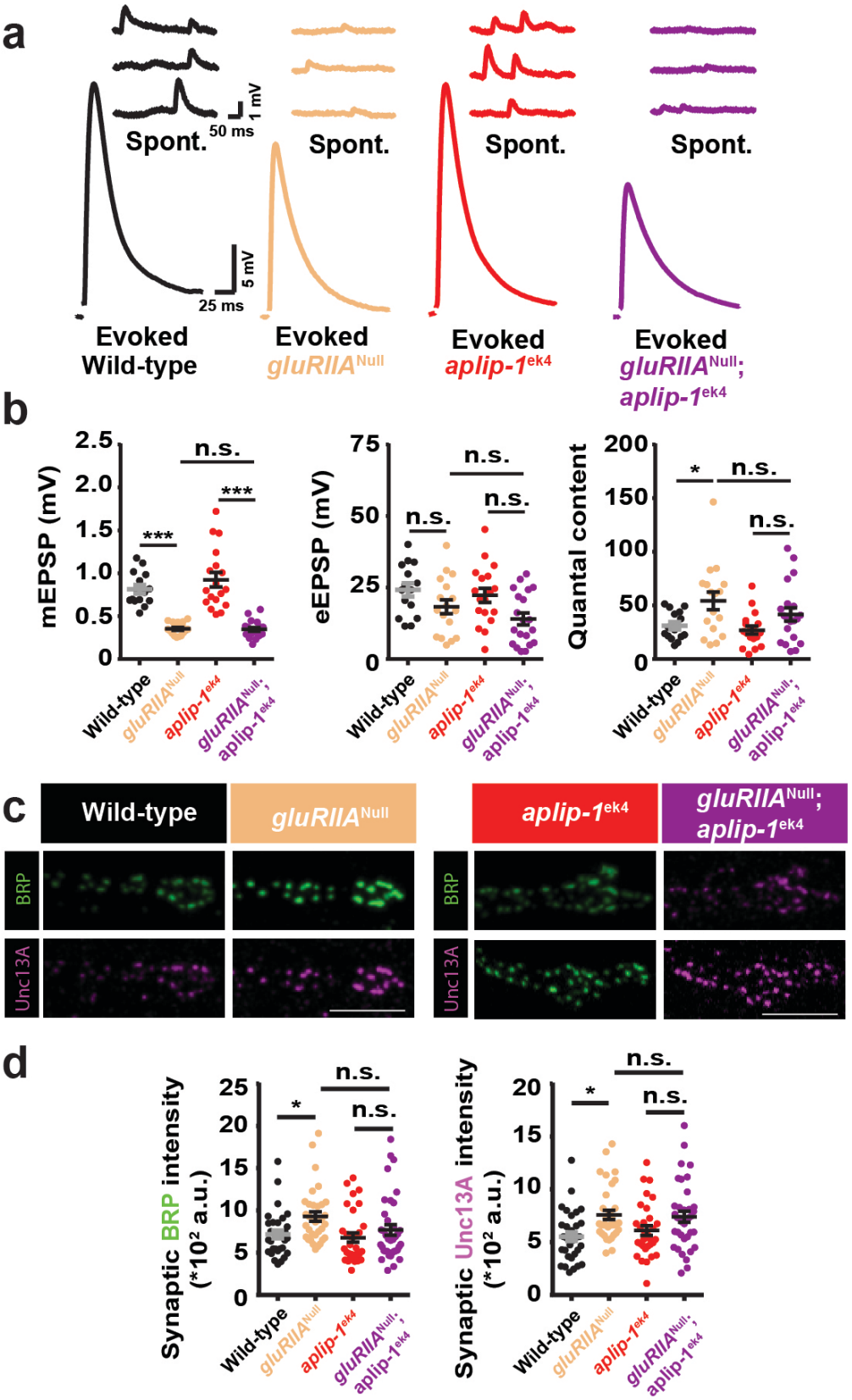

Figure 19: Transport adapter Aplip-1 is essential for both functional PHP and structural rearrangement with chronic loss of GluRIIA.

Figure 19 continued (a) Representative eEPSP (evoked) and mEPSP (spontaneous) traces of wild-type control (black), *gluRIIA*^{Null} (gold), *aplip-1*^{ek4} (red) and *gluRIIA*^{Null}; *aplip-1*^{ek4} (purple) larvae. **(b)** Quantification of mEPSP amplitude, eEPSP amplitude and Quantal Content. mEPSP amplitudes are decreased in both *gluRIIA*^{Null} genotypes. eEPSP amplitudes are slightly decreased in both *gluRIIA*^{Null} genotypes. Quantal content is increased comparing *gluRIIA*^{Null} to wild-type animals. There is only a slight increase in Quantal Content of *gluRIIA*^{Null}; *aplip-1*^{ek4} animals compared to *aplip-1*^{ek4} animals. **(c)** Representative confocal images of third instar NMJs at muscle 4 abdominal segments A2-A4 immunolabelled for BRP and Unc13A (scale bars: 5 µm) **(d)** Quantification of synaptic BRP and Unc13A. Left: BRP intensity increased in *gluRIIA*^{Null} animals compared to wild-type. BRP intensity was unchanged comparing both *aplip-1*^{ek4} genotypes. Right: Unc13A intensity was increased in *gluRIIA*^{Null} animals compared to wild-type. Unc13A intensity was unchanged comparing both *aplip-1*^{ek4} genotypes. One-way ANOVA with Tukey's multiple comparison test, *$p \leq 0.05$, ***$p \leq 0.001$, not significant (n.s.) $p > 0.05$, mean ± SEM. For details see Table 2. Data in c, d provided by Mathias Böhme. Modified from Böhme et al. (2019).

5.8 Summary of Results

The key findings of these experiments were as follows:

Lipid modulation of cellular processes and neurotransmission

- It is possible to efficiently load, uncage and observe PI(4,5)P_2 localisation in vivo.
- Acutely uncaged PI(4,5)P_2 has detectable effects on actin reorganisation and exocytosis.
- PMA enhances NT release and the RRP at the *Drosophila* NMJ but has no obvious effect on spontaneous neurotransmission.

Presynaptic Homeostatic Plasticity

- The priming protein Unc13A is essential for rapid functional PHP.
- The N-terminus of Unc13A is also essential for rapid functional PHP.
- The scaffold protein BRP is not necessary for rapid functional PHP.
- Axonal transport of BRP increases following application of PhTx.
- BRP and the adapter protein Aplip-1 are important during both functional PHP and structural reorganisation at the AZ during chronic induction of homeostatic plasticity.

6 Discussion

Initially inositol phospholipids were discovered to be important for exocytosis as their metabolism affected secretion in chromaffin cells (Eberhard et al., 1990). Secretion of tritiated norepinephrine from these chromaffin cells was inhibited by PLC metabolism of $PI(4,5)P_2$ in a reaction requiring ATP. It was subsequently discovered that the generation of $PI(4,5)P_2$ was important for dense core vesicle (DCV) secretion and that this was Ca^{2+} dependent (Hay et al., 1995; Holz et al., 2000). In regard to SVs at the membrane, $PI(4,5)P_2$ was found to positively modulate the RRP and priming (Di Paolo et al., 2004; Gong et al., 2005; Milosevic et al., 2005). $PI(4,5)P_2$ is enriched at sites of vesicle docking in microdomains of the plasma membrane (James et al., 2008; van den Bogaart et al., 2011). Most of these early experiments were performed by making fairly disruptive alterations to cellular systems and without the ability to uncage PI(4,5)P2 acutely .

6.1 Benefits of uncaging $PI(4,5)P_2$

Previous studies involving the study of protein-lipid interactions have taken broadly different approaches to unearth the specifics of exocytosis at the synapse. Mutation of amino acid residues in relevant lipid binding proteins was one such approach. The C2 domains of syt-1 and Munc13 were altered in an attempt to inhibit $PI(4,5)P_2$ binding (Li et al., 2006; Shin et al., 2010). Release probability was reduced in the case of syt-1 C_2B mutants (Li et al., 2006). Exocytosis with sustained stimulation was lower in Munc13 C_2B mutants (Shin et al., 2010). These mutations interfere with sites of Ca^{2+}-dependent lipid binding however so it becomes difficult to ascertain if it is rather the perturbed Ca^{2+} interaction at physiological conditions that affects exocytosis or phospholipid binding itself, if indeed these are separate at all.

Lipids cannot be easily manipulated (i.e. mutation of the encoding genes) as is the case for proteins, and so we must rely on altering their levels instead. Interference with the kinases responsible for the generation of phospholipids

was approach previously used (Di Paolo et al., 2004). Knockout of the neuronal phosphatidylinositol-4-phosphate 5-kinase type Iγ, PIPKIγ, lead to a reduction of the RRP, spontaneous events and a vesicle recycling defect consistent with impaired vesicular trafficking in neurons cultured from mice that die within 24 hours of birth (Di Paolo et al., 2004). In mouse chromaffin cells, large dense core vesicle (LDCV) exocytosis was also affected by PIPKIγ KO. There was a reduction of $PI(4,5)P_2$ at the membrane and a subsequent reduction of the RRP and priming rate (Gong et al., 2005).

Conversely, upregulation of $PI(4,5)P_2$ levels by overexpressing PIPKIγ or injecting it directly was shown to be successful in increasing $PI(4,5)P_2$ and hence the RRP and LDVC secretion. The effect on exocytosis can be reversed by expression of a phosphatase against $PI(4,5)P_2$, synatpojanin-1 (Chang-Ileto et al., 2011; Milosevic et al., 2005). A major downside of these approaches is that modulation occurs over long timescales, or in the case of the invasive injection, is already biologically active prior to localisation. A benefit of the method I describe here is the speed of $PI(4,5)P_2$ modulation (Walter et al., 2017). Rather than tens of seconds, $PI(4,5)P_2$ is uncaged immediately and already localised at the plasma membrane (Figure 7). However, defined localisation within the cell of uncaged $PI(4,5)P_2$ is uncertain, leading to possible $PI(4,5)P_2$ increases elsewhere (Walter et al., 2017). $PI(4,5)P_2$ localises not only over the plasma membrane but at other membranes throughout the cell, including internal cellular structures (Figure 7b). There is additional potential for knock-on effects as it metabolised to agents such as DAG.

Despite the confirmation of $PI(4,5)P_2$ potentiating exocytosis in other systems, no immediate change in the probability of release was observed with uncaging at the *Drosophila* NMJ, only a slight protective effect against reductions in amplitude due to subsequent stimulation (Figure 9). It is unknown to what degree the caged lipid is loaded and access to *Drosophila* larval NMJ synapses is uncertain. Uncaging experiments in cell culture provide much greater access to the membrane than the *Drosophila* NMJ (Figure 8).

6.2 PI(4,5)P_2 & Actin

Phosphoinositides play a vital role in cell migration due to its role in regulating the actin cytoskeleton. PI(4,5)P_2 is produced at focal adhesions. When local PI(4,5)P_2 synthesis is lost, cell adhesion by integrin-ligand binding and ultimately integrin-actin force coupling are perturbed (Legate et al., 2011). PI(4,5)P_2 is concentrated at patches of ruffling lamella in migrating cells that also exhibit high levels of filamentous actin (f-actin) (Golub and Caroni, 2005). Focal adhesion proteins such as α-actinin, kindlin, talin and vinculin bind PI(4,5)P_2 (Saarikangas et al., 2010; Senju and Lappalainen, 2019). Vinculin-talin binding and binding of vinculin to actin filaments, is regulated by PI(4,5)P_2, and serves as part of the important bridge between the cytoskeleton and focal adhesions (Chinthalapudi et al., 2014; Ezzell et al., 1997). Cellular migration dependent on adhesion is referred to as mesenchymal migration. At the leading edges of such migrating cells, lamellipodia are centres of actin cytoskeletal rearrangement (Senju and Lappalainen, 2019). Actin nucleation of f-actin branches is initiated by the Arp2/3 complex, which itself is activated by neuronal Wiskott-Aldrich Syndrome protein (N-WASP). N-WASP moves from a closed inactive state to an open conformation by interaction with Cdc42, a rho family GTPase, and PI(4,5)P_2 (Prehoda et al., 2000; Rohatgi et al., 2000). Formins are involved in actin nucleation and polymerisation. mDia1 and mDia2 are targeted to the membrane via their N-terminus. (Gorelik et al., 2011; Ramalingam et al., 2010). Conversely, depolymerisation by Actin-depolymerizing-factor (ADF)/cofilins and inhibition of elongation by heterodimeric actin-capping protein (CP) is reversed by PI(4,5)P_2. Proteins that downregulate the formation of actin structures are bound by PI(4,5)P_2 at the membrane and restricted to an inactive state (Kim et al., 2007; Zhao et al., 2010). Moving away from nucleation of existing f-actin at lamellipodia, the actin polymerisation protein, profilin, has also been shown to interact with PI(4,5)P_2 (Skare and Karlsson, 2002).

Actin and PI(4,5)P_2 play a part in regulating clathrin-mediated endocytosis. Coat and actin network assembly is linked to higher levels of PI(4,5)P_2. Disassembly is associated with lower PI(4,5)P_2 levels and coincides with higher synaptojanin-1 (Perera et al., 2006; Sun et al., 2007). Filamentous actin production via Arp2/3 is also reduced with lower PI(4,5)P_2 (Zoncu et al., 2007). BAR and F-BAR

domain proteins interact with $PI(4,5)P_2$ activity during endocytosis. They are present in members of the WASP-family of proteins. The BAR domain protein SNX9 activates actin assembly via N-WASP for example (Yarar et al., 2007). The Arp2/3 complex is also activated by Type I myosins which in turn interact with $PI(4,5)P_2$ (Fernández-Golbano et al., 2014).

I made use of LifeAct tagged with RFP to visualise f-actin (Figure 8). LifeAct is composed of the first 17 aa of Abp140 from *Saccharomyces cerevisiae* (Riedl et al., 2008). A benefit of using LifeAct is that it is less disruptive to actin function than use of actin-fluorophore fusion proteins. In such cases, untagged actin must compensate and mitigate for dysfunction caused by tagged actin. A downside of LifeAct however, is a large degree of background fluorescence likely due to it binding soluble g-actin (Riedl et al., 2008). Another downside is the possible side effects on normal actin organisation. In *Drosophila* germline cells, high expression of LifeAct leads to sterility and strong actin disorganisation (Spracklen et al., 2014). It is proposed that the strong UAS/GAL4 germline driver used is at fault as previous studies making use of considerably weaker germline drivers (Huelsmann et al., 2013; Zanet et al., 2012). Similarly, it has been shown that LifeAct expressed at differing concentrations can have variable effects on severing or elongation of actin in fission-yeast cells (Courtemanche et al., 2016). While these studies claim level of LifeAct to be the primary cause of these aberrant phenotypes, underlying explanations are the sequestration of g-actin by LifeAct or competition and interference with endogenous actin-binding proteins. Nevertheless, as Melak et al. (2017) has noted, there is a host of studies successfully making use of the low toxicity of LifeAct without issue for the visualisation of actin in mice, zebrafish, plants and fungi.

LifeAct has been used as a probe to identify the role of actin and $PI(4,5)P_2$ in determining cell polarity in *C. elegans* (Scholze et al., 2018). $PI(4,5)P_2$ colocalises to similar regions of the embryos and moves ahead of it. Vitally, both rely on the presence of the other. $PI(4,5)P_2$ structures depend on f-actin function, and $PI(4,5)P_2$ alteration affects actin organisation (Scholze et al., 2018). I observed similar actin reorganisation following $PI(4,5)P_2$ uncaging (Figure 8) (Walter et al., 2017).

6.3 PMA as an analogue for DAG

$PI(4,5)P_2$ modulates release further by generation of second messengers and initiating signalling pathways due to its metabolism. $PI(4,5)P_2$ is metabolised by phospholipase C (PLC) enzymes to DAG and inositol 1,4,5-triphoshate (IP_3) (Brose et al., 2004). At the synapse, DAG binds the C1 domains of Protein Kinase Cs (PKC) and Unc13. Experiments performed on bovine adrenal chromaffin cells or hippocampal neurons claimed that the potentiation induced by PMA was via activation of PKC, leading to an increase in the RRP (Gillis et al., 1996; Stevens and Sullivan, 1998). Bisindolylmaleimide (BIS), a PKC inhibitor, interfered with PMA induced potentiation of release and RRP (Stevens and Sullivan, 1998). BIS binds to the catalytic site of PKC and not the DAG binding C1 domain. Stevens and Sullivan also showed an increase in the refiling rate of SVs with PMA that was blocked by BIS. At the *Drosophila* larval NMJ however, it was shown that PMA induced potentiation could increase evoked release despite the use of PKC inhibitors (Song et al., 2002). BIS applied in conjunction with PMA failed to prevent facilitation after 16 minutes, indicating that another target of PMA rather than PKC is responsible for potentiation at the *Drosophila* NMJ. I could confirm that PMA induced potentiation was possible at the *Drosophila* NMJ (Figure 10e, f, g, h). To investigate whether this was due to an increase in the RRP, I performed high frequency stimulation. The data indeed indicate an increase in the RRP (Figure 10i, j).

It has more recently been claimed that PMA induces an increase in Ca^{2+} sensitivity, not RRP size, and BIS blocks this, indicating that PKC is vital (pituitary gonadotropes) (Zhu et al., 2002). At Calyx of Held synapses, where PdBu leads to an increase in exocytosis and spontaneous release, an increase in affinity for Ca^{2+} of the release machinery has likewise been postulated (Lou et al., 2005). With PMA application and subsequent BIS inhibition this was shown to be PKC dependent (Wu and Wu, 2001). Increased potentiation via Ca^{2+} sensitivity has been suggested to occur due to lowering of the energy barrier for vesicular fusion (Basu et al., 2007).

I did not observe an increase in the amplitude of spontaneous release (Figure10 c). The inability of phorbol esters to potentiate spontaneous amplitudes has been observed with PdBu application in *Drosophila* (Ortega et al., 2018). Likewise, in hippocampal culture spontaneous amplitudes were not potentiated by phorbol esters, but the frequency of these events was increased (Stevens and Sullivan, 1998). Increased spontaneous frequency due to phorbol ester application is well established in mammals (Lou et al., 2008). I cannot report any change of spontaneous frequency at the *Drosophila* NMJ following PMA application (Figure10 d). It has been suggested that this effect is due to the maturity of synapses, as young hippocampal culture synapses lacked the effect of PMA application on the frequency while older synapses displayed a far greater number of spontaneous events (Virmani et al., 2005). The claim that this is due to the lack of an established RRP at these synapses is perhaps not comparable to the *Drosophila* larval NMJ however.

Due to the partial effects of PKC inhibitors and similar experiments, it was known that there must be other factors involved in the upregulation of release. Unc13 is a primary target for DAG and phorbol esters. In fact, Unc13 is the primary contributor as explored in hippocampal neurons. (Basu et al., 2007; Rhee et al., 2002). PKC mediated effects are often secondary and Unc18 for example can be activated downstream of PKC (Cijsouw et al., 2014; Edwards et al., 2012; Genç et al., 2014; Nili et al., 2006).

Of course DAG/phorbol esters have functional roles in activating signalling pathways and processes other than exocytosis, some of these receptors include protein kinase D, diacylglycerol kinases α, β, and γ, RasGRPs and chimaerins (Brose et al., 2004).

6.4 Summary of Lipid Signalling and Modulation of Neurotransmission

It can be concluded that loading cg-PI(4,5)P_2 into mammalian cells and acutely uncaging it is an effective way to alter cellular processes such as actin reorganisation. Uncaged PI(4,5)P_2 at the *Drosophila* NMJ does not increase release probability but may prevent a decrease in response to multiple stimulations.

The metabolism of PI(4,5)P2 was not directly examined following uncaging. Rather pharmacological PMA application was used to mimic DAG function. PMA successfully potentiates evoked NT release but has no effect on spontaneous release. This highlights a difference to PMA modulation of neurotransmission at mammalian synapses, which exhibit a sharp increase in the frequency of spontaneous release.

6.5 Presynaptic Homeostatic Plasticity

At the *Drosophila* NMJ, block or deletion of glutamate receptors at the postsynapse leads to a compensatory increase in presynaptic neurotransmitter release to account for the reduced sensitivity of the postsynapse. For this to reliably occur on both short and long timescales the information that receptors are perturbed must travel retrogradely across the synapse. Receptor blockade initiates a signalling pathway or pathways within the muscle postsynapse. This in turn activates retrograde trans-synaptic signalling which links to necessary changes at the presynaptic neuron. The presynapse responds with altered structural organisation of proteins, particularly at the AZ cytomatrix, as well as increased functional neurotransmitter exocytosis.

6.5.1 The postsynaptic origin of presynaptic homeostatic plasticity

The initiation of signalling during induction of presynaptic homeostatic plasticity must originate at the postsynapse. Glutamate receptor activation leads to Ca^{2+} influx and it was speculated that loss of Ca^{2+} influx due to glutamate receptor loss/block was responsible for signal initiation (Haghighi et al., 2003). During normal neurotransmission, Ca^{2+} influx leads to activation and phosphorylation of Ca^{2+}/calmodulin-dependent protein kinase II (CaMKII). Inhibition of CaMKII at the postsynapse by expression of CaMKII inhibitory peptides in the muscle reduces presynaptic neurotransmitter release. Deletion of glutamate receptors should also increase presynaptic neurotransmitter release but muscle expression of constitutively active CaMKII supresses the ability of synapses to upregulate presynaptic release (Haghighi et al., 2003; Li et al., 2018). This indicates that CaMKII signalling in the muscle is required following chronic glutamate receptor loss. On the rapid timescale, levels of observed phosphorylated CaMKII are reduced following PhTx application (Goel et al., 2017). Extracellular Ca^{2+} concentration does not alter the levels of active pCaMKII however, suggesting that Ca^{2+} influx does not influence CaMKII during rapid plasticity. As I will discuss later however, observed changes in protein level cannot always be related to the functional reality and the timing of plasticity can reveal dramatic differences at the *Drosophila* NMJ.

Dystrophin is another negative regulator of synaptic homeostasis at the postsynapse (van der Plas, Mariska C et al., 2006). As a part of the Dystrophin-glycoprotein complex (DGC), it acts to link the muscle actin cytoskeleton to the extracellular matrix. Increased neurotransmitter release occurs due to muscle specific loss of Dystrophin isoforms. Rho GTPases as part of Rho signalling are another important mediator of cytoskeletal changes and vesicle trafficking (Hall, 1998). Rho GTPases move between an active GTP bound state, catalysed by Rho-type guanine nucleotide exchange factors (RhoGEFs), and an inactive GDP bound state, catalysed by Rho GTPase activating proteins (RhoGAPs). Dystrophin interacts with the RhoGAP crossveinless-c (cv-c). Just as with Dystrophin mutation, cv-c mutation (loss of function) results in a significant increase of presynaptic release, without affecting postsynaptic responses (Pilgram et al., 2011). This Dystrophin or cv-c mediated increase of release can be reversed by targeting Cdc42 for mutation, indicating that the Rho GTPase Cdc42 functions downstream of both Dystrophin and cv-c in this pathway (Pilgram et al., 2011). Cdc42 might function in a system with the RhoGEF, Ephexin (Exn), to activate presynaptic Ephs receptor and ultimately modulate $Ca_V2.1$ Ca^{2+} channels during induction of synaptic homeostasis. Exn appears to be more important for long-term synaptic homeostasis and dispensable for rapid PHP however (Frank et al., 2009).

An interesting candidate for plasticity regulation, Importin 13 (imp13) is observed around nuclei of muscles and neurons and is involved in transport of proteins across the nuclear membrane (Giagtzoglou et al., 2009). Similarly to Dystrophin and cv-c, it acts as a negative regulator of presynaptic release. Imp13 mutation results in stronger presynaptic release at low or normal extracellular Ca^{2+}. It is claimed that this phenotype is lost at higher Ca^{2+} concentrations; however, the experiments were performed in current clamp, where it is possible that the maximum stimulated response in both cases has been reached. The probability of release, determined by PPR, is also higher in imp13 mutants (Giagtzoglou et al., 2009). This increase can be reversed by postsynaptic-specific, but not presynaptic-specific, overexpression of imp13. The assumption is made that because visualised BRP is unchanged in these mutants, release site number is also unchanged. Unc13 is more likely to be the

release site generating molecule (Reddy-Alla et al., 2017). It would be appropriate to perform variance-mean analysis to determine the number of release sites (Scheuss and Neher, 2001). In imp13 mutants there is a slight increase in presynaptic intracellular Ca^{2+}, observed by forward filling the cut end of the motoneuron with a Ca^{2+} sensitive dye and imaging at the synaptic bouton (Giagtzoglou et al., 2009).

Target of rapamycin (TOR) has been shown to be important for long-term synaptic homeostasis (Penney et al., 2012). In a chronic homeostatic situation, glutamate receptor mutants lacked presynaptic exocytotic compensation when TOR was specifically lost at the postsynapse, indicating that it controls the retrograde signal. Further supporting this, postsynaptic overexpression of TOR increases presynaptic release. TOR phosphorylates proteins such p70 S6 ribosomal kinases (S6Ks). Cap-dependent translation is modulated by TOR signalling and as an enhancer of cap-dependent translation, S6K is likewise vital for synaptic homeostasis (Penney et al., 2012). Postsynaptic constitutive overexpression of S6K increases presynaptic release. Mutants lacking GluRIIA and one copy of cap-binding complex protein eIF4E, which is also activated by TOR, lack synaptic homeostasis. eIF4E is a translation initiation factor and is required for the increased presynaptic release due to postsynaptic TOR and S6K overexpression. Translation is initiated after eIF4E binds eIF4G, and is inhibited by 4E-BP. As a consequence 4E-BP along with the transcription factor Forkhead box O (Foxo) can act as negative regulators of changes in presynaptic neurotransmitter release (Kauwe et al., 2016).

6.5.2 Retrograde signalling in homeostatic plasticity

There have been several attempts to define the exact molecule responsible for relaying the signal of postsynaptic receptor blockade across the synaptic cleft. For such a process, a presynaptic receptor for this signal would also be required. An initial candidate for retrograde signalling was via secretion of Bone Morphogenic Proteins (BMPs), most being members of the TGF-β superfamily (Marqués et al., 2002). The BMP type II receptor, wishful thinking (Wit), was shown to be important for NMJ synapse development, as abnormal synapse

size, ultrastructure and reduced transmission is reported upon its mutation (Aberle et al., 2002). Mutants of the BMP ligand glass bottom boat (Gbb) were subsequently discovered to display similar synapse abnormalities (McCabe et al., 2003). The phosphorylated transcription factor Mad is a known effector protein of wit signalling and would normally accumulate in motoneuron but is lacking in Gbb mutants. Gbb and Wit are vital for rapid PHP (Goold and Davis, 2007). However, in the case of motoneuronal loss of Gbb it is possible to reverse PHP deficiency by motoneuronal Gbb rescue. Gbb generated in the muscle was not required. This indicates that Gbb is not acting retrogradely as a signal across the synapse. Neuronal retrograde axonal transport and continuous developmental presence of Mad in the neuron is however required for synaptic homeostasis (Goold and Davis, 2007). While the presence of these processes may be important during development, as previously mentioned, rapid and acute increase of vesicular release occurs despite the use of translation blockers and severing the nerve axon, indicating fresh protein from the soma is unnecessary (Böhme et al., 2019; Frank et al., 2006).

One of the best candidates as a retrograde signal is semaphorin 2b (Sema2b) (Orr et al., 2017). Plexins act as receptors for proteins from the semaphorin family. It was postulated that sema2b, secreted from the muscle postsynaptically was binding to presynaptic plexin B (PlexB). Sema2b and PlexB mutants lack rapid PHP. RNAi knockdown of Sema2b postsynaptically in the muscle and PlexB presynaptically in the motoneuron block rapid PHP. The reverse, knockdown of Sema2b presynaptically and PlexB postsynaptically had no effect on PHP. Interestingly, purified SemaB protein applied to SemaB mutants could also rescue rapid PHP. The presynaptic cytoplasmic actin-depolymerisation mediating protein Mical is essential downstream of PlexB (Orr et al., 2017).

Multiplexin, a matrix protein that can be cleaved to produce the signalling factor Endostatin, is involved in presynaptic neurotransmitter release and Ca^{2+} channel upregulation (Wang et al., 2014). PhTx application or co-mutation of glutamate receptors in multiplexin mutants reveals that it is vital during both rapid and chronic PHP, as presynaptic compensation is absent in these two situations. Multiplexin mutants also exhibit decreased Ca^{2+} channel abundance

and reduced Ca^{2+} influx. During induction of homeostasis it is proposed that multiplexin is processed in the synaptic cleft by an unknown protease, producing endostatin that subsequently interacts with $Ca_V2.1$ channels at the presynapse to increase Ca^{2+} influx.

Finally, a candidate for the involvement of immune signalling has been found. Immune Receptor PGRP-LC (Harris et al., 2015). This receptor is located presynaptically and it is proposed to detect a trans-synaptic signal to regulate the RRP during rapid PHP.

6.5.3 Presynaptic molecular components

Increased Ca^{2+} influx is a central observation during the induction of rapid homeostatic plasticity, likely contributing to greater vesicular fusion (Müller and Davis, 2012). Ca^{2+} influx has a direct effect on the probability of vesicular release. The Cac subunit containing Ca^{+}-channel is a vital presynaptic component contributing to PHP. Cac mutants are unable to maintain synaptic homeostasis and so Cac is a downstream target of the retrograde signal (Müller and Davis, 2012). Cac mutants have lower baseline transmission which decreases further with the additional block of postsynaptic glutamate receptors, confirming a defect in rapid PHP (Frank et al., 2006). Cac channels accumulate at the presynapse during rapid homeostatic plasticity and this increase occurs early after PhTx treatment (Böhme et al., 2019; Gratz et al., 2019). Another Ca^{2+} channel subunit, the auxiliary α2δ-3, is presynaptically vital for sustained rapid PHP (Wang et al., 2016). Degenerin/Epithelial Sodium channels (DEG/ENaC) may provide a route for differential Ca^{2+} influx via Cac channels during induction of rapid PHP (Younger et al., 2013). Two subunits of ENaCs are coded for by pickpocket11 and pickpocket16 (ppk11 & ppk16) and are required presynaptically for rapid PHP. Mutation or knockdown of ppk11 & ppk16 abolishes rapid PHP. In the absence of postsynaptic blockade, mutation or knockdown of ppk11 and ppk16 does not affect baseline transmission. Pharmacological application of an ENaC blocker Benzamil also does not affect baseline transmission; however subsequent application of PhTx unveils a defect in induction of rapid PHP. This proves that ENaCs are less important for normal

synaptic release and play a larger role in a situation where PHP becomes necessary. Several propositions are made about how ENaC might contribute to the increase of exocytotic release during PHP. One possibility is that K+ channel inactivation occurs due to ENaC-mediated membrane depolarisation, subsequently broadening action potentials (Younger et al., 2013). The second proposal is that sub threshold membrane depolarisation via ENaC increases basal Ca^{2+} concentration and hence Ca^{2+}-dependent channel facilitation (Younger et al., 2013). It is also not possible to discount that Ca^{2+} itself flows through ENaCs (Younger et al., 2013).

Loss of scaffolding RIMs proteins leads to reduced Ca^{2+} influx and reduced exocytotic release (Müller et al., 2012). RIM mutants lack PHP and fail to upregulate their already low vesicular release in response to glutamate receptor blockade. RIMs are responsible for regulating Ca^{2+} channel level increases and the RRP (Graf et al., 2012). Nonetheless, they still maintain the ability to increase Ca^{2+} influx during acute postsynaptic challenge (Müller et al., 2012). The reduced release of SVs is due to an inability to regulate the RRP during rapid homeostasis (Müller et al., 2012). Another scaffolding protein, Fife, interacts with RIM and is central to proper cytomatrix formation. Rapid PHP is perturbed in fife mutants (Bruckner et al., 2012; Bruckner et al., 2016).

RBP is also required for induction of homeostatic plasticity (Müller et al., 2015). Like RIM mutants, RBP mutants fail to expand the RRP. Unlike RIM however, they also fail to increase Ca^{2+} influx (Müller et al., 2015). This indicates that Ca^{2+} channel accumulation and SV release changes are both downstream of RBP. SV recovery in RBP mutants is reduced compared to wildtype, and the divide between genotypes widens drastically with induction of homeostatic plasticity (Müller et al., 2015).

BRP is a core scaffold protein at the AZ, and as the other AZ scaffold proteins had been determined to be essential for rapid PHP, I wondered if the same might be true for BRP. PHP requires Ca^{2+} channel clustering and increases in vesicular exocytosis, both of which BRP is known to influence (Kittel et al., 2006). BRP null mutants exhibit lower postsynaptic responses to presynaptic stimulation, compared to wildtype (Figure 15). Surprisingly, loss of BRP did not

affect the ability of synapses to maintain this response. Vesicular release was increased due to rapid PHP, indicating that BRP is not essential for rapid PHP.

A range of non-scaffolding proteins are implicated in homeostasis at the presynapse. Complete loss of Unc18/Rop is lethal. Nevertheless, RNAi knockdown or heterozygous mutation have been used to examine its role during rapid PHP (Ortega et al., 2018). Unc18 knockdown confirms that even partial loss has a negative impact on induction of rapid PHP. Unc18 is also implicated in interacting with RIM to establish PHP. Heterozygous loss of both Unc18 and RIM completely abolishes PHP, compared to the partial defect seen in either individual heterozygous null mutant. Syx-1A loss is shown to reverse the defect of PHP seen in the heterozygous Unc18 null mutant (Ortega et al., 2018).

Dysbindin, a gene associated with schizophrenia, in *Drosophila* is involved in establishing PHP at the presynapse in a manner independent of Ca^{2+} influx and Cac, although it may also be downstream of either (Dickman and Davis, 2009). Rab3-GAP (Müller et al., 2011), SNAP-25 and Snapin have been identified as candidates regulating PHP (Dickman et al., 2012). Presynaptic kainate receptor (KAR) subunit KaiRID is required for rapid PHP, as seen in loss of function mutants (Kiragasi et al., 2017). The accessory subunit Neto can modulate KARs and two are expressed at the *Drosophila* NMJ, Neto-α and Netoβ (Han et al., 2019). Although Neto-β is the predominant isoform at the NMJ, it is restricted to the postsynapse and only Neto-α is expressed pre- and postsynaptically. Neto-α null mutants display a deficit of maintaining rapid PHP. Presynaptic overexpression of Neto-α can rescue and even overcompensate for deficient PHP at the NMJ, in animals lacking endogenous Neto-α and KaiRID. It is claimed that Neto-α is crucial and sufficient for rapid PHP (Han et al., 2019).

6.5.4 Unc13 and Homeostatic Plasticity

I investigated the contribution of Unc13 to homeostatic plasticity. As it is a vital SV priming protein, I hypothesised that it would be essential to homeostatic plasticity. There are two isoforms, Unc13A and Unc13B. Previous work showed the differential distribution of each isoform (Böhme et al., 2016). Defining the centre of the AZ by GFP labelled Ca^{2+} channels (Cac-GFP), Unc13A is located

closer to the centre of the AZ than Unc13B. Combining high pressure freeze (HPF) embedding with electron microscopy, it is possible to determine that loss of Unc13A leads to the lack of defined SV docking close to the centre of the AZ. Loss of Unc13A also drastically decreases stimulated exocytosis and synapses have a greatly reduced probability of release. (Böhme et al., 2016) Exocytosis at Unc13A null synapses is also more sensitive than wildtype to Ca^{2+} buffering (EGTA-AM), indicating that activity and hence Ca^{2+} influx at these synapses results in exocytosis of SVs placed further from the Ca^{2+} channel.

Unc13A is responsible for localisation of primed and docked SVs with tight coupling to Ca^{2+} channels. As I show here, PHP is abolished upon loss of Unc13A, even when Unc13B remains (Figure 12). The low NT release of the Unc13A null mutant is unable to compensate for postsynaptic receptor blockade. Homeostatic plasticity relies on Unc13A to provide the necessary release sites (N), as well as Ca^{2+} influx (via Cac) increasing SV release probability (p). From this it can be concluded that Unc13A is vital for rapid PHP to occur reliably.

Unc13B on the other hand is less important for exocytosis, as its loss leads to a much less severe deficit in neurotransmission compared to Unc13A loss (Böhme et al., 2016). It could be inferred based on the SV distribution of Unc13A null mutants that if SVs are positioned by Unc13B, they do so at a greater distance. Importantly, it appears Unc13B is not necessary for rapid induction of PHP, as evidenced by re-expression of Unc13A in the null background exhibiting normal induction of PHP (Figure 13a). This suggests that PHP relies on SV placement close to the centre of the AZ, at least at these Ca^{2+} concentrations.

Focusing on Unc13A, I was interested in the function of the N-terminus of the protein and how it relates to homeostatic plasticity. The N-terminus is important for localisation (Reddy-Alla et al., 2017). Overexpression of the N-terminus in a wildtype background, leads to competition with endogenous Unc13A, blocking functional release sites and overall reduction of docked/primed SVs (Reddy-Alla et al., 2017). Stimulated exocytosis is reduced compared to control animals. SVs require the C-terminal portion of the protein to properly dock and prime.

Expression of the C-terminus of Unc13A in a null background results in protein that cannot localise with specific distribution at the AZ (Reddy-Alla et al., 2017). It heterogeneously covers the membrane and is observed at close proximity to the Ca^{2+} channels where it would usually be excluded. Unc13A C-term maintains the ability to form independent release sites, although the number of these is vastly increased. Consequently, the number of docked SVs is also increased. There is a reduction in stimulated exocytosis compared to full length Unc13A rescue that becomes more pronounced with increased extracellular Ca^{2+}. My data confirms the defect in release, with a ~20% reduction in amplitude observed (Figure 13).

Application of PhTx uncovers a severe defect in the induction of PHP (Figure 13, 14). Quantal content does not increase. The induction of rapid homeostatic plasticity occurs within 10 minutes. The conclusion can be made that the C-terminal portion of Unc13A alone is not sufficient for homeostatic plasticity. Accurate localisation of Unc13A is required at synapses for a fast increase in vesicular release, supporting the idea that release site generation by Unc13A is just as important for PHP as priming alone.

It is possible however that the CaM-binding domain may play some role in modulating homeostatic synaptic plasticity as it does in other forms of plasticity, notably STP in mammals (Lipstein et al., 2012). Synapses do not exclusively display one form of plasticity at any one time and there may be mechanistic overlap. In worms, the UNC-13L isoform possesses a CaM site that accelerates NT release (Hu et al., 2013). In C-term-GFP mutants lacked this site due to the nature of the deletion as the CaM binding-site is proximal to the N-terminus. This will need to be explored further with specific targeting of the domain.

As mentioned in the Introduction, a C_2A domain exists in the N-terminus of mouse and worm Munc13/UNC-13 that is lacking in *Drosophila* Unc13, and this interacts with RIM to prime SVs (Andrews-Zwilling et al., 2006; Camacho et al., 2017; Deng et al., 2011; Zhou et al., 2013). RIM-BP in mammals also appears to be involved in this interaction of Unc13 and RIM to prime SVs (Brockmann et al., 2019). It is possible such activating function is nevertheless still present in the N-terminus of *Drosophila* Unc13 and that a domain like the CaM-binding site

may fulfil this function, leading to activation of Unc13 already present at the AZ during PHP.

Finally, it is interesting to consider how the mechanisms and components important for presynaptic homeostatic plasticity may apply to other forms of plasticity or neurotransmission (as I mentioned above for STP), focusing on Unc13 as the release site molecule. Dysfunction of Unc13 can have wide ranging effects and genetic variability in Munc13-1 has been identified as a risk factor for neurodegenerative diseases in humans, including amyotrophic lateral sclerosis and frontotemporal dementia (Diekstra et al., 2014). Deletion of the N-terminus of Unc13A was shown to inhibit learning and short-term memory formation when expressed in the mushroom body of the adult fly, indicating that the specific loss of this region of the protein is not only necessary for PHP but may be involved in other forms of plasticity (Böhme et al., 2019). There is a great degree of conservation in plasticity and learning mechanisms. Taking the example of olfactory conditioning in *Drosophila*, it additionally involves cAMP-PKA signalling with PKA being further implicated in many other forms of plasticity including presynaptic facilitation in the sea slug *Aplysia* or mammalian LTP (Michel et al., 2011). It seems natural then that Unc13, with such a vital role in potentiation (homeostatic or otherwise), would be another possible conserved candidate for the convergence of synaptic adaptation pathways.

6.6 Differences in Homeostatic Plasticity - Structural versus Functional

Presynaptic homeostatic plasticity presents as two distinct phenomena. As discussed, the first involves the increase in presynaptic vesicular release due to a greater number independent release sites, compensating for loss of glutamate sensitivity at the postsynapse, a form of functional plasticity (Böhme et al., 2019; Müller et al., 2012). The second involves the rapid rearrangement of cytomatrix AZ proteins, a form of structural plasticity at *Drosophila* 1b boutons. I propose that while both often occur in tandem, structural and functional plasticity can be completely separated.

A host of AZ proteins visualised at the AZ increase rapidly during homeostatic plasticity, including BRP, RBP, Cac, Unc13A and Syx-1A (Böhme et al., 2019;

Goel et al., 2017; Gratz et al., 2019; Weyhersmüller et al., 2011). In fact, BRP and RBP are required for the structural rearrangement of other AZ proteins such as Unc13A (Böhme et al., 2019). Combining immunohistochemistry with super-resolution STED microscopy unveils the arrangement of these proteins at the AZ. When looking at many AZs, a regular geometric pattern can be observed for Unc13A, BRP and RBP. AZs consist of clusters of these proteins arranged in a very regular shape. On application with PhTx or deletion of GluRIIA, the number of AZs with a greater number of clusters of Unc13A, BRP and RBP increases. Referring to these clusters as “nano-modules”, it appears that under conditions that induce homeostatic plasticity, additional nano-modules of certain AZ proteins are inserted at AZs or larger nano-modules fragment into smaller ones. This is not true for all AZ proteins, as it was observed that Syx-1A and Unc18 do not cluster. Unc18 also does not undergo rapid structural homeostatic plasticity, but is vital for rapid PHP (Böhme et al., 2019; Ortega et al., 2018).

A major question surrounding this phenomenon is where this protein comes from, as a storage pool is not immediately obvious. One possibility is rearrangement of protein already at the AZ. We know that inhibition of translation prevents neither rapid structural or rapid functional plasticity (Böhme et al., 2019; Frank et al., 2006), however I elaborate on these experiments later.

Immunohistochemistry only reveals the location of protein at a particular point in time and not its transport. Unc13A and BRP for example had been visualised being co-transported in the axon (Böhme et al., 2019). I looked at motoneuronal axons of larvae expressing BRP-mCherry and observed particles of BRP moving as well as remaining stationary (Figure 16). On treatment with PhTx, the number of motile particles increased while the number of stationary particles decreased. The movement of motile particles is not uniform, often stopping and starting again. Vesicles carrying dendritic proteins have been described moving in similar fashion with such vesicles pausing at patches of actin (Watanabe et al., 2012). It is proposed that proteins are conveyed along axons and dendrites, stopping at regions of high actin for sorting and filtering, such as at the axon initial segment.

Proper actin function is vital for AZ-remodelling. Actin polymerisation blocker Latrunculin B inhibits rapid structural plasticity at AZs (Böhme et al., 2019). It is thus plausible that AZ proteins are transported via actin into the AZ during rapid structural plasticity. Immunohistochemistry experiments as well as live imaging experiments of Cac at individual AZs were performed with the segmental nerve intact (Böhme et al., 2019; Gratz et al., 2019). Proteins associated with transport of AZ components BRP/RBP, such as serine-arginine (SR) protein kinase at location 79D (Srpk79D) (Driller et al., 2019) and transport adapter App-like interacting protein 1 (Aplip-1) (Siebert et al., 2015), when mutated lead to co-accumulations of BRP/Unc13A in the axon (Böhme et al., 2019). These mutants are incapable of AZ protein rearrangement during homeostatic plasticity. Interestingly, while rapid structural plasticity is lost, rapid functional plasticity remains, further supporting the idea that rapid structural plasticity is separate from PHP.

I have shown this separation of functional and structural aspects is true for BRP (Figure 15). It was assumed that such an important component regarding AZ-remodelling would also be important for PHP. Loss of BRP had been observed to prevent an increase of the release site factor Unc13A (Böhme et al., 2019). As mentioned previously, this is not the case however, as treatment with PhTx in mutants lacking BRP maintain PHP (Figure 15). Likewise, interference with transport of BRP/RBP by mutation of Srpk79D or Aplip-1, while affecting AZ-remodelling, does not inhibit induction of rapid PHP (Böhme et al., 2019). It is possible that AZ-remodelling occurs in preparation for a long-term perturbation of synapses as a form of consolidation, and Srpk79D/Aplip-1 are involved in moving sufficient quantities of AZ proteins to the NMJ. Unc13A present at the AZ and previously inactive may be sufficient to upregulate release during rapid induction of PHP. It can be concluded, that while it was once assumed that the upregulation of presynaptic release during homeostatic plasticity was inseparable from the acute remodelling of the proteins at the AZ, this is revealed to no longer be the case. The two mechanisms do not necessarily directly relate to each other on very short timescales of a few minutes.

6.7 Differences in Homeostatic Plasticity - Rapid versus Chronic

Presynaptic homeostatic plasticity occurring in response postsynaptic challenge involves rapid plasticity following pharmacological blockade of glutamate receptors or long-term plasticity observed when glutamate receptors are chronically absent (Figure 17). These data support the possibility that these two types of homeostatic plasticity are distinct, in phenotype and mechanism. Proteins that were only required for AZ-remodelling on short timescales become vital for PHP on longer timescales. During rapid homeostatic plasticity there is no change in Unc18 but during chronic plasticity Unc18 drastically increases at the presynapse. AZ-remodelling and PHP is also generally more robust during chronic plasticity compared to rapid plasticity. The fact remains that genetic deletion of receptors is very different from pharmacological blockade. Loss of GluRIIA receptors occurs over the lifetime of the organism and so the consequence may be widespread, knock-on effects that distinguish this form of plasticity from the rapid form. BRP, while dispensable for rapid PHP, is required on the long-term for both structural plasticity and chronic PHP (Figure 18). Likewise, transport associated proteins Srpk79D and Aplip-1 are also required for both structural plasticity and PHP but only upon chronic glutamate receptor loss (Figure 19). Axonal transport is likely vital on long term timescales, involving transport of protein from the soma.

Regarding production of new protein, rapid homeostatic plasticity is hypothesised to be independent of translation. Severing the axon does not prevent rapid PHP (Frank et al., 2006), an observation that perhaps implied that rapid homeostatic plasticity is independent of translation. The presence of presynaptic ribosomal components and active translation at mammalian glutamate synapses has recently been identified however (Scarnati et al., 2018). Regions of active protein synthesis are determined by SUrface SEnsing of Translation (SUnSET), whereby puromycin is acutely applied, incorporated into polypeptides followed by removal, tissue fixation and immunostaining for the newly generated puromycin polypeptides. It is possible that similar processes exist at the *Drosophila* NMJ presynapse.

Acute application of the translation blocker Cycloheximide directly to larvae has been used to inhibit translation and presumably would do so postsynaptically

and presynaptically. Rapid PHP induction is unperturbed by Cycloheximide use (Böhme et al., 2019; Frank et al., 2006). Chronic plasticity on the other hand is mediated by TOR signalling and so postsynaptic translation is thought to be necessary (Kauwe et al., 2016; Penney et al., 2012). A recent study has reported that application of Cycloheximide to GluRIIA mutants did not affect chronic PHP, nor did application to larvae overexpressing TOR reduce their increased release (Goel et al., 2017). One could conclude from this that translation is unimportant for chronic PHP also and that TOR signalling is not directly involved in potentiated presynaptic release.

The use of Cycloheximide as a translation blocker has been confirmed to inhibit memory retention as long-term memory is sensitive to its use. Adult flies were fed Cycloheximide at least 12 hours before testing (Tully et al., 1994). Both the method of application and length of time prior to testing differs greatly from experiments where it was acutely applied to larvae (Böhme et al., 2019; Frank et al., 2006). The incubation time may be insufficient to block PHP as for example Unc13 is very stable at the NMJ, taking many hours to recover from fluorescence recovery after photobleaching (FRAP) (Reddy-Alla et al., 2017). Further evidence that presynaptic plasticity requires protein synthesis is seen at mammalian hippocampal synapses (Han and Stevens, 2009). Application of TTX and subsequent silencing of nerve firing for 1 day leads to a presynaptic increase in the probability of NT release. This has been shown to be transcription dependent, as it is inhibited by use of the transcription blocker A-D.

In order to quantify the level of translation inhibition and determine the origin of AZ proteins, fluorescent timers (FTs) may be useful. FTs involve a chromophore that changes wavelength over time and can aid in determining the age and trafficking of proteins. FTs exist with suitably long blue to red fluorescence conversion rates (Subach et al., 2009; Terskikh et al., 2000). As an alternative to pharmacological blockade of translation, an optogenetic approach to disable translation might be possible. Chromophore-assisted light inactivation (CALI) involves tagging a protein with a chromophore that upon stimulation with light, rapidly generates oxygen radicals that oxidise residues elsewhere on the tagged protein. As a result, the function of the tagged protein is acutely temporally and spatially disrupted (Lin et al., 2013; Tour et al., 2003). By

targeting proteins, essential for translation, the importance for induction of homeostatic plasticity could be more confidently explored. CALI could also potentially be used to induce plasticity, targeting GluRIIA for example. Manipulation of postsynaptic receptors over the medium time scale might shed more light on the separation between rapid and chronic plasticity, making use of an optogenetic approach to disable receptors over a few hours.

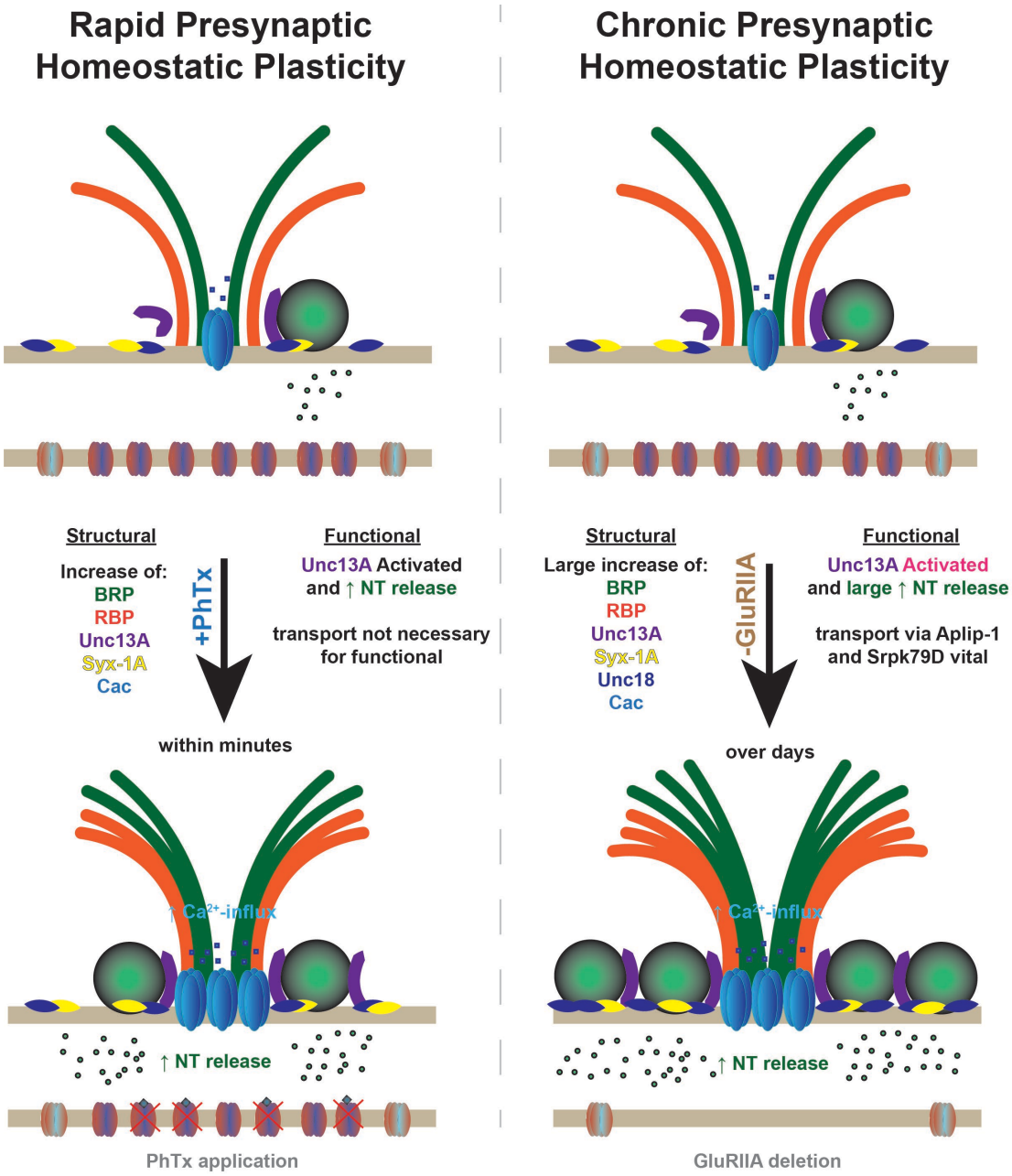

Figure 20: The functional and structural aspects of Presynaptic Homeostatic Plasticity differ depending on induction method.

Homeostatic plasticity at the *Drosophila* NMJ can be induced in two ways, the acute pharmacological (Rapid) application of PhTx or the genetic (Chronic) deletion of GluRIIA. Both methods manifest as distinct functional and structural changes at the presynaptic AZ.

6.8 Presynaptic Homeostatic Plasticity - Conclusion and Outlook

While it might previously have been assumed that the structural rearrangement and increase of AZ proteins is fundamentally linked to the functional aspect of presynaptic homeostatic plasticity, the work described here proves that this is not the case. On rapid timescales, despite the fact the scaffold (BRP) undergoes such change, it is unnecessary for PHP. The release site molecule Unc13A on the other hand is essential, and it is likely that material already at the AZ becomes activated to increase NT release in such a situation (Figure 20).

The answer to why the AZ undergoes structural reorganisation is perhaps due to the need to consolidate functional potentiation over long timescales, as during chronic presynaptic homeostatic plasticity. Plastic modulation is stronger, both functionally and structurally, and efficient transport of AZ proteins is mandatory. Increased supply of protein such as Unc13A may increase the ceiling for potentiation.

The two induction methods are quite different however, as it is a comparison of pharmacological block of glutamate receptors over the course of minutes versus the genetic deletion and absence of receptors over the life of the animal. Investigation of whether further potentiation is possible by application of phorbol ester, converging on Unc13A during rapid of chronic plasticity, would be interesting.

It remains to be seen whether these two situations (rapid versus chronic) reflect a common form of presynaptic homeostatic plasticity. If there is a switch between the two, it may purely be the duration and extent of postsynaptic receptor challenge that steers synapses towards either form of plasticity. Nevertheless, presynaptic homeostatic plasticity as a whole is a vital process for stable neurotransmission.

7 References

Aberle, H., Haghighi, A.P., Fetter, R. D., McCabe, B. D., Magalhães, T. R. and Goodman, C. S. (2002) 'wishful thinking Encodes a BMP Type II Receptor that Regulates Synaptic Growth in Drosophila', *Neuron*, vol. 33, no. 4, pp. 545–558.

Acuna, C., Liu, X. and Südhof, T. C. (2016) 'How to Make an Active Zone: Unexpected Universal Functional Redundancy between RIMs and RIM-BPs', *Neuron*, vol. 91, no. 4, pp. 792–807.

Adams, M. D., Celniker, S. E., Holt, R. A., Evans, C. A., Gocayne, J. D., Amanatides, P. G., Scherer, S. E., Li, P. W., Hoskins, R. A., Galle, R. F., George, R. A., Lewis, S. E., Richards, S., Ashburner, M., Henderson, S. N., Sutton, G. G., Wortman, J. R., Yandell, M. D., Zhang, Q., Chen, L. X., Brandon, R. C., Rogers, Y.-H. C., Blazej, R. G., Champe, M. and Pfeiffer, B. D., et al. (2000) 'The Genome Sequence of Drosophila melanogaster', *Science*, vol. 287, no. 5461, p. 2185.

Allocca, M., Zola, S. and Bellosta, P. (2018) 'The Fruit Fly, Drosophila melanogaster: The Making of a Model (Part I)', in Perveen, F. K. (ed) *Drosophila melanogaster: Model for recent advances in genetics and therapeutics,* Rijeka, InTech.

Andrews-Zwilling, Y. S., Kawabe, H., Reim, K., Varoqueaux, F. and Brose, N. (2006) 'Binding to Rab3A-interacting molecule RIM regulates the presynaptic recruitment of Munc13-1 and ubMunc13-2', *The Journal of biological chemistry*, vol. 281, no. 28, pp. 19720–19731.

Aoyagi, K., Sugaya, T., Umeda, M., Yamamoto, S., Terakawa, S. and Takahashi, M. (2005) 'The activation of exocytotic sites by the formation of phosphatidylinositol 4,5-bisphosphate microdomains at syntaxin clusters', *The Journal of biological chemistry*, vol. 280, no. 17, pp. 17346–17352.

Aravamudan, B., Fergestad, T., Davis, W. S., Rodesch, C. K. and Broadie, K. (1999) 'Drosophila UNC-13 is essential for synaptic transmission', *Nature Neuroscience*, vol. 2, no. 11, pp. 965–971.

Ashburner, M., Golic, K. G. and Hawley, R. S. (2005) *Drosophila: A laboratory handbook / Michael Ashburner, Kent G. Golic, R. Scott Hawley*, 2nd edn, New York, Cold Spring Harbor Laboratory Press; [Oxford : Lavis Marketing.

Atwood, B. K., Lovinger, D. M. and Mathur, B. N. (2014) 'Presynaptic long-term depression mediated by Gi/o-coupled receptors', *Trends in Neurosciences*, vol. 37, no. 11, pp. 663–673.

Augustin, I., Rosenmund, C., Südhof, T. C. and Brose, N. (1999) 'Munc13-1 is essential for fusion competence of glutamatergic synaptic vesicles', *Nature*, vol. 400, no. 6743, pp. 457–461.

Barg, S., Knowles, M. K., Chen, X., Midorikawa, M. and Almers, W. (2010) 'Syntaxin clusters assemble reversibly at sites of secretory granules in live cells', *Proceedings of the National Academy of Sciences of the United States of America*, vol. 107, no. 48, pp. 20804–20809.

Basu, J., Betz, A., Brose, N. and Rosenmund, C. (2007) 'Munc13-1 C1 Domain Activation Lowers the Energy Barrier for Synaptic Vesicle Fusion', *The Journal of Neuroscience*, vol. 27, no. 5, p. 1200.

Basu, J., Shen, N., Dulubova, I., Lu, J., Guan, R., Guryev, O., Grishin, N. V., Rosenmund, C. and Rizo, J. (2005) 'A minimal domain responsible for Munc13 activity', *Nature Structural & Molecular Biology*, vol. 12, no. 11, pp. 1017–1018.

Betz, A., Thakur, P., Junge, H. J., Ashery, U., Rhee, J.-S., Scheuss, V., Rosenmund, C., Rettig, J. and Brose, N. (2001) 'Functional Interaction of the Active Zone Proteins Munc13-1 and RIM1 in Synaptic Vesicle Priming', *Neuron*, vol. 30, no. 1, pp. 183–196.

Blanco, F. A., Czikora, A., Kedei, N., You, Y., Mitchell, G. A., Pany, S., Ghosh, A., Blumberg, P. M. and Das, J. (2019) 'Munc13 Is a Molecular Target of Bryostatin 1', *Biochemistry*, vol. 58, no. 27, pp. 3016–3030.

Böhme, M. A., Beis, C., Reddy-Alla, S., Reynolds, E., Mampell, M. M., Grasskamp, A. T., Lützkendorf, J., Bergeron, D. D., Driller, J. H., Babikir, H., Göttfert, F., Robinson, I. M., O'Kane, C. J., Hell, S. W., Wahl, M. C., Stelzl, U., Loll, B., Walter, A. M. and Sigrist, S. J. (2016) 'Active zone scaffolds differentially accumulate Unc13 isoforms to tune Ca2+ channel–vesicle coupling', *Nature Neuroscience*, vol. 19, no. 10, pp. 1311–1320.

Böhme, M. A., Grasskamp, A. T. and Walter, A. M. (2018) 'Regulation of synaptic release-site Ca2+ channel coupling as a mechanism to control release probability and short-term plasticity', *FEBS Letters*, vol. 592, no. 21, pp. 3516–3531.

Böhme, M. A., McCarthy, A. W., Grasskamp, A. T., Beuschel, C. B., Goel, P., Jusyte, M., Laber, D., Huang, S., Rey, U., Petzoldt, A. G., Lehmann, M., Göttfert, F., Haghighi, P., Hell, S. W., Owald, D., Dickman, D., Sigrist, S. J. and Walter, A. M. (2019) 'Rapid

active zone remodeling consolidates presynaptic potentiation', *Nature Communications*, vol. 10, no. 1, p. 1085.

Brand, A. H. and Perrimon, N. (1993) 'Targeted gene expression as a means of altering cell fates and generating dominant phenotypes', *Development*, vol. 118, no. 2, p. 401.

Brockmann, M. M., Maglione, M., Willmes, C. G., Stumpf, A., Bouazza, B. A., Velasquez, L. M., Grauel, M. K., Beed, P., Lehmann, M., Gimber, N., Schmoranzer, J., Sigrist, S. J., Rosenmund, C., Schmitz, D., Bartos, M., Westbrook, G. L. and Garner, C. C. (2019) 'RIM-BP2 primes synaptic vesicles via recruitment of Munc13-1 at hippocampal mossy fiber synapses', *eLife*, vol. 8, e43243.

Brose, N., Betz, A. and Wegmeyer, H. (2004) 'Divergent and convergent signaling by the diacylglycerol second messenger pathway in mammals', *Current opinion in neurobiology*, vol. 14, no. 3, pp. 328–340.

Brose, N., Hofmann, K., Hata, Y. and Südhof, T. C. (1995) 'Mammalian homologues of Caenorhabditis elegans unc-13 gene define novel family of C2-domain proteins', *The Journal of biological chemistry*, vol. 270, no. 42, pp. 25273–25280.

Bruckner, J. J., Gratz, S. J., Slind, J. K., Geske, R. R., Cummings, A. M., Galindo, S. E., Donohue, L. K., O&#039 and Connor-Giles, K. M. (2012) 'Fife, a Drosophila Piccolo-RIM Homolog, Promotes Active Zone Organization and Neurotransmitter Release', *The Journal of Neuroscience*, vol. 32, no. 48, p. 17048.

Bruckner, J. J., Zhan, H., Gratz, S. J., Rao, M., Ukken, F., Zilberg, G. and O'Connor-Giles, K. M. (2016) 'Fife organizes synaptic vesicles and calcium channels for high-probability neurotransmitter release', *The Journal of Cell Biology*, vol. 216, no. 1, pp. 231–246.

Bruckner, J. J., Zhan, H. and O'Connor-Giles, K. M. (2015) 'Advances in imaging ultrastructure yield new insights into presynaptic biology', *Frontiers in Cellular Neuroscience*, vol. 9, p. 196.

Camacho, M., Basu, J., Trimbuch, T., Chang, S., Pulido-Lozano, C., Chang, S.-S., Duluvova, I., Abo-Rady, M., Rizo, J. and Rosenmund, C. (2017) 'Heterodimerization of Munc13 C2A domain with RIM regulates synaptic vesicle docking and priming', *Nature Communications*, vol. 8, no. 1, p. 15293.

Campbell, D. B. and Nash, H. A. (1994) ‘Use of Drosophila mutants to distinguish among volatile general anesthetics’, *Proceedings of the National Academy of Sciences of the United States of America*, vol. 91, no. 6, pp. 2135–2139.

Castelfranco, A. M. and Hartline, D. K. (2015) ‘The evolution of vertebrate and invertebrate myelin: a theoretical computational study’, *Journal of computational neuroscience*, vol. 38, no. 3, pp. 521–538.

Catterall, W. A. (2010) ‘Ion Channel Voltage Sensors: Structure, Function, and Pathophysiology’, *Neuron*, vol. 67, no. 6, pp. 915–928.

Catterall, W. A. (2011) ‘Voltage-gated calcium channels’, *Cold Spring Harbor perspectives in biology*, vol. 3, no. 8, a003947-a003947.

Chang-Ileto, B., Frere, S. G., Chan, R. B., Voronov, S. V., Roux, A. and Di Paolo, G. (2011) ‘Synaptojanin 1-mediated PI(4,5)P2 hydrolysis is modulated by membrane curvature and facilitates membrane fission’, *Developmental cell*, vol. 20, no. 2, pp. 206–218.

Chernomordik, L. V. and Kozlov, M. M. (2008) ‘Mechanics of membrane fusion’, *Nature Structural & Molecular Biology*, vol. 15, no. 7, pp. 675–683.

Chinthalapudi, K., Rangarajan, E. S., Patil, D. N., George, E. M., Brown, D. T. and Izard, T. (2014) ‘Lipid binding promotes oligomerization and focal adhesion activity of vinculin’, *The Journal of Cell Biology*, vol. 207, no. 5, pp. 643–656.

Cijsouw, T., Weber, J. P., Broeke, J. H., Broek, J. A.C., Schut, D., Kroon, T., Saarloos, I., Verhage, M. and Toonen, R. F. (2014) ‘Munc18-1 redistributes in nerve terminals in an activity- and PKC-dependent manner’, *The Journal of Cell Biology*, vol. 204, no. 5, pp. 759–775.

Courtemanche, N., Pollard, T. D. and Chen, Q. (2016) ‘Avoiding artefacts when counting polymerized actin in live cells with LifeAct fused to fluorescent proteins’, *Nature Cell Biology*, vol. 18, no. 6, pp. 676–683.

Deguchi-Tawarada, M., Inoue, E., Takao-Rikitsu, E., Inoue, M., Ohtsuka, T. and Takai, Y. (2004) ‘CAST2: identification and characterization of a protein structurally related to the presynaptic cytomatrix protein CAST’, *Genes to Cells*, vol. 9, no. 1, pp. 15–23.

del Castillo, J. and Katz, B. (1954) ‘Quantal components of the end-plate potential’, *The Journal of physiology*, vol. 124, no. 3, pp. 560–573.

Delvendahl, I. and Müller, M. (2019) 'Homeostatic plasticity—a presynaptic perspective', *Current opinion in neurobiology*, vol. 54, pp. 155–162.

Deng, L., Kaeser, P. S., Xu, W. and Sudhof, T. C. (2011) 'RIM proteins activate vesicle priming by reversing autoinhibitory homodimerization of Munc13', *Neuron*, vol. 69, no. 2, pp. 317–331.

Denker, A., Kröhnert, K. and Rizzoli, S. O. (2009) 'Revisiting synaptic vesicle pool localization in the Drosophila neuromuscular junction', *The Journal of physiology*, vol. 587, Pt 12, pp. 2919–2926.

Denker, A. and Rizzoli, S. O. (2010) 'Synaptic Vesicle Pools: An Update', *Frontiers in Synaptic Neuroscience*, vol. 2.

Di Paolo, G., Moskowitz, H. S., Gipson, K., Wenk, M. R., Voronov, S., Obayashi, M., Flavell, R., Fitzsimonds, R. M., Ryan, T. A. and Camilli, P. de (2004) 'Impaired PtdIns(4,5)P2 synthesis in nerve terminals produces defects in synaptic vesicle trafficking', *Nature*, vol. 431, no. 7007, pp. 415–422.

DiAntonio, A., Petersen, S. A., Heckmann, M. and Goodman, C. S. (1999) 'Glutamate Receptor Expression Regulates Quantal Size and Quantal Content at the Drosophila Neuromuscular Junction', *The Journal of Neuroscience*, vol. 19, no. 8, p. 3023.

Dickman, D. K. and Davis, G. W. (2009) 'The schizophrenia susceptibility gene dysbindin controls synaptic homeostasis', *Science*, vol. 326, no. 5956, pp. 1127–1130.

Dickman, D. K., Tong, A. and Davis, G. W. (2012) 'Snapin is Critical for Presynaptic Homeostatic Plasticity', *The Journal of Neuroscience*, vol. 32, no. 25, p. 8716.

Diekstra, F. P., van Deerlin, V. M., van Swieten, J. C., Al-Chalabi, A., Ludolph, A. C., Weishaupt, J. H., Hardiman, O., Landers, J. E., Brown, R. H., van Es, M. A., Pasterkamp, R. J., Koppers, M., Andersen, P. M., Estrada, K., Rivadeneira, F., Hofman, A., Uitterlinden, A. G., van Damme, P., Melki, J., Meininger, V., Shatunov, A., Shaw, C. E., Leigh, P. N., Shaw, P. J. and Morrison, K. E., et al. (2014) 'C9orf72 and UNC13A are shared risk loci for amyotrophic lateral sclerosis and frontotemporal dementia: a genome-wide meta-analysis', *Annals of neurology*, vol. 76, no. 1, pp. 120–133.

Driller, J. H., Lützkendorf, J., Depner, H., Siebert, M., Kuropka, B., Weise, C., Piao, C., Petzoldt, A. G., Lehmann, M., Stelzl, U., Zahedi, R., Sickmann, A., Freund, C., Sigrist, S. J. and Wahl, M. C. (2019) 'Phosphorylation of the Bruchpilot N-terminus in

Drosophila unlocks axonal transport of active zone building blocks', *Journal of cell science*, vol. 132, no. 6.

Eberhard, D. A., Cooper, C. L., Low, M. G. and Holz, R. W. (1990) 'Evidence that the inositol phospholipids are necessary for exocytosis. Loss of inositol phospholipids and inhibition of secretion in permeabilized cells caused by a bacterial phospholipase C and removal of ATP', *The Biochemical journal*, vol. 268, no. 1, pp. 15–25.

Edwards, M. R., Johnson, J. R., Rankin, K., Jenkins, R. E., Maguire, C., Morgan, A., Burgoyne, R. D. and Barclay, J. W. (2012) 'PKC-2 phosphorylation of UNC-18 Ser322 in AFD neurons regulates temperature dependency of locomotion', *The Journal of neuroscience : the official journal of the Society for Neuroscience*, vol. 32, no. 20, pp. 7042–7051.

Ezzell, R. M., Goldmann, W. H., Wang, N., Parasharama, N. and Ingber, D. E. (1997) 'Vinculin Promotes Cell Spreading by Mechanically Coupling Integrins to the Cytoskeleton', *Experimental Cell Research*, vol. 231, no. 1, pp. 14–26.

Fatt, P. and Katz, B. (1952) 'Spontaneous subthreshold activity at motor nerve endings', *The Journal of Physiology*, vol. 117, no. 1, pp. 109–128.

Fernández-Golbano, I. M., Idrissi, F.-Z., Giblin, J. P., Grosshans, B. L., Robles, V., Grötsch, H., Borrás, M. d. M. and Geli, M. I. (2014) 'Crosstalk between PI(4,5)P2 and CK2 Modulates Actin Polymerization during Endocytic Uptake', *Developmental cell*, vol. 30, no. 6, pp. 746–758.

Fouquet, W., Owald, D., Wichmann, C., Mertel, S., Depner, H., Dyba, M., Hallermann, S., Kittel, R. J., Eimer, S. and Sigrist, S. J. (2009) 'Maturation of active zone assembly by Drosophila Bruchpilot', *The Journal of Cell Biology*, vol. 186, no. 1, pp. 129–145.

Frank, C. A., Kennedy, M. J., Goold, C. P., Marek, K. W. and Davis, G. W. (2006) 'Mechanisms underlying the rapid induction and sustained expression of synaptic homeostasis', *Neuron*, vol. 52, no. 4, pp. 663–677.

Frank, C. A., Pielage, J. and Davis, G. W. (2009) 'A Presynaptic Homeostatic Signaling System Composed of the Eph Receptor, Ephexin, Cdc42, and CaV2.1 Calcium Channels', *Neuron*, vol. 61, no. 4, pp. 556–569.

Freeman, S. A., Desmazières, A., Fricker, D., Lubetzki, C. and Sol-Foulon, N. (2016) 'Mechanisms of sodium channel clustering and its influence on axonal impulse conduction', *Cellular and Molecular Life Sciences*, vol. 73, no. 4, pp. 723–735.

Gaviño, M. A., Ford, K. J., Archila, S., Davis, G. W. and Calabrese, R. L. (2015) 'Homeostatic synaptic depression is achieved through a regulated decrease in presynaptic calcium channel abundance', *eLife*, vol. 4, e05473.

Genç, Ö., Kochubey, O., Toonen, R. F., Verhage, M., Schneggenburger, R. and Rosenmund, C. (2014) 'Munc18-1 is a dynamically regulated PKC target during short-term enhancement of transmitter release', *eLife*, vol. 3, e01715.

Giagtzoglou, N., Lin, Y. Q., Haueter, C. and Bellen, H. J. (2009) 'Importin 13 regulates neurotransmitter release at the Drosophila neuromuscular junction', *The Journal of neuroscience : the official journal of the Society for Neuroscience*, vol. 29, no. 17, pp. 5628–5639.

Gillis, K. D., Mößner, R. and Neher, E. (1996) 'Protein Kinase C Enhances Exocytosis from Chromaffin Cells by Increasing the Size of the Readily Releasable Pool of Secretory Granules', *Neuron*, vol. 16, no. 6, pp. 1209–1220.

Goel, P., Li, X. and Dickman, D. (2017) 'Disparate Postsynaptic Induction Mechanisms Ultimately Converge to Drive the Retrograde Enhancement of Presynaptic Efficacy', *Cell reports*, vol. 21, no. 9, pp. 2339–2347.

Gois, S. de, Schäfer, M. K.-H., Defamie, N., Chen, C., Ricci, A., Weihe, E., Varoqui, H. and Erickson, J. D. (2005) 'Homeostatic Scaling of Vesicular Glutamate and GABA Transporter Expression in Rat Neocortical Circuits', *The Journal of Neuroscience*, vol. 25, no. 31, p. 7121.

Golub, T. and Caroni, P. (2005) 'PI(4,5)P2-dependent microdomain assemblies capture microtubules to promote and control leading edge motility', *The Journal of Cell Biology*, vol. 169, no. 1, pp. 151–165.

Gong, L.-W., Di Paolo, G., Diaz, E., Cestra, G., Diaz, M.-E., Lindau, M., Camilli, P. de and Toomre, D. (2005) 'Phosphatidylinositol phosphate kinase type Iγ regulates dynamics of large dense-core vesicle fusion', *Proceedings of the National Academy of Sciences of the United States of America*, vol. 102, no. 14, p. 5204.

Goold, C. P. and Davis, G. W. (2007) 'The BMP ligand Gbb gates the expression of synaptic homeostasis independent of synaptic growth control', *Neuron*, vol. 56, no. 1, pp. 109–123.

Gorelik, R., Yang, C., Kameswaran, V., Dominguez, R. and Svitkina, T. (2011) 'Mechanisms of plasma membrane targeting of formin mDia2 through its amino terminal domains', *Molecular biology of the cell*, vol. 22, no. 2, pp. 189–201.

Graf, E. R., Valakh, V., Wright, C. M., Wu, C., Liu, Z., Zhang, Y. Q. and DiAntonio, A. (2012) 'RIM Promotes Calcium Channel Accumulation at Active Zones of the Drosophila Neuromuscular Junction', *The Journal of Neuroscience*, vol. 32, no. 47, p. 16586.

Gratz, S. J., Goel, P., Bruckner, J. J., Hernandez, R. X., Khateeb, K., Macleod, G. T., Dickman, D. and Connor-Giles, K. M. (2019) 'Endogenous Tagging Reveals Differential Regulation of Ca2+ Channels at Single Active Zones during Presynaptic Homeostatic Potentiation and Depression', *The Journal of Neuroscience*, vol. 39, no. 13, p. 2416.

Grauel, M. K., Maglione, M., Reddy-Alla, S., Willmes, C. G., Brockmann, M. M., Trimbuch, T., Rosenmund, T., Pangalos, M., Vardar, G., Stumpf, A., Walter, A. M., Rost, B. R., Eickholt, B. J., Haucke, V., Schmitz, D., Sigrist, S. J. and Rosenmund, C. (2016) 'RIM-binding protein 2 regulates release probability by fine-tuning calcium channel localization at murine hippocampal synapses', *Proceedings of the National Academy of Sciences of the United States of America*, vol. 113, no. 41, pp. 11615–11620.

Haghighi, A.P., McCabe, B. D., Fetter, R. D., Palmer, J. E., Hom, S. and Goodman, C. S. (2003) 'Retrograde Control of Synaptic Transmission by Postsynaptic CaMKII at the Drosophila Neuromuscular Junction', *Neuron*, vol. 39, no. 2, pp. 255–267.

Hall, A. (1998) 'Rho GTPases and the Actin Cytoskeleton', *Science*, vol. 279, no. 5350, p. 509.

Hallermann, S., Kittel, R. J., Wichmann, C., Weyhersmüller, A., Fouquet, W., Mertel, S., Owald, D., Eimer, S., Depner, H., Schwärzel, M., Sigrist, S. J. and Heckmann, M. (2010) 'Naked Dense Bodies Provoke Depression', *The Journal of Neuroscience*, vol. 30, no. 43, p. 14340.

Han, E. B. and Stevens, C. F. (2009) 'Development regulates a switch between post- and presynaptic strengthening in response to activity deprivation', *Proceedings of the National Academy of Sciences of the United States of America*, vol. 106, no. 26, pp. 10817–10822.

Han, J., Pluhackova, K. and Böckmann, R. A. (2017) 'The Multifaceted Role of SNARE Proteins in Membrane Fusion', *Frontiers in physiology*, vol. 8, p. 5.

Han, T. H., Dharkar, P., Mayer, M. L. and Serpe, M. (2015) 'Functional reconstitution of Drosophila melanogaster NMJ glutamate receptors', *Proceedings of the National Academy of Sciences of the United States of America*, vol. 112, no. 19, pp. 6182–6187.

Han, T. H., Vicidomini, R., Ramos, C. I., Wang, Q., Nguyen, P., Jarnik, M., Li, M., Stawarski, M., Hernandez, R. X., Macleod, G. T. and Serpe, M. (2019) 'Neto-α controls synapse organization and homeostasis at the Drosophila neuromuscular junction', *bioRxiv*, p. 812040.

Han, Y., Kaeser, P. S., Südhof, T. C. and Schneggenburger, R. (2011) 'RIM Determines Ca2+ Channel Density and Vesicle Docking at the Presynaptic Active Zone', *Neuron*, vol. 69, no. 2, pp. 304–316.

Harris, N., Braiser, D. J., Dickman, D. K., Fetter, R. D., Tong, A. and Davis, G. W. (2015) 'The Innate Immune Receptor PGRP-LC Controls Presynaptic Homeostatic Plasticity', *Neuron*, vol. 88, no. 6, pp. 1157–1164.

Hay, J. C., Fisette, P. L., Jenkins, G. H., Fukami, K., Takenawa, T., Anderson, R. A. and Martin, T. F. (1995) 'ATP-dependent inositide phosphorylation required for Ca(2+)-activated secretion', *Nature*, vol. 374, no. 6518, pp. 173–177.

Held, R. G., Liu, C., Kaeser, P. S. and Jahn, R. (2016) 'ELKS controls the pool of readily releasable vesicles at excitatory synapses through its N-terminal coiled-coil domains', *eLife*, vol. 5, e14862.

Hibino, H., Pironkova, R., Onwumere, O., Vologodskaia, M., Hudspeth, A. J. and Lesage, F. (2002) 'RIM binding proteins (RBPs) couple Rab3-interacting molecules (RIMs) to voltage-gated Ca(2+) channels', *Neuron*, vol. 34, no. 3, pp. 411–423.

Hida, Y. and Ohtsuka, T. (2010) 'CAST and ELKS proteins: structural and functional determinants of the presynaptic active zone', *The Journal of Biochemistry*, vol. 148, no. 2, pp. 131–137.

Hodgkin, A. L. and Huxley, A. F. (1952) 'A quantitative description of membrane current and its application to conduction and excitation in nerve', *The Journal of physiology*, vol. 117, no. 4, pp. 500–544.

Holz, R. W., Hlubek, M. D., Sorensen, S. D., Fisher, S. K., Balla, T., Ozaki, S., Prestwich, G. D., Stuenkel, E. L. and Bittner, M. A. (2000) 'A pleckstrin homology domain specific for phosphatidylinositol 4, 5-bisphosphate (PtdIns-4,5-P2) and fused to green fluorescent protein identifies plasma membrane PtdIns-4,5-P2 as being important in exocytosis', *The Journal of biological chemistry*, vol. 275, no. 23, pp. 17878–17885.

Horiuchi, D., Barkus, R. V., Pilling, A. D., Gassman, A. and Saxton, W. M. (2005) 'APLIP1, a kinesin binding JIP-1/JNK scaffold protein, influences the axonal transport

of both vesicles and mitochondria in Drosophila', *Current biology : CB*, vol. 15, no. 23, pp. 2137–2141.

Hu, Z., Tong, X.-J. and Kaplan, J. M. (2013) 'UNC-13L, UNC-13S, and Tomosyn form a protein code for fast and slow neurotransmitter release in Caenorhabditis elegans', *eLife*, vol. 2.

Huelsmann, S., Ylänne, J. and Brown, N. H. (2013) 'Filopodia-like Actin Cables Position Nuclei in Association with Perinuclear Actin in Drosophila Nurse Cells', *Developmental cell*, vol. 26, no. 6, pp. 604–615.

Imig, C., Min, S.-W., Krinner, S., Arancillo, M., Rosenmund, C., Südhof, T. C., Rhee, J., Brose, N. and Cooper, B. H. (2014) 'The Morphological and Molecular Nature of Synaptic Vesicle Priming at Presynaptic Active Zones', *Neuron*, vol. 84, no. 2, pp. 416–431.

James, D. J., Khodthong, C., Kowalchyk, J. A. and Martin, T. F. J. (2008) 'Phosphatidylinositol 4,5-bisphosphate regulates SNARE-dependent membrane fusion', *The Journal of Cell Biology*, vol. 182, no. 2, pp. 355–366.

Jan, L. Y. and Jan, Y. N. (1976) 'Properties of the larval neuromuscular junction in Drosophila melanogaster', *The Journal of physiology*, vol. 262, no. 1, pp. 189–214.

Junge, H. J., Rhee, J.-S., Jahn, O., Varoqueaux, F., Spiess, J., Waxham, M. N., Rosenmund, C. and Brose, N. (2004) 'Calmodulin and Munc13 form a Ca2+ sensor/effector complex that controls short-term synaptic plasticity', *Cell*, vol. 118, no. 3, pp. 389–401.

Kabachinski, G., Yamaga, M., Kielar-Grevstad, D. M., Bruinsma, S. and Martin, T. F. J. (2014) 'CAPS and Munc13 utilize distinct PIP2-linked mechanisms to promote vesicle exocytosis', *Molecular biology of the cell*, vol. 25, no. 4, pp. 508–521.

Kaeser, P. S., Deng, L., Chávez, A. E., Liu, X., Castillo, P. E. and Südhof, T. C. (2009) 'ELKS2α/CAST Deletion Selectively Increases Neurotransmitter Release at Inhibitory Synapses', *Neuron*, vol. 64, no. 2, pp. 227–239.

Kaeser, P. S., Deng, L., Wang, Y., Dulubova, I., Liu, X., Rizo, J. and Sudhof, T. C. (2011) 'RIM proteins tether Ca2+ channels to presynaptic active zones via a direct PDZ-domain interaction', *Cell*, vol. 144, no. 2, pp. 282–295.

Kandel, E. R., Schwartz, J. H. and Jessell, T. M. (2000) *Principles of neural science*, 4th edn, New York, McGraw-Hill, Health Professions Division.

Karunanithi, S., Marin, L., Wong, K. and Atwood, H. L. (2002) 'Quantal Size and Variation Determined by Vesicle Size in Normal and Mutant Drosophila Glutamatergic Synapses', *The Journal of neuroscience : the official journal of the Society for Neuroscience*, vol. 22, no. 23, pp. 10267–10276.

Kauwe, G., Tsurudome, K., Penney, J., Mori, M., Gray, L., Calderon, M. R., Elazouzzi, F., Chicoine, N., Sonenberg, N. and Haghighi, A. P. (2016) 'Acute Fasting Regulates Retrograde Synaptic Enhancement through a 4E-BP-Dependent Mechanism', *Neuron*, vol. 92, no. 6, pp. 1204–1212.

Kawabe, H., Mitkovski, M., Kaeser, P. S., Hirrlinger, J., Opazo, F., Nestvogel, D., Kalla, S., Fejtova, A., Verrier, S. E., Bungers, S. R., Cooper, B. H., Varoqueaux, F., Wang, Y., Nehring, R. B., Gundelfinger, E. D., Rosenmund, C., Rizzoli, S. O., Südhof, T. C., Rhee, J.-S. and Brose, N. (2017) 'ELKS1 localizes the synaptic vesicle priming protein bMunc13-2 to a specific subset of active zones', *The Journal of Cell Biology*, vol. 216, no. 4, pp. 1143–1161.

Keshishian, H., Chiba, A., Chang, T. N., Halfon, M. S., Harkins, E. W., Jarecki, J., Wang, L., Anderson, M., Cash, S. and Halpern, M. E. (1993) 'Cellular mechanisms governing synaptic development in Drosophila melanogaster', *Journal of Neurobiology*, vol. 24, no. 6, pp. 757–787.

Khuong, T. M., Habets, R. L. P., Kuenen, S., Witkowska, A., Kasprowicz, J., Swerts, J., Jahn, R., van den Bogaart, G. and Verstreken, P. (2013) 'Synaptic PI(3,4,5)P3 is required for Syntaxin1A clustering and neurotransmitter release', *Neuron*, vol. 77, no. 6, pp. 1097–1108.

Kim, K., McCully, M. E., Bhattacharya, N., Butler, B., Sept, D. and Cooper, J. A. (2007) 'Structure/function analysis of the interaction of phosphatidylinositol 4,5-bisphosphate with actin-capping protein: implications for how capping protein binds the actin filament', *The Journal of biological chemistry*, vol. 282, no. 8, pp. 5871–5879.

Kiragasi, B., Wondolowski, J., Li, Y. and Dickman, D. K. (2017) 'A Presynaptic Glutamate Receptor Subunit Confers Robustness to Neurotransmission and Homeostatic Potentiation', *Cell reports*, vol. 19, no. 13, pp. 2694–2706.

Kittel, R. J., Wichmann, C., Rasse, T. M., Fouquet, W., Schmidt, M., Schmid, A., Wagh, D. A., Pawlu, C., Kellner, R. R., Willig, K. I., Hell, S. W., Buchner, E., Heckmann, M. and Sigrist, S. J. (2006) 'Bruchpilot promotes active zone assembly, Ca2+ channel clustering, and vesicle release', *Science*, vol. 312, no. 5776, pp. 1051–1054.

Kobayashi, S., Hida, Y., Ishizaki, H., Inoue, E., Tanaka-Okamoto, M., Yamasaki, M., Miyazaki, T., Fukaya, M., Kitajima, I., Takai, Y., Watanabe, M., Ohtsuka, T. and Manabe, T. (2016) 'The active zone protein CAST regulates synaptic vesicle recycling and quantal size in the mouse hippocampus', *European Journal of Neuroscience*, vol. 44, no. 5, pp. 2272–2284.

Koike-Tani, M., Kanda, T., Saitoh, N., Yamashita, T. and Takahashi, T. (2008) 'Involvement of AMPA receptor desensitization in short-term synaptic depression at the calyx of Held in developing rats', *The Journal of physiology*, vol. 586, no. 9, pp. 2263–2275.

Kuo, W., Herrick, D. Z. and Cafiso, D. S. (2011) 'Phosphatidylinositol 4,5-bisphosphate alters synaptotagmin 1 membrane docking and drives opposing bilayers closer together', *Biochemistry*, vol. 50, no. 13, pp. 2633–2641.

Lam, A. D., Tryoen-Toth, P., Tsai, B., Vitale, N. and Stuenkel, E. L. (2008) 'SNARE-catalyzed fusion events are regulated by Syntaxin1A-lipid interactions', *Molecular biology of the cell*, vol. 19, no. 2, pp. 485–497.

Lang, T., Bruns, D., Wenzel, D., Riedel, D., Holroyd, P., Thiele, C. and Jahn, R. (2001) 'SNAREs are concentrated in cholesterol-dependent clusters that define docking and fusion sites for exocytosis', *The EMBO Journal*, vol. 20, no. 9, pp. 2202–2213.

Legate, K. R., Takahashi, S., Bonakdar, N., Fabry, B., Boettiger, D., Zent, R. and Fässler, R. (2011) 'Integrin adhesion and force coupling are independently regulated by localized PtdIns(4,5)2 synthesis', *The EMBO Journal*, vol. 30, no. 22, pp. 4539–4553.

Li, L., Shin, O.-H., Rhee, J.-S., Araç, D., Rah, J.-C., Rizo, J., Südhof, T. and Rosenmund, C. (2006) 'Phosphatidylinositol Phosphates as Co-activators of Ca2+ Binding to C2 Domains of Synaptotagmin 1', *Journal of Biological Chemistry*, vol. 281, no. 23, pp. 15845–15852.

Li, X., Goel, P., Chen, C., Angajala, V., Chen, X., Dickman, D. K. and Calabrese, R. L. (2018) 'Synapse-specific and compartmentalized expression of presynaptic homeostatic potentiation', *eLife*, vol. 7, e34338.

Liebeskind, B. J., Hofmann, H. A., Hillis, D. M. and Zakon, H. H. (2017) 'Evolution of Animal Neural Systems', *Annual Review of Ecology, Evolution, and Systematics*, vol. 48, no. 1, pp. 377–398.

Lin, J. Y., Sann, S. B., Zhou, K., Nabavi, S., Proulx, C. D., Malinow, R., Jin, Y. and Tsien, R. Y. (2013) 'Optogenetic Inhibition of Synaptic Release with Chromophore-Assisted Light Inactivation (CALI)', *Neuron*, vol. 79, no. 2, pp. 241–253.

Lipstein, N., Sakaba, T., Cooper, B. H., Lin, K.-H., Strenzke, N., Ashery, U., Rhee, J.-S., Taschenberger, H., Neher, E. and Brose, N. (2013) 'Dynamic control of synaptic vesicle replenishment and short-term plasticity by Ca(2+)-calmodulin-Munc13-1 signaling', *Neuron*, vol. 79, no. 1, pp. 82–96.

Lipstein, N., Schaks, S., Dimova, K., Kalkhof, S., Ihling, C., Kölbel, K., Ashery, U., Rhee, J., Brose, N., Sinz, A. and Jahn, O. (2012) 'Nonconserved Ca(2+)/calmodulin binding sites in Munc13s differentially control synaptic short-term plasticity', *Molecular and cellular biology*, vol. 32, no. 22, pp. 4628–4641.

Liu, C., Bickford, L. S., Held, R. G., Nyitrai, H., Südhof, T. C. and Kaeser, P. S. (2014) 'The active zone protein family ELKS supports Ca2+ influx at nerve terminals of inhibitory hippocampal neurons', *The Journal of neuroscience : the official journal of the Society for Neuroscience*, vol. 34, no. 37, pp. 12289–12303.

Liu, H., Li, L., Nedelcu, D., Hall, Q., Zhou, L., Wang, W., Yu, Y., Kaplan, J. M. and Hu, Z. (2019) 'Heterodimerization of UNC-13/RIM regulates synaptic vesicle release probability but not priming in C. elegans', *eLife*, vol. 8.

Liu, K. S. Y., Siebert, M., Mertel, S., Knoche, E., Wegener, S., Wichmann, C., Matkovic, T., Muhammad, K., Depner, H., Mettke, C., Bückers, J., Hell, S. W., Müller, M., Davis, G. W., Schmitz, D. and Sigrist, S. J. (2011) 'RIM-binding protein, a central part of the active zone, is essential for neurotransmitter release', *Science (New York, N.Y.)*, vol. 334, no. 6062, pp. 1565–1569.

Loewen, C. A., Lee, S.-M., Shin, Y.-K. and Reist, N. E. (2006) 'C2B polylysine motif of synaptotagmin facilitates a Ca2+-independent stage of synaptic vesicle priming in vivo', *Molecular biology of the cell*, vol. 17, no. 12, pp. 5211–5226.

Lou, X., Korogod, N., Brose, N. and Schneggenburger, R. (2008) 'Phorbol esters modulate spontaneous and Ca2+-evoked transmitter release via acting on both Munc13 and protein kinase C', *The Journal of neuroscience : the official journal of the Society for Neuroscience*, vol. 28, no. 33, pp. 8257–8267.

Lou, X., Scheuss, V. and Schneggenburger, R. (2005) 'Allosteric modulation of the presynaptic Ca2+ sensor for vesicle fusion', *Nature*, vol. 435, no. 7041, pp. 497–501.

Ma, C., Li, W., Xu, Y. and Rizo, J. (2011) 'Munc13 mediates the transition from the closed syntaxin-Munc18 complex to the SNARE complex', *Nature Structural & Molecular Biology*, vol. 18, no. 5, pp. 542–549.

Ma, C., Su, L., Seven, A. B., Xu, Y. and Rizo, J. (2013) 'Reconstitution of the vital functions of Munc18 and Munc13 in neurotransmitter release', *Science*, vol. 339, no. 6118, pp. 421–425.

Mackler, J. M., Drummond, J. A., Loewen, C. A., Robinson, I. M. and Reist, N. E. (2002) 'The C(2)B Ca(2+)-binding motif of synaptotagmin is required for synaptic transmission in vivo', *Nature*, vol. 418, no. 6895, pp. 340–344.

Markow, T. A. (2015) 'The secret lives of Drosophila flies', *eLife*, vol. 4, e06793.

Marqués, G., Bao, H., Haerry, T. E., Shimell, M. J., Duchek, P., Zhang, B. and O'Connor, M. B. (2002) 'The Drosophila BMP Type II Receptor Wishful Thinking Regulates Neuromuscular Synapse Morphology and Function', *Neuron*, vol. 33, no. 4, pp. 529–543.

Martin, T. F. J. (2012) 'Role of PI(4,5)P(2) in vesicle exocytosis and membrane fusion', *Sub-cellular biochemistry*, vol. 59, pp. 111–130.

Maruyama, I. N. and Brenner, S. (1991) 'A phorbol ester/diacylglycerol-binding protein encoded by the unc-13 gene of Caenorhabditis elegans', *Proceedings of the National Academy of Sciences of the United States of America*, vol. 88, no. 13, pp. 5729–5733.

Matkovic, T., Siebert, M., Knoche, E., Depner, H., Mertel, S., Owald, D., Schmidt, M., Thomas, U., Sickmann, A., Kamin, D., Hell, S. W., Burger, J., Hollmann, C., Mielke, T., Wichmann, C. and Sigrist, S. J. (2013) 'The Bruchpilot cytomatrix determines the size of the readily releasable pool of synaptic vesicles', *The Journal of Cell Biology*, vol. 202, no. 4, pp. 667–683.

McCabe, B. D., Marqués, G., Haghighi, A.P., Fetter, R. D., Crotty, M.L., Haerry, T. E., Goodman, C. S. and O'Connor, M. B. (2003) 'The BMP Homolog Gbb Provides a Retrograde Signal that Regulates Synaptic Growth at the Drosophila Neuromuscular Junction', *Neuron*, vol. 39, no. 2, pp. 241–254.

Melak, M., Plessner, M. and Grosse, R. (2017) 'Actin visualization at a glance', *Journal of cell science*, vol. 130, no. 3, pp. 525–530.

Menon, K. P., Carrillo, R. A. and Zinn, K. (2013) 'Development and plasticity of the Drosophila larval neuromuscular junction', *Wiley interdisciplinary reviews. Developmental biology*, vol. 2, no. 5, pp. 647–670.

Michel, M., Green, C. L. and Lyons, L. C. (2011) 'PKA and PKC are required for long-term but not short-term in vivo operant memory in Aplysia', *Learning & memory (Cold Spring Harbor, N.Y.)*, vol. 18, no. 1, pp. 19–23.

Michelassi, F., Liu, H., Hu, Z. and Dittman, J. S. (2017) 'A C1–C2 Module in Munc13 Inhibits Calcium-Dependent Neurotransmitter Release', *Neuron*, vol. 95, no. 3, 577-590.e5.

Milosevic, I., Sørensen, J. B., Lang, T., Krauss, M., Nagy, G., Haucke, V., Jahn, R. and Neher, E. (2005) 'Plasmalemmal Phosphatidylinositol-4,5-Bisphosphate Level Regulates the Releasable Vesicle Pool Size in Chromaffin Cells', *The Journal of Neuroscience*, vol. 25, no. 10, p. 2557.

Müller, M. and Davis, G. W. (2012) 'Transsynaptic control of presynaptic Ca^{2+} influx achieves homeostatic potentiation of neurotransmitter release', *Current biology : CB*, vol. 22, no. 12, pp. 1102–1108.

Müller, M., Genç, Ö. and Davis, G. W. (2015) 'RIM-binding protein links synaptic homeostasis to the stabilization and replenishment of high release probability vesicles', *Neuron*, vol. 85, no. 5, pp. 1056–1069.

Müller, M., Liu, K. S. Y., Sigrist, S. J. and Davis, G. W. (2012) 'RIM controls homeostatic plasticity through modulation of the readily-releasable vesicle pool', *The Journal of neuroscience : the official journal of the Society for Neuroscience*, vol. 32, no. 47, pp. 16574–16585.

Müller, M., Pym, E. C.G., Tong, A. and Davis, G. W. (2011) 'Rab3-GAP Controls the Progression of Synaptic Homeostasis at a Late Stage of Vesicle Release', *Neuron*, vol. 69, no. 4, pp. 749–762.

Nili, U., Wit, H. de, Gulyas-Kovacs, A., Toonen, R. F., Sorensen, J. B., Verhage, M. and Ashery, U. (2006) 'Munc18-1 phosphorylation by protein kinase C potentiates vesicle pool replenishment in bovine chromaffin cells', *Neuroscience*, vol. 143, no. 2, pp. 487–500.

Orr, B. O., Fetter, R. D. and Davis, G. W. (2017) 'Retrograde semaphorin–plexin signalling drives homeostatic synaptic plasticity', *Nature*, vol. 550, no. 7674, pp. 109–113.

Ortega, J. M., Genç, Ö., Davis, G. W., Goda, Y. and Marder, E. (2018) 'Molecular mechanisms that stabilize short term synaptic plasticity during presynaptic homeostatic plasticity', *eLife*, vol. 7, e40385.

Osterwalder, T., Yoon, K. S., White, B. H. and Keshishian, H. (2001) 'A conditional tissue-specific transgene expression system using inducible GAL4', *Proceedings of the National Academy of Sciences of the United States of America*, vol. 98, no. 22, pp. 12596–12601.

Peled, E. S., Newman, Z. L. and Isacoff, E. Y. (2014) 'Evoked and spontaneous transmission favored by distinct sets of synapses', *Current biology : CB*, vol. 24, no. 5, pp. 484–493.

Penney, J., Tsurudome, K., Liao, E. H., Elazzouzi, F., Livingstone, M., Gonzalez, M., Sonenberg, N. and Haghighi, A. P. (2012) 'TOR Is Required for the Retrograde Regulation of Synaptic Homeostasis at the Drosophila Neuromuscular Junction', *Neuron*, vol. 74, no. 1, pp. 166–178.

Perera, R. M., Zoncu, R., Lucast, L., Camilli, P. de and Toomre, D. (2006) 'Two synaptojanin 1 isoforms are recruited to clathrin-coated pits at different stages', *Proceedings of the National Academy of Sciences*, vol. 103, no. 51, p. 19332.

Pérez-Moreno, J. J. and O'Kane, C. J. (2019) 'GAL4 Drivers Specific for Type Ib and Type Is Motor Neurons in Drosophila', *G3 (Bethesda, Md.)*, vol. 9, no. 2, pp. 453–462.

Petersen, S. A., Fetter, R. D., Noordermeer, J. N., Goodman, C. S. and DiAntonio, A. (1997) 'Genetic Analysis of Glutamate Receptors in Drosophila Reveals a Retrograde Signal Regulating Presynaptic Transmitter Release', *Neuron*, vol. 19, no. 6, pp. 1237–1248.

Petzoldt, A. G., Lee, Y.-H., Khorramshahi, O., Reynolds, E., Plested, A. J. R., Herzel, H. and Sigrist, S. J. (2014) 'Gating characteristics control glutamate receptor distribution and trafficking in vivo', *Current biology : CB*, vol. 24, no. 17, pp. 2059–2065.

Pilgram, G. S. K., Potikanond, S., van der Plas, Mariska C, Fradkin, L. G. and Noordermeer, J. N. (2011) 'The RhoGAP crossveinless-c interacts with Dystrophin and is required for synaptic homeostasis at the Drosophila neuromuscular junction', *The Journal of neuroscience : the official journal of the Society for Neuroscience*, vol. 31, no. 2, pp. 492–500.

Plomp, J. J., van Kempen, G. T. and Molenaar, P. C. (1992) 'Adaptation of quantal content to decreased postsynaptic sensitivity at single endplates in alpha-bungarotoxin-treated rats', *The Journal of physiology*, vol. 458, no. 1, pp. 487–499.

Posor, Y., Eichhorn-Gruenig, M., Puchkov, D., Schöneberg, J., Ullrich, A., Lampe, A., Müller, R., Zarbakhsh, S., Gulluni, F., Hirsch, E., Krauss, M., Schultz, C., Schmoranzer,

J., Noé, F. and Haucke, V. (2013) ‘Spatiotemporal control of endocytosis by phosphatidylinositol-3,4-bisphosphate’, *Nature*, vol. 499, no. 7457, pp. 233–237.

Prehoda, K. E., Scott, J. A., Mullins, R. D. and Lim, W. A. (2000) ‘Integration of Multiple Signals Through Cooperative Regulation of the N-WASP-Arp2/3 Complex’, *Science*, vol. 290, no. 5492, p. 801.

Pulido, C. and Marty, A. (2017) ‘Quantal Fluctuations in Central Mammalian Synapses: Functional Role of Vesicular Docking Sites’, *Physiological Reviews*, vol. 97, no. 4, pp. 1403–1430.

Radhakrishnan, A., Stein, A., Jahn, R. and Fasshauer, D. (2009) ‘The Ca2+ affinity of synaptotagmin 1 is markedly increased by a specific interaction of its C2B domain with phosphatidylinositol 4,5-bisphosphate’, *The Journal of biological chemistry*, vol. 284, no. 38, pp. 25749–25760.

Ramalingam, N., Zhao, H., Breitsprecher, D., Lappalainen, P., Faix, J. and Schleicher, M. (2010) ‘Phospholipids regulate localization and activity of mDia1 formin’, *European Journal of Cell Biology*, vol. 89, no. 10, pp. 723–732.

Reddy-Alla, S., Böhme, M. A., Reynolds, E., Beis, C., Grasskamp, A. T., Mampell, M. M., Maglione, M., Jusyte, M., Rey, U., Babikir, H., McCarthy, A. W., Quentin, C., Matkovic, T., Bergeron, D. D., Mushtaq, Z., Göttfert, F., Owald, D., Mielke, T., Hell, S. W., Sigrist, S. J. and Walter, A. M. (2017) ‘Stable Positioning of Unc13 Restricts Synaptic Vesicle Fusion to Defined Release Sites to Promote Synchronous Neurotransmission’, *Neuron*, vol. 95, no. 6, 1350-1364.e12.

Regehr, W. G. (2012) ‘Short-term presynaptic plasticity’, *Cold Spring Harbor perspectives in biology*, vol. 4, no. 7, a005702.

Rhee, J.-S., Betz, A., Pyott, S., Reim, K., Varoqueaux, F., Augustin, I., Hesse, D., Südhof, T. C., Takahashi, M., Rosenmund, C. and Brose, N. (2002) ‘β Phorbol Ester- and Diacylglycerol-Induced Augmentation of Transmitter Release Is Mediated by Munc13s and Not by PKCs’, *Cell*, vol. 108, no. 1, pp. 121–133.

Richmond, J. E., Davis, W. S. and Jorgensen, E. M. (1999) ‘UNC-13 is required for synaptic vesicle fusion in C. elegans’, *Nature Neuroscience*, vol. 2, no. 11, pp. 959–964.

Riedl, J., Crevenna, A. H., Kessenbrock, K., Yu, J. H., Neukirchen, D., Bista, M., Bradke, F., Jenne, D., Holak, T. A., Werb, Z., Sixt, M. and Wedlich-Soldner, R. (2008)

'Lifeact: a versatile marker to visualize F-actin', *Nature Methods*, vol. 5, no. 7, pp. 605–607.

Rizzoli, S. O. and Betz, W. J. (2004) 'The structural organization of the readily releasable pool of synaptic vesicles', *Science (New York, N.Y.)*, vol. 303, no. 5666, pp. 2037–2039.

Rizzoli, S. O. and Betz, W. J. (2005) 'Synaptic vesicle pools', *Nature Reviews Neuroscience*, vol. 6, no. 1, pp. 57–69.

Robertis, E. D. de and Bennett, H. S. (1955) 'Some features of the submicroscopic morphology of synapses in frog and earthworm', *The Journal of biophysical and biochemical cytology*, vol. 1, no. 1, pp. 47–58.

Rohatgi, R., Ho, H.-y. H. and Kirschner, M. W. (2000) 'Mechanism of N-Wasp Activation by Cdc42 and Phosphatidylinositol 4,5-Bisphosphate', *The Journal of Cell Biology*, vol. 150, no. 6, pp. 1299–1310.

Rudolph, S., Tsai, M.-C., Gersdorff, H. von and Wadiche, J. I. (2015) 'The ubiquitous nature of multivesicular release', *Trends in Neurosciences*, vol. 38, no. 7, pp. 428–438.

Saarikangas, J., Zhao, H. and Lappalainen, P. (2010) 'Regulation of the Actin Cytoskeleton-Plasma Membrane Interplay by Phosphoinositides', *Physiological Reviews*, vol. 90, no. 1, pp. 259–289.

Sakamoto, H., Ariyoshi, T., Kimpara, N., Sugao, K., Taiko, I., Takikawa, K., Asanuma, D., Namiki, S. and Hirose, K. (2018) 'Synaptic weight set by Munc13-1 supramolecular assemblies', *Nature Neuroscience*, vol. 21, no. 1, pp. 41–49.

Scarnati, M. S., Kataria, R., Biswas, M., Paradiso, K. G., Monteggia, L. M. and Westbrook, G. L. (2018) 'Active presynaptic ribosomes in the mammalian brain, and altered transmitter release after protein synthesis inhibition', *eLife*, vol. 7, e36697.

Scheuss, V. and Neher, E. (2001) 'Estimating synaptic parameters from mean, variance, and covariance in trains of synaptic responses', *Biophysical Journal*, vol. 81, no. 4, pp. 1970–1989.

Schneggenburger, R. and Neher, E. (2000) 'Intracellular calcium dependence of transmitter release rates at a fast central synapse', *Nature*, vol. 406, no. 6798, pp. 889–893.

Schoch, S., Castillo, P. E., Jo, T., Mukherjee, K., Geppert, M., Wang, Y., Schmitz, F., Malenka, R. C. and Südhof, T. C. (2002) 'RIM1alpha forms a protein scaffold for

regulating neurotransmitter release at the active zone', *Nature*, vol. 415, no. 6869, pp. 321–326.

Scholze, M. J., Barbieux, K. S., Simone, A. de, Boumasmoud, M., Süess, C. C. N., Wang, R. and Gönczy, P. (2018) 'PI(4,5)P2 forms dynamic cortical structures and directs actin distribution as well as polarity in Caenorhabditis elegans embryos', *Development*, vol. 145, no. 11, dev164988.

Senju, Y. and Lappalainen, P. (2019) 'Regulation of actin dynamics by PI(4,5)P2 in cell migration and endocytosis', *Current Opinion in Cell Biology*, vol. 56, pp. 7–13.

Seven, A. B., Brewer, K. D., Shi, L., Jiang, Q.-X. and Rizo, J. (2013) 'Prevalent mechanism of membrane bridging by synaptotagmin-1', *Proceedings of the National Academy of Sciences of the United States of America*, vol. 110, no. 34, E3243-52.

Shapiro, H. (1932) 'The Rate of Oviposition in the Fruit Fly, Drosophila', *Biological Bulletin*, vol. 63, no. 3, pp. 456–471.

Shin, O.-H., Lu, J., Rhee, J.-S., Tomchick, D. R., Pang, Z. P., Wojcik, S. M., Camacho-Perez, M., Brose, N., Machius, M., Rizo, J., Rosenmund, C. and Südhof, T. C. (2010) 'Munc13 C2B domain is an activity-dependent Ca2+ regulator of synaptic exocytosis', *Nature Structural & Molecular Biology*, vol. 17, no. 3, pp. 280–288.

Shin, O.-H., Xu, J., Rizo, J. and Südhof, T. C. (2009) 'Differential but convergent functions of Ca2+ binding to synaptotagmin-1 C2 domains mediate neurotransmitter release', *Proceedings of the National Academy of Sciences*, vol. 106, no. 38, p. 16469.

Siebert, M., Böhme, M. A., Driller, J. H., Babikir, H., Mampell, M. M., Rey, U., Ramesh, N., Matkovic, T., Holton, N., Reddy-Alla, S., Göttfert, F., Kamin, D., Quentin, C., Klinedinst, S., Andlauer, T. F., Hell, S. W., Collins, C. A., Wahl, M. C., Loll, B. and Sigrist, S. J. (2015) 'A high affinity RIM-binding protein/Aplip1 interaction prevents the formation of ectopic axonal active zones', *eLife*, vol. 4.

Sigrist, S. J., Reiff, D. F., Thiel, P. R., Steinert, J. R. and Schuster, C. M. (2003) 'Experience-Dependent Strengthening of Drosophila Neuromuscular Junctions', *The Journal of neuroscience : the official journal of the Society for Neuroscience*, vol. 23, no. 16, pp. 6546–6556.

Simms, B. A. and Zamponi, G. W. (2014) 'Neuronal Voltage-Gated Calcium Channels: Structure, Function, and Dysfunction', *Neuron*, vol. 82, no. 1, pp. 24–45.

Skare, P. and Karlsson, R. (2002) ‘Evidence for two interaction regions for phosphatidylinositol(4,5)-bisphosphate on mammalian profilin I’, *FEBS Letters*, vol. 522, 1-3, pp. 119–124.

Smith, L. A., Peixoto, A. A., Kramer, E. M., Villella, A. and Hall, J. C. (1998) ‘Courtship and visual defects of cacophony mutants reveal functional complexity of a calcium-channel alpha1 subunit in Drosophila’, *Genetics*, vol. 149, no. 3, pp. 1407–1426.

Sollner, T., Whiteheart, S. W., Brunner, M., Erdjument-Bromage, H., Geromanos, S., Tempst, P. and Rothman, J. E. (1993) ‘SNAP receptors implicated in vesicle targeting and fusion’, *Nature*, vol. 362, no. 6418, pp. 318–324.

Song, W., Ranjan, R., Dawson-Scully, K., Bronk, P., Marin, L., Seroude, L., Lin, Y.-J., Nie, Z., Atwood, H. L., Benzer, S. and Zinsmaier, K. E. (2002) ‘Presynaptic Regulation of Neurotransmission in Drosophila by the G Protein-Coupled Receptor Methuselah’, *Neuron*, vol. 36, no. 1, pp. 105–119.

Song, Y., Ailenberg, M. and Silverman, M. (1998) ‘Cloning of a novel gene in the human kidney homologous to rat munc13s: its potential role in diabetic nephropathy’, *Kidney international*, vol. 53, no. 6, pp. 1689–1695.

Spracklen, A. J., Fagan, T. N., Lovander, K. E. and Tootle, T. L. (2014) ‘The pros and cons of common actin labeling tools for visualizing actin dynamics during Drosophila oogenesis’, *Developmental Biology*, vol. 393, no. 2, pp. 209–226.

Stanton, P. K., Winterer, J., Bailey, C. P., Kyrozis, A., Raginov, I., Laube, G., Veh, R. W., Nguyen, C. Q. and Müller, W. (2003) ‘Long-Term Depression of Presynaptic Release from the Readily Releasable Vesicle Pool Induced by NMDA Receptor-Dependent Retrograde Nitric Oxide’, *The Journal of neuroscience : the official journal of the Society for Neuroscience*, vol. 23, no. 13, pp. 5936–5944.

Stevens, C. F. and Sullivan, J. M. (1998) ‘Regulation of the Readily Releasable Vesicle Pool by Protein Kinase C’, *Neuron*, vol. 21, no. 4, pp. 885–893.

Stevens, C. F. and Tsujimoto, T. (1995) ‘Estimates for the pool size of releasable quanta at a single central synapse and for the time required to refill the pool’, *Proceedings of the National Academy of Sciences of the United States of America*, vol. 92, no. 3, pp. 846–849.

Stevens, D. R., Wu, Z.-X., Matti, U., Junge, H. J., Schirra, C., Becherer, U., Wojcik, S. M., Brose, N. and Rettig, J. (2005) ‘Identification of the Minimal Protein Domain

Required for Priming Activity of Munc13-1', *Current biology : CB*, vol. 15, no. 24, pp. 2243–2248.

Stewart, B. A., Atwood, H. L., Renger, J. J., Wang, J. and Wu, C. F. (1994) 'Improved stability of Drosophila larval neuromuscular preparations in haemolymph-like physiological solutions', *Journal of comparative physiology. A, Sensory, neural, and behavioral physiology*, vol. 175, no. 2, pp. 179–191.

Stocker, B., Bochow, C., Damrau, C., Mathejczyk, T., Wolfenberg, H., Colomb, J., Weber, C., Ramesh, N., Duch, C., Biserova, N. M., Sigrist, S. and Pflüger, H.-J. (2018) 'Structural and Molecular Properties of Insect Type II Motor Axon Terminals', *Frontiers in systems neuroscience*, vol. 12, p. 5.

Subach, F. V., Subach, O. M., Gundorov, I. S., Morozova, K. S., Piatkevich, K. D., Cuervo, A. M. and Verkhusha, V. V. (2009) 'Monomeric fluorescent timers that change color from blue to red report on cellular trafficking', *Nature chemical biology*, vol. 5, no. 2, pp. 118–126.

Südhof, T. C. (2012) 'The presynaptic active zone', *Neuron*, vol. 75, no. 1, pp. 11–25.

Sun, Y., Carroll, S., Kaksonen, M., Toshima, J. Y. and Drubin, D. G. (2007) 'PtdIns(4,5)P2 turnover is required for multiple stages during clathrin- and actin-dependent endocytic internalization', *The Journal of Cell Biology*, vol. 177, no. 2, pp. 355–367.

Sutton, R. B., Fasshauer, D., Jahn, R. and Brunger, A. T. (1998) 'Crystal structure of a SNARE complex involved in synaptic exocytosis at 2.4 Å resolution', *Nature*, vol. 395, no. 6700, pp. 347–353.

Takahashi, T. (2015) 'Strength and precision of neurotransmission at mammalian presynaptic terminals', *Proceedings of the Japan Academy. Series B, Physical and biological sciences*, vol. 91, no. 7, pp. 305–320.

Terskikh, A., Fradkov, A., Ermakova, G., Zaraisky, A., Tan, P., Kajava, A. V., Zhao, X., Lukyanov, S., Matz, M., Kim, S., Weissman, I. and Siebert, P. (2000) '"Fluorescent timer": protein that changes color with time', *Science*, vol. 290, no. 5496, pp. 1585–1588.

Tour, O., Meijer, R. M., Zacharias, D. A., Adams, S. R. and Tsien, R. Y. (2003) 'Genetically targeted chromophore-assisted light inactivation', *Nature Biotechnology*, vol. 21, no. 12, pp. 1505–1508.

Tully, T., Preat, T., Boynton, S. C. and Del Vecchio, M. (1994) 'Genetic dissection of consolidated memory in Drosophila', *Cell*, vol. 79, no. 1, pp. 35–47.

Ugur, B., Chen, K. and Bellen, H. J. (2016) 'Drosophila tools and assays for the study of human diseases', *Disease Models & Mechanisms*, vol. 9, no. 3, p. 235.

van den Bogaart, G., Meyenberg, K., Risselada, H. J., Amin, H., Willig, K. I., Hubrich, B. E., Dier, M., Hell, S. W., Grubmüller, H., Diederichsen, U. and Jahn, R. (2011) 'Membrane protein sequestering by ionic protein-lipid interactions', *Nature*, vol. 479, no. 7374, pp. 552–555.

van der Plas, Mariska C, Pilgram, G. S. K., Plomp, J. J., Jong, A. de, Fradkin, L. G. and Noordermeer, J. N. (2006) 'Dystrophin is required for appropriate retrograde control of neurotransmitter release at the Drosophila neuromuscular junction', *The Journal of neuroscience : the official journal of the Society for Neuroscience*, vol. 26, no. 1, pp. 333–344.

Varoqueaux, F., Sigler, A., Rhee, J.-S., Brose, N., Enk, C., Reim, K. and Rosenmund, C. (2002) 'Total arrest of spontaneous and evoked synaptic transmission but normal synaptogenesis in the absence of Munc13-mediated vesicle priming', *Proceedings of the National Academy of Sciences of the United States of America*, vol. 99, no. 13, pp. 9037–9042.

Verhage, M. and Sørensen, J. B. (2008) 'Vesicle docking in regulated exocytosis', *Traffic (Copenhagen, Denmark)*, vol. 9, no. 9, pp. 1414–1424.

Virmani, T., Ertunc, M., Sara, Y., Mozhayeva, M. and Kavalali, E. T. (2005) 'Phorbol Esters Target the Activity-Dependent Recycling Pool and Spare Spontaneous Vesicle Recycling', *The Journal of neuroscience : the official journal of the Society for Neuroscience*, vol. 25, no. 47, pp. 10922–10929.

Wagh, D. A., Rasse, T. M., Asan, E., Hofbauer, A., Schwenkert, I., DÃ¼rrbeck, H., Buchner, S., Dabauvalle, M.-C., Schmidt, M., Qin, G., Wichmann, C., Kittel, R., Sigrist, S. J. and Buchner, E. (2006) 'Bruchpilot, a Protein with Homology to ELKS/CAST, Is Required for Structural Integrity and Function of Synaptic Active Zones in Drosophila', *Neuron*, vol. 49, no. 6, pp. 833–844.

Wagner, M. L. and Tamm, L. K. (2001) 'Reconstituted syntaxin1a/SNAP25 interacts with negatively charged lipids as measured by lateral diffusion in planar supported bilayers', *Biophysical Journal*, vol. 81, no. 1, pp. 266–275.

Walter, A. M., Böhme, M. A. and Sigrist, S. J. (2018) 'Vesicle release site organization at synaptic active zones', *Neuroscience Research*, vol. 127, pp. 3–13.

Walter, A. M., Groffen, A. J., Sørensen, J. B. and Verhage, M. (2011) 'Multiple Ca2+ sensors in secretion: teammates, competitors or autocrats?', *Trends in Neurosciences*, vol. 34, no. 9, pp. 487–497.

Walter, A. M., Müller, R., Tawfik, B., Wierda, K. D. B., Pinheiro, P. S., Nadler, A., McCarthy, A. W., Ziomkiewicz, I., Kruse, M., Reither, G., Rettig, J., Lehmann, M., Haucke, V., Hille, B., Schultz, C., Sørensen, J. B. and Pfeffer, S. R. (2017) 'Phosphatidylinositol 4,5-bisphosphate optical uncaging potentiates exocytosis', *eLife*, vol. 6, e30203.

Wang, T., Hauswirth, A. G., Tong, A., Dickman, D. K. and Davis, G. W. (2014) 'Endostatin Is a Trans-Synaptic Signal for Homeostatic Synaptic Plasticity', *Neuron*, vol. 83, no. 3, pp. 616–629.

Wang, T., Jones, R. T., Whippen, J. M. and Davis, G. W. (2016) 'α2δ-3 Is Required for Rapid Transsynaptic Homeostatic Signaling', *Cell reports*, vol. 16, no. 11, pp. 2875–2888.

Wang, X., Wang, Q., Engisch, K. L. and Rich, M. M. (2010) 'Activity-dependent regulation of the binomial parameters p and n at the mouse neuromuscular junction in vivo', *Journal of neurophysiology*, vol. 104, no. 5, pp. 2352–2358.

Watanabe, K., Al-Bassam, S., Miyazaki, Y., Wandless, T. J., Webster, P. and Arnold, D. B. (2012) 'Networks of polarized actin filaments in the axon initial segment provide a mechanism for sorting axonal and dendritic proteins', *Cell reports*, vol. 2, no. 6, pp. 1546–1553.

Weimer, R. M., Gracheva, E. O., Meyrignac, O., Miller, K. G., Richmond, J. E. and Bessereau, J.-L. (2006) 'UNC-13 and UNC-10/rim localize synaptic vesicles to specific membrane domains', *The Journal of neuroscience : the official journal of the Society for Neuroscience*, vol. 26, no. 31, pp. 8040–8047.

Weyhersmüller, A., Hallermann, S., Wagner, N. and Eilers, J. (2011) 'Rapid Active Zone Remodeling during Synaptic Plasticity', *The Journal of Neuroscience*, vol. 31, no. 16, p. 6041.

Wu, X.-S. and Wu, L.-G. (2001) 'Protein Kinase C Increases the Apparent Affinity of the Release Machinery to Ca2+ by Enhancing the Release Machinery Downstream of the Ca2+ Sensor', *The Journal of Neuroscience*, vol. 21, no. 20, p. 7928.

Xu, X. Z., Wes, P. D., Chen, H., Li, H. S., Yu, M., Morgan, S., Liu, Y. and Montell, C. (1998) 'Retinal targets for calmodulin include proteins implicated in synaptic transmission', *The Journal of biological chemistry*, vol. 273, no. 47, pp. 31297–31307.

Yang, Y. and Calakos, N. (2013) 'Presynaptic long-term plasticity', *Frontiers in Synaptic Neuroscience*, vol. 5.

Yarar, D., Waterman-Storer, C. M. and Schmid, S. L. (2007) 'SNX9 Couples Actin Assembly to Phosphoinositide Signals and Is Required for Membrane Remodeling during Endocytosis', *Developmental cell*, vol. 13, no. 1, pp. 43–56.

Younger, M. A., Müller, M., Tong, A., Pym, E. C. and Davis, G. W. (2013) 'A presynaptic ENaC channel drives homeostatic plasticity', *Neuron*, vol. 79, no. 6, pp. 1183–1196.

Zanet, J., Jayo, A., Plaza, S., Millard, T., Parsons, M. and Stramer, B. (2012) 'Fascin promotes filopodia formation independent of its role in actin bundling', *The Journal of Cell Biology*, vol. 197, no. 4, pp. 477–486.

Zeidler, M. P., Tan, C., Bellaiche, Y., Cherry, S., Hader, S., Gayko, U. and Perrimon, N. (2004) 'Temperature-sensitive control of protein activity by conditionally splicing inteins', *Nature Biotechnology*, vol. 22, no. 7, pp. 871–876.

Zhai, R. G. and Bellen, H. J. (2004) 'The Architecture of the Active Zone in the Presynaptic Nerve Terminal', *Physiology*, vol. 19, no. 5, pp. 262–270.

Zhang, B. and Stewart, B. (2010a) 'Electrophysiological recording from Drosophila larval body-wall muscles', *Cold Spring Harbor protocols*, vol. 2010, no. 9, pdb.prot5487.

Zhang, B. and Stewart, B. (2010b) 'Synaptic Electrophysiology of the Drosophila Neuromuscular Junction: Chapter 12', in Zhang, B., Freeman, M. R. and Waddell, S. (eds) *Drosophila neurobiology: A laboratory manual / edited by Bing Zhang, Marc R. Freeman, Scott Waddell,* Cold Spring Harbor, N.Y., Cold Spring Harbor Laboratory Press.

Zhang, B. and Stewart, B. (2010c) 'Voltage-clamp analysis of synaptic transmission at the Drosophila larval neuromuscular junction', *Cold Spring Harbor protocols*, vol. 2010, no. 9, pdb.prot5488.

Zhao, H., Hakala, M. and Lappalainen, P. (2010) 'ADF/Cofilin Binds Phosphoinositides in a Multivalent Manner to Act as a PIP2-Density Sensor', *Biophysical Journal*, vol. 98, no. 10, pp. 2327–2336.

Zhou, K., Stawicki, T. M., Goncharov, A. and Jin, Y. (2013) 'Position of UNC-13 in the active zone regulates synaptic vesicle release probability and release kinetics', *eLife*, vol. 2, e01180.

Zhou, Q., Zhou, P., Wang, A. L., Wu, D., Zhao, M., Südhof, T. C. and Brunger, A. T. (2017) 'The primed SNARE–complexin–synaptotagmin complex for neuronal exocytosis', *Nature*, vol. 548, no. 7668, pp. 420–425.

Zhu, H., Hille, B. and Xu, T. (2002) 'Sensitization of regulated exocytosis by protein kinase C', *Proceedings of the National Academy of Sciences*, vol. 99, no. 26, p. 17055.

Zikich, D., Mezer, A., Varoqueaux, F., Sheinin, A., Junge, H. J., Nachliel, E., Melamed, R., Brose, N., Gutman, M. and Ashery, U. (2008) 'Vesicle Priming and Recruitment by ubMunc13-2 Are Differentially Regulated by Calcium and Calmodulin', *The Journal of Neuroscience*, vol. 28, no. 8, p. 1949.

Zoncu, R., Perera, R. M., Sebastian, R., Nakatsu, F., Chen, H., Balla, T., Ayala, G., Toomre, D. and Camilli, P. V. de (2007) 'Loss of endocytic clathrin-coated pits upon acute depletion of phosphatidylinositol 4,5-bisphosphate', *Proceedings of the National Academy of Sciences*, vol. 104, no. 10, p. 3793.

8 Appendix

8.1 List of publications

Grasskamp, A. T., Jusyte, M., **McCarthy, A. W.,** Walter, A. M. 'Molecular and functional interdependence of spontaneous and action potential evoked neurotransmission at individual synapses', *in preparation*.

Böhme, M. A.*, **McCarthy, A. W.***, Grasskamp, A. T., Beuschel, C. B., Goel, P., Jusyte, M., Laber, D., Huang, S., Rey, U., Petzoldt, A. G., Lehmann, M., Göttfert, F., Haghighi, P., Hell, S. W., Owald, D., Dickman, D., Sigrist, S. J. and Walter, A. M. (2019) 'Rapid active zone remodeling consolidates presynaptic potentiation', *Nature Communications*, vol. 10, no. 1, p. 1085

*Co-first author

Walter, A. M., Müller, R., Tawfik, B., Wierda, K. D. B., Pinheiro, P. S., Nadler, A., **McCarthy, A. W.**, Ziomkiewicz, I., Kruse, M., Reither, G., Rettig, J., Lehmann, M., Haucke, V., Hille, B., Schultz, C., Sørensen, J. B. and Pfeffer, S. R. (2017) 'Phosphatidylinositol 4,5-bisphosphate optical uncaging potentiates exocytosis', *eLife*, vol. 6, e30203.

Reddy-Alla, S., Böhme, M. A., Reynolds, E., Beis, C., Grasskamp, A. T., Mampell, M. M., Maglione, M., Jusyte, M., Rey, U., Babikir, H., **McCarthy, A. W.**, Quentin, C., Matkovic, T., Bergeron, D. D., Mushtaq, Z., Göttfert, F., Owald, D., Mielke, T., Hell, S. W., Sigrist, S. J. and Walter, A. M. (2017) 'Stable Positioning of Unc13 Restricts Synaptic Vesicle Fusion to Defined Release Sites to Promote Synchronous Neurotransmission', *Neuron*, vol. 95, no. 6, 1350-1364.e12

8.2 Abbreviations

αBTX	α-bungarotoxin
AMPA	a-amino-3-hdroxy-5-methyl-4-isooxazolepropionic acid
AP	action potential
Aplip1	APP-like protein interacting protein 1
ATP	adenosine triphosphate
AZ	active zone
BIS	Bisindolylmaleimide
BMP	bone morphogenic factor
BRP	Bruchpilot
Cac	Cacophony
CALI	chromophore assisted light inactivation
CaM	Calmodulin
CaMKII	Ca^{2+}/calmodulin-dependent protein kinase II
cAMP	cyclic adenosine monophosphate
CAST	CAZ-Associated STructural protein
cg-PI(4,5)P_2	caged phosphatidylinositol 4,5-bisphosphate
cv-c	crossveinless-c
DAG	diacylglycerol
DEG/ENaC	Degenerin/Epithelial Sodium channel
DMSO	dimethyl sulfoxide
eEPSC/P	evoked excitatory postsynaptic potential
EGTA	ethylene glycol-*bis*(β-aminoethyl ether)-N,N,N′,N′-tetraacetic acid
ELKS	protein rich in the amino acids E, L, K and S
EM	electron microscopy
EMS	ethyl methanesulfonate
Exn	Ephexin
Foxo	Forkhead box O
FRAP	fluorescence recovery after photobleaching

GAL4	galactose-responsive transcription factor GAL4
GFP	green fluorescent protein
Gbb	glass bottom boat
GluR	glutamate receptor
imp13	Importin13
ISI	interstimulus interval
KAR	kainate receptor
KLC	kinesin light chain
LDCV	large dense core vesicle
LTD	long-term depression
LTP	long-term potentiation
mEPSC/P	mini excitatory postsynaptic current/potential
(M)unc13	(mammalian) Uncoordinated-13
(M)unc18	(mammalian) Uncoordinated-18
NMJ	neuromuscular junction
NT	neurotransmitter
PdBu	4β-phorbol-12, 13-dibutyrate
PHP	presynaptic homeostatic potentiation
PIPKIγ	phosphatidylinositol-4-phosphate 5-kinase type Iγ
PhTx	Philanthotoxin
PKA	protein kinase A
PKC	protein kinase C
PLC	phospholipase C
PlexB	plexin B
PMA	phorbol 12-myristate 13-acetate
PPR	paired-pulse ratio
QC	quantal content
RBP	RIM binding protein
RFP	red fluorescent protein
RhoGAP	Rho GTPase activating protein

RhoGEF	Rho-type guanine nucleotide exchange factor
RIM	Rab3 interacting molecule
RNAi	RNA interference
ROI	region of interest
RRP	readily releasable pool
S6K	p70 S6 ribosomal kinase
SEM	standard error of the mean
Sema2b	semaphorin 2b
SNARE	Soluble N-ethylmaleimide sensitive factor Attachment protein Receptor
Srpk79D	serine arginine protein kinase at cytological position 79D
STED	stimulated emission depletion (microscopy)
STP	short-term plasticity
SUnSET	SUrface SEnsing of Translation
SV	synaptic vesicle
Syt	synaptotagmin
Syx	syntaxin
TEVC	two-electrode current clamp
TIRF	total internal reflection fluorescence (microscopy)
TOR	target of rapamycin
TTX	tetrodotoxin
UAS	upstream activating sequence
UV	ultraviolet
VAMP	vesicle associated membrane protein
Wit	wishful thinking

8.3 Figure Index

8.4 Statistics summary

Table 2: Summary of experimental parameters.

Figure	Description	Mean ± SEM (n)		p value	Statistical test
Figure 7a	488 nm channel intensity	before uncaging	after uncaging		
		857.9 ± 23.17 (10)	1518 ± 80.72 (10)	< 0.0001***	Paired t-test
Figure 7b	405 nm channel intensity	Frame 1	Frame 60		
	cg-PI(4,5)P_2	416.9 ± 122.4 (14)	182.6 ± 34.61 (14)	0.0328*	Paired t-test
	DMSO	30.33 ± 13.71 (5)	36.89 ± 15.11 (5)	0.6392	Paired t-test
Figure 8a	488 nm channel intensity	DMSO	cg-PI(4,5)P_2		
		0.9869 ± 0.004366 (15)	1.009 ± 0.004972 (15)	0.0005***	Mann-Whitney U test
Figure 8b	561 nm channel intensity	DMSO	cg-PI(4,5)P_2		
		0.9805 ± 0.002376 (5)	1.00 ± 0.005143 (6)	0.0043**	Mann-Whitney U test

Figure	Description	Mean ± SEM (n)		p value	Statistical test
Figure 9b	Paired-pulse ratios	Before	After		
	No flash	0.9137 ± 0.02038 (7)	0.9242 ± 0.03308 (7)	0.5345	Paired t-test
	Flash	0.9436 ± 0.02200 (7)	0.9452 ± 0.01421 (7)	0.9518	Paired t-test
	First amplitudes (nA)	Before	After		
	No flash	-90.546 ± 6.651 (7)	-84.961 ± 6.497 (7)	0.0082**	Paired t-test
	Flash	-99.034 ± 4.872 (7)	-93.720 ± 4.758 (7)	0.0643	Paired t-test
		DMSO	PMA		
Figure 10c	mEPSC amplitude (nA)	-5.622 ± 0.2002 (9)	-5.437 ± 0.222 (9)	0.3347	Mann-Whitney U test
Figure 10d	mEPSC frequency (Hz)	2.296 ± 0.2076 (9)	2.489 ± 0.2067 (9)	0.5202	Unpaired t-test
Figure 10e	eEPSC amplitude (nA)	-55.861 ± 8.181 (9)	-81.931 ± 6.824 (9)	0.0142*	Mann-Whitney U test
Figure 10f	Quantal content	99.55 ± 14.27 (9)	152.6 ± 14.11 (9)	0.0078**	Mann-Whitney U test
Figure 10h	Paired-pulse ratio	0.9004 ± 0.04298 (9)	0.7155 ± 0.07297 (9)	0.0442*	Unpaired t-test
Figure 10j	y-intercept	-284.171 ± 78.881 (9)	-549.913 ± 87.024 (9)	0.0379*	Unpaired t-test
Figure 10k	Slope	-78.823 ± 3.965 (9)	-72.221 ± 4.892 (9)	0.31	Unpaired t-test

Figure	Description	Mean ± SEM (n)		p value	Statistical test
		before PhTx	after PhTx		
Figure 11a	mEPSP frequency (Hz)	2.417 ± 0.1329 (18)	2.226 ± 0.1917 (18)	0.0435*	Paired t-test
	mEPSP amplitude (mV)	0.8902 ± 0.03051 (18)	0.5702 ± 0.02297 (18)	<0.0001***	Paired t-test
		after PhTx, before no stim	after PhTx, after no stim		
Figure 11c	mEPSP frequency (Hz)	2.163 ± 0.2705 (9)	2.144 ± 0.2429 (9)	0.8962	Paired t-test
	mEPSP amplitude (mV)	0.5261 ± 0.03291 (9)	0.5218 ± 0.02073 (9)	0.8328	Paired t-test
		after PhTx, before stim	after PhTx, after stim		
Figure 11d	mEPSP frequency (Hz)	2.289 ± 0.2863 (9)	1.726 ± 0.1790 (9)	0.0027**	Paired t-test
	mEPSP amplitude (mV)	0.6144 ± 0.02594 (9)	0.5675 ± 0.04475 (9)	0.1371	Paired t-test
	Wild-type	Ctrl	PhTx		
Figure 12b, 17b	mEPSP amplitude (mV)	0.8074 ± 0.03153 (8)	0.4539 ± 0.03266 (8)	< 0.0001***	Unpaired t-test
	eEPSP amplitude (mV)	17.32 ± 2.681 (8)	15.57 ± 1.609 (8)	0.5844	Unpaired t-test
	Quantal content	21.15 ± 2.758 (8)	34.4 ± 2.616 (8)	0.0036**	Unpaired t-test
	unc13A^{Null}				
Figure 12d	mEPSP amplitude (mV)	0.9881 ± 0.06958 (9)	0.9881 ± 0.06958 (9)	0.0006***	Unpaired t-test
	eEPSP amplitude (mV)	3.296 ± 0.6671 (9)	1.453 ± 0.3050 (9)	0.0188*	Mann-Whitney U test
	Quantal content	3.395 ± 0.6906 (9)	2.795 ± 0.8457 (9)	0.3799	Mann-Whitney U test

Figure	Description	Mean ± SEM (n)		p value	Statistical test
	Unc13A-GFP	Ctrl	PhTx		
Figure 13b	mEPSP amplitude (mV)	1.372 ± 0.09085 (12)	0.7788 ± 0.05711 (13)	<0.0001***	Unpaired t-test
	eEPSP amplitude (mV)	21.59 ± 2.756 (12)	21.44 ± 3.101 (13)	0.9714	Unpaired t-test
	Quantal content	16.63 ± 2.498 (12)	29.20 ± 4.383 (13)	0.0396*	Mann-Whitney U test
	C-term-GFP				
Figure 13d	mEPSP amplitude (mV)	1.194 ± 0.06731 (10)	0.7063 ± 0.03215 (11)	<0.0001***	Mann-Whitney U test
	eEPSP amplitude (mV)	16.77 ± 2.326 (10)	6.800 ± 1.744 (11)	0.0028**	Mann-Whitney U test
	Quantal content	14.77 ± 2.405 (10)	9.416 ± 2.115 (11)	0.1096	Unpaired t-test
	Values 400s after PhTx	Unc13A-GFP	C-term-GFP		
Figure 14b	mEPSP amplitude (mV)	0.4891 ± 0.01298 (14)	0.5129 ± 0.02204 (15)	0.7148	Mann-Whitney U test
Figure 14c	mEPSP frequency (Hz)	1.016 ± 0.1134 (14)	1.128 ± 0.1244 (15)	0.5124	Unpaired t-test
Figure 14d	eEPSP amplitude (mV)	14.77 ± 2.400 (14)	8.927 ± 0.9712 (15)	0.0769	Mann-Whitney U test
Figure 14e	Quantal content	30.49 ± 5.068 (14)	17.65 ± 1.897 (15)	0.0292*	Mann-Whitney U test

Figure	Description	Mean ± SEM (n)		p value	Statistical test
	Wild-type	Ctrl	PhTx		
Figure 15b	mEPSP amplitude (mV)	1.031 ± 0.06045 (18)	0.4999 ± 0.04065 (23)	<0.0001***	Unpaired t-test
	eEPSP amplitude (mV)	28.41 ± 2.743 (18)	22.77 ± 2.075 (23)	0.1024	Unpaired t-test
	Quantal content	30.66 ± 4.253 (18)	54.34 ± 7.698 (23)	0.0217*	Mann-Whitney U test
	brp^{Null}				
Figure 15d	mEPSP amplitude (mV)	1.381 ± 0.08217 (11)	0.5881 ± 0.03854 (11)	<0.0001***	Mann-Whitney U test
	eEPSP amplitude (mV)	9.931 ± 1.850 (11)	8.793 ± 1.804 (11)	0.6643	Unpaired t-test
	Quantal content	7.632 ± 1.679 (11)	15.54 ± 3.108 (11)	0.0368*	Unpaired t-test
		Ctrl	PhTx		
Figure 16b	Motile	39.45 ± 7.431 (10)	66.06 ± 7.391 (9)	0.0216*	Unpaired t-test
	Stable	60.55 ± 7.431 (10)	33.94 ± 7.391 (9)		
Figure 17b	See Figure 12b				

Figure	Description	Mean ± SEM (n)		p value	Statistical test
	Wild-type	Ctrl	PhTx		
Figure 17c	BRP intensity	641.9 ± 45.84 (21)	940.3 ± 74.49 (23)	0.0044**	Mann-Whitney U test
	Unc13A intensity	530.5 ± 34.74 (21)	842.7 ± 54.48 (23)	0.0002***	Mann-Whitney U test
	gluRIIA^{Null}	Ctrl	PhTx		
Figure 17e	mEPSP amplitude (mV)	1.144 ± 0.06038 (10)	0.3680 ± 0.02385 (9)	<0.0001***	Mann-Whitney U test
	eEPSP amplitude (mV)	22.17 ± 1.759 (10)	21.09 ± 1.771 (9)	0.671	Unpaired t-test
	Quantal content	19.99 ± 2.005 (10)	60.95 ± 8.605 (9)	<0.0001***	Mann-Whitney U test
	gluRIIA^{Null}	Ctrl	PhTx		
Figure 17f	BRP intensity	21.51 ± 3.006 (20)	27.97 ± 1.772 (29)	0.0029**	Mann-Whitney U test
	Unc13A intensity	17.30 ± 2.059 (20)	20.11 ± 1.654 (29)	0.291	Unpaired t-test

Figure	Description	Mean ± SEM (n)		p value	Statistical test
Figure 18b	mEPSP amplitude (mV)				
	Wild-type vs. *gluRIIA*^{Null}	0.940 ± 0.03 (9)	0.488 ± 0.02 (8)	< 0.0001***	One way ANOVA with Tukey's multiple comparison test
	brp^{Null} vs. *brp*^{Null};*gluRIIA*^{Null}	1.07 ± 0.04 (8)	0.497 ± 0.01 (9)	< 0.0001***	
	gluRIIA^{Null} vs. *brp*^{Null};*gluRIIA*^{Null}	0.488 ± 0.02 (8)	0.497 ± 0.01 (9)	0.99	
	eEPSP amplitude (mV)				
	Wild-type vs. *gluRIIA*^{Null}	33.82 ± 0.75 (9)	26.67 ± 0.93 (8)	< 0.0001***	One way ANOVA with Tukey's multiple comparison test
	brp^{Null} vs. *brp*^{Null};*gluRIIA*^{Null}	25.52 ± 1.16 (8)	14.79 ± 1.16 (9)	< 0.0001***	
	gluRIIA^{Null} vs. *brp*^{Null};*gluRIIA*^{Null}	26.67 ± 0.93 (8)	14.79 ± 1.16 (9)	< 0.0001***	
	Quantal content				
	Wild-type vs. *gluRIIA*^{Null}	36.18 ± 1.147 (9)	59.04 ± 2.81 (8)	< 0.0001***	One way ANOVA with Tukey's multiple comparison test
	brp^{Null} vs. *brp*^{Null};*gluRIIA*^{Null}	23.92 ± 1.157 (8)	29.61 ± 1.79 (9)	0.144	
	gluRIIA^{Null} vs. *brp*^{Null};*gluRIIA*^{Null}	59.04 ± 2.81 (8)	29.61 ± 1.79 (9)	< 0.0001***	
Figure 18d	BRP intensity				
	Wild-type vs. *gluRIIA*^{Null}	21.51 ± 3.006 (20)	27.97 ± 1.772 (29)	0.0432*	One way ANOVA with Tukey's multiple comparison test
	brp^{Null} vs. *brp*^{Null};*gluRIIA*^{Null}	1.031 ± 0.07860 (22)	1.026 ± 0.09475 (20)	> 0.9999	
	gluRIIA^{Null} vs. *brp*^{Null};*gluRIIA*^{Null}	27.97 ± 1.772 (29)	1.026 ± 0.09475 (20)	< 0.0001***	
	Unc13A intensity				
	Wild-type vs. *gluRIIA*^{Null}	17.30 ± 2.059 (20)	20.11 ± 1.654 (29)	0.5523	One way ANOVA with Tukey's multiple comparison test
	brp^{Null} vs. *brp*^{Null};*gluRIIA*^{Null}	11.65 ± 1.199 (22)	10.52 ± 0.6132 (20)	0.959	
	gluRIIA^{Null} vs. *brp*^{Null};*gluRIIA*^{Null}	20.11 ± 1.654 (29)	10.52 ± 0.6132 (20)	< 0.0001***	

Figure	Description	Mean ± SEM (n)		p value	Statistical test
Figure 19b	mEPSP amplitude (mV)				
	Wild-type vs. *gluRIIA*^{Null}	0.813 ± 0.04 (15)	0.353 ± 0.01 (17)	< 0.0001***	One way ANOVA with Tukey's multiple comparison test
	aplip1^{ek4} vs. *aplip1*^{ek4};*gluRIIA*^{Null}	0.924 ± 0.08 (18)	0.346 ± 0.02 (20)	< 0.0001***	
	gluRIIA^{Null} vs. *aplip1*^{ek4};*gluRIIA*^{Null}	0.353 ± 0.01 (17)	0.346 ± 0.02 (20)	0.99	
	eEPSP amplitude (mV)				
	Wild-type vs. *gluRIIA*^{Null}	24.19 ± 2.321 (15)	18.28 ± 2.45 (17)	0.31	One way ANOVA with Tukey's multiple comparison test
	aplip1^{ek4} vs. *aplip1*^{ek4};*gluRIIA*^{Null}	22.31 ± 2.44 (18)	14.03 ± 2.040 (20)	0.05	
	gluRIIA^{Null} vs. *aplip1*^{ek4};*gluRIIA*^{Null}	18.28 ± 2.45 (17)	14.03 ± 2.040 (20)	0.54	
	Quantal content				
	Wild-type vs. *gluRIIA*^{Null}	31.03 ± 3.41 (15)	54.32 ± 8.19 (17)	0.04*	One way ANOVA with Tukey's multiple comparison test
	aplip1^{ek4} vs. *aplip1*^{ek4};*gluRIIA*^{Null}	26.96 ± 3.74 (18)	41.64 ± 6.22 (20)	0.026	
	gluRIIA^{Null} vs. *aplip1*^{ek4};*gluRIIA*^{Null}	54.32 ± 8.19 (17)	41.64 ± 6.22 (20)	0.4	
Figure 19d	BRP intensity				
	Wild-type vs. *gluRIIA*^{Null}	716.9 ± 45.52 (33)	929.2 ± 55.15 (34)	0.04*	One way ANOVA with Tukey's multiple comparison test
	aplip1^{ek4} vs. *aplip1*^{ek4};*gluRIIA*^{Null}	678.8 ± 55.82 (31)	770.4 ± 62.67 (37)	0.651	
	gluRIIA^{Null} vs. *aplip1*^{ek4};*gluRIIA*^{Null}	929.2 ± 55.15 (34)	770.4 ± 62.67 (37)	0.17	
	Unc13A intensity				
	Wild-type vs. *gluRIIA*^{Null}	551.9 ± 40.71 (33)	758.7 ± 44.26 (34)	0.011*	One way ANOVA with Tukey's multiple comparison test
	aplip1^{ek4} vs. *aplip1*^{ek4};*gluRIIA*^{Null}	610.4 ± 46.23 (31)	741.2 ± 51.86 (37)	0.1963	
	gluRIIA^{Null} vs. *aplip1*^{ek4};*gluRIIA*^{Null}	758.7 ± 44.26 (34)	741.2 ± 51.86 (37)	0.9928	